**The Study of Dopamine Dynamics in Transgenic Mouse Models**

Brian M. Kile

A dissertation submitted to the faculty of the University of North Carolina at Chapel Hill in partial fulfillment for the degree of Doctor of Philosophy in the Department of Chemistry.

Chapel Hill
2009

Approved By:

Dr. R. Mark Wightman

Dr. James Jorgenson

Dr. Gary Glish

Dr. Paul Manis

Dr. Muhammad Yousaf

## Abstract

Brian M. Kile: The Study of Dopamine Dynamics in Transgenic Mouse Models
(Under the direction of Dr. R. Mark Wightman)

Brain slice experiments are a robust and controlled platform for the study of neurotransmitter dynamics using electrochemistry. The isolation and study of brain slices from genetically altered animals is critical for the understanding of neurotransmitter dynamics. The dynamics of biogenic amine neurotransmitters are important for movement and addiction studies. This dissertation focuses on the use of five separate transgenic mouse models to increase the understanding of biogenic amine transmission in the brain. Fast scan cyclic voltammetry and amperometry at carbon fiber microelectrodes were used to directly monitor the dynamics of dopamine, serotonin, and norepinephrine. The amount of neurotransmitter available to act on neuronal targets is a balance of release and uptake. A transgenic mouse model lacking the presynaptic protein synapsin was used to show that dopamine has a unique presynaptic architecture making it susceptible to release facilitation by cocaine, a drug of abuse. Additionally, mice expressing different amounts of the dopamine transporter were studied to show that the dopamine transporter is a critical regulator of extracellular dopamine concentrations. The importance of mitochondrial energy output was studied in animals lacking uncoupling protein 2, a regulator of mitochondrial function and two disease state mouse models indicated a relationship between obesity and dopamine release that does not extend to mental retardation. High performance liquid chromatography was used to support the conclusions drawn from the electrochemical measurements in brain tissue. Finally, methodologies related to brain slice experimentation were evaluated to better understand how these measurements can be improved.

To Eric L. Kile
(April 6, 1951-July 14, 2000).

This Work Fulfills My Promise To You.

**Acknowledgements**

The research in this dissertation would not have been possible without the guidance and support of Dr. Mark Wightman. The vast majority of work presented here was done in collaboration with other researchers. At Duke University, I would like to acknowledge Dr. Marc Caron, Dr. Ali Salahpour, and Dr. George Augustine. At Harvard University, I would like to acknowledge Dr. Brad Lowell, Dr. Helen Freeman, and Dr. Dong Kong. Funding for this research was provided by the National Institutes for Health. Finally, I would like to thank all of my collaborators in the Wightman Lab. I would also like to acknowledge Rachel and all of my family and friends without whom I would not have had the opportunity to make this accomplishment.

## Table of Contents

## List of Tables

## List of Figures

## List of Abbreviations

| | |
|---|---|
| 5-HT | 5 hydroxytryptamine or serotonin |
| $[DA]_{max}$ | The maximum extracellular dopamine concentration |
| aCSF | Artificial cerebrospinal fluid |
| AMPH | Amphetamine |
| AP | Acetamidophenol |
| ATP | Adenosine triphosphate |
| BAC | Bacterial vector |
| CFME | Carbon fiber microelectrode |
| CNQX | 6-cyano-7-nitroquinoxaline-2,3-dione |
| CV | Cyclic voltammogram or cyclic voltammetry |
| DA | Dopamine |
| DAT | Dopamine transporter |
| DNA | Deoxydribonucleic acid |
| E | Epinephrine |
| ECD | Electrochemical detector or electrochemical detection |
| EDTA | Ethylenediaminetetra-acetic acid |
| eGFP | Enhanced green fluorescent protein |
| EM | Electron micrograph |
| EOF | Electroosmotic flow |
| ES | Embryonic stem cell |
| Fmrp | Fragile X mental retardation protein |
| FSCV | Fast scan cyclic voltammetry |
| FXS | Fragile X syndrome |

| | |
|---|---|
| GABA | Gamma (γ)-amino butyric acid |
| HPLC | High performance (pressure) liquid chromatography |
| HSVTK | Transgenic cassette containing the *NEO* and *TK* genes |
| $K_{ca}^{2+}$ | Calcium constant for dopamine release |
| $K_i$ | Inhibition constant for a competitive inhibitor of DAT |
| $K_m$ | Michaelis-Menten constant (also listed with subscript app when inhibitor present) |
| KO | Knock-out |
| L-dopa | 3,4-dihydroxy-L-phenyalanine (dopamine precursor) |
| MAO | Monoamine oxidase |
| MAOI | Monoamine oxidase inhibitor |
| METH | Methamphetamine |
| MFB | Medial forebrain bundle |
| MPP+ | (1-methyl-4-phenylpyridinium)$^+$ |
| MPTP | 1-methyl-4-phenyl-1,2,3,6-tetrahydropyridine |
| mRNA | Messenger ribonucleic acid |
| Nac | Nucleus accumbens |
| NE | Norepinephrine |
| NET | Norepinephrine transporter |
| NPE | 2-(4-nitrophenoxy) ethanol |
| PCR | Polymerase chain reaction |
| PTT | 2β-propanoyl-3β-(4-tolyl)-tropane |
| Quin | quinelorane |
| RNA | Ribonucleic acid |
| ROS | Reactive oxygen species |
| RP-HPLC | Reversed phase high performance liquid chromatography |

| | |
|---|---|
| SEM | Standard error in the mean |
| SERT | Serotonin transporter |
| SNr | Substantia nigra pars reticulata |
| SNc | Substantian nigra pars compacta |
| T-650 | Thornel® 650 carbon fiber |
| TKO | Triple knockout |
| $t_r$ | Retention time |
| UCP2 | Uncoupling protein 2 |
| *v*BNST | Ventral bed nucleus of the stria terminalis |
| VMAT2 | Vesicle monoamine transporter |
| $V_{max}$ | Maximal uptake velocity in µM $s^{-1}$ |
| VTA | Ventral tegmental area |
| WT | Wild type |

# Chapter 1

## Analytical Neuroscience and Transgenic Animals

### Introduction

Information is transmitted through the brain via electrical impulses carried along neurons, specialized cells capable of propagating electrical and chemical signals (Figure 1.1). Electrical signals are carried along the dendrites and axon of the neuron by ion movement (primarily $Na^+$, $K^+$, and $Cl^-$) across the plasma membrane (Hodgkin and Huxley, 1952a, b). The ion gradient that is created due to this movement changes the relative potential of the plasma membrane. Wave like potential changes along the plasma membrane allow for information to pass along the axon, dendrites, and cell body (Figure 1.2). The normal resting potential of a neuron is negative; positive deflections in membrane potential are considered excitatory while negative changes are considered inhibitory. A neuron will receive excitatory and inhibitory electrical inputs at its dendrites where they will be summated at the cell body. If the summated inputs exceed a predetermined threshold, the cell will fire an action potential that propagates down its axon. The axon synapses with the dendrites of target neurons at which point electrical propagation of the signal switches to a chemical form of communication. Information is transmitted at synapses through the use of chemical messengers termed neurotransmitters. When the action potential reaches the synapse, voltage gated $Ca^{2+}$ channels open and $Ca^{2+}$ enters the presynaptic terminal. The influx of $Ca^{2+}$ triggers exocytosis, the fusion of intracellular vesicles with the plasma

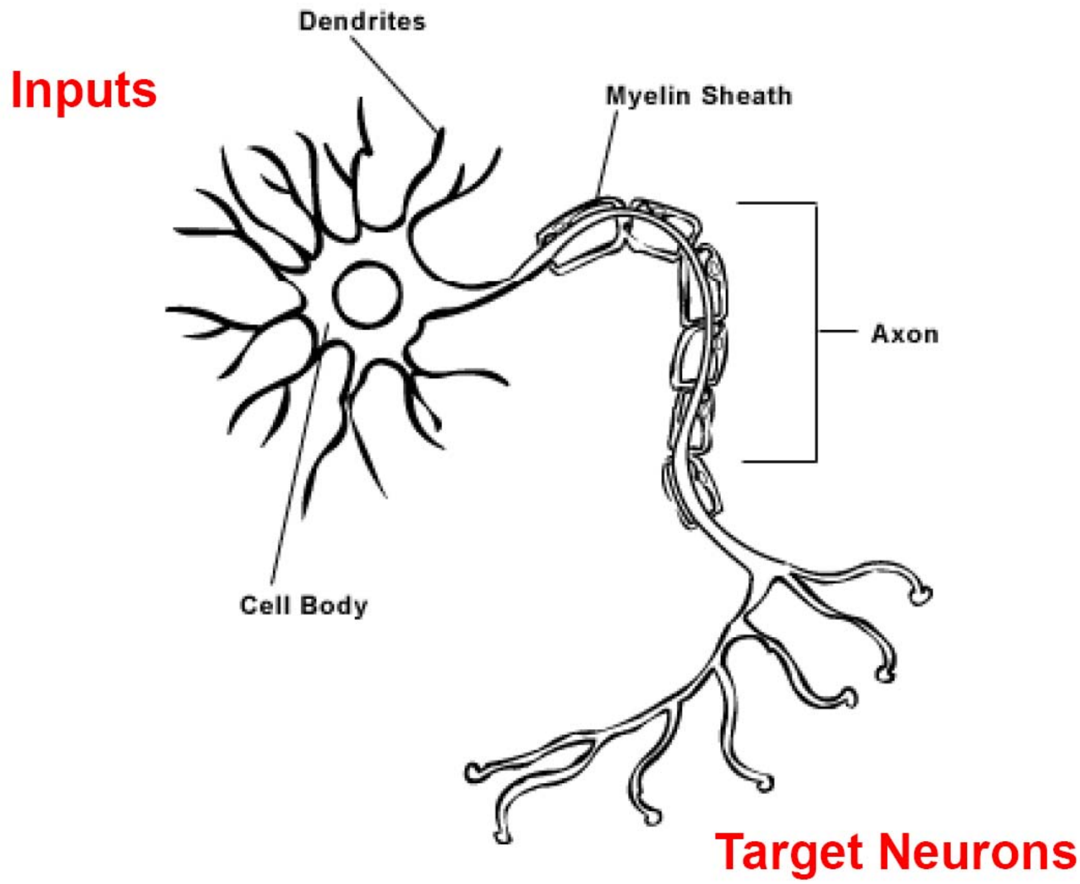


**Figure 1.1** A schematic of a unipolar neuron depicting the major structures associated with this cell type. Electrical inputs (both excitatory and inhibitory) are received at the dendrites, summated at the cell body, and propagated down the axon to target neurons. Some neurons have a myelin sheath around their axons helping to propagate axon potentials more quickly (biogenic amine neurons do not). The axon branches forming multiple synapses (the site of neurotransmitter release) with target neurons. This figure has been modified from a similar illustration found at www.drugabuse.gov.

membrane followed by the expulsion of neurotransmitters into the extracellular space. These chemicals diffuse to pre- and postsynaptic targets where they trigger responses via specific receptors.

The action of neurotransmitters at their targets depends upon the location of synapse, the type of neurotransmitter, and the type of receptor that it binds. In general, neurotransmitters will act either to open an ion channel, affecting the polarity of the postsynaptic cell, or to begin an intracellular messenger cascade, changing how the target cell operates on a longer time scale (Brown and Birnbaumer, 1989; Unwin, 1993). The duration of action for most neurotransmitters is short; therefore, clearance mechanisms exist to cease neurotransmitter action. These include uptake into neurons by membrane bound transport proteins, a relatively rapid process, and the slower process of degradation by free-floating enzymes in the extracellular space (Kandel, 2008).

The biogenic amine neurotransmitters primarily act as modulators of neuronal activity in the brain. The biogenic amines include serotonin (5-HT), dopamine, and norepinephrine (NE). These chemicals are known to modulate movement, wakefulness, mood, pleasure, addiction, and appetite (Cooper et al., 2003). Proper understanding of neuronal function related to these neurotransmitters has implications for disease state and addiction studies. An example of the ability of these neurotransmitters to modulate behavior is the 5-HT modulation of dopamine release (Fink and Gothert, 2007). Selective antagonism of 5-$HT_{2A}$ receptors can alleviate movement phenotypes commonly associated with hyperdopaminergia (Barr et al., 2004). 5-HT innervation of the dopamine cell bodies in the midbrain changes their firing rate which affects the amount of dopamine released in the striatum. In the striatum, dopamine is responsible for modulation of the synaptic strength between γ-aminobutyric acid (GABA) (the main inhibitory neurotransmitter) neurons and glutamate (the main excitatory neurotransmitter) neurons (Chase and Oh, 2000). Released dopamine acts on the glutamate-sensitive medium spiny neurons (GABAergic neurons that project to motor cortex) altering the ability of released glutamate to initiate movement. This example demonstrates how biogenic amines can regulate each other as well as other neurotransmitters and how this regulation relates to behavioral responses.

**Murine Brain Slices**

Neurons exist in tightly packed networks that weave throughout the brain to different targets of action. In many cases the neurotransmitter target is distal to the location of the cell bodies. A cluster of cell bodies, known as a nucleus, will project a bundle, or tract, of axons to multiple sites of termination. This organization can be seen in the serotonergic system where three cell nuclei are responsible for distributing 5-HT to 17 different target regions (Heimer, 1995). Dissection of live tissue by techniques such as the preparation of brain slices facilitates the isolation of these systems for study. Isolation can involve the selection of a specific neurotransmitter tract (eg: isolation of the nigrostriatal dopamine pathway) or portions of the same neurotransmitter tract (eg: separation of 5-HT terminals in the ventral tegmental area from 5-HT cell bodies in the dorsal raphe nucleus).

Mouse brain slices are a robust and controlled preparation for the isolation and maintenance of brain regions for analytical studies. The brain can be divided along three planes: horizontal, sagittal, and coronal. Figure 1.3 shows examples of these three sections and how they are taken from a human brain. The nomenclature described in Figure 1.3 is identical for sections taken from the mouse brain. Using a reference atlas such as <u>The Mouse Brain in Stereotaxic Coordinates</u> by Keith Franklin and George Paxinos (Paxinos et al., 1985), it is possible to pinpoint an anatomical location within a brain slice. When the area of interest is contained within a thin section of live tissue, it can be maintained under physiological conditions for study. The brain slice preparation is particularly useful for

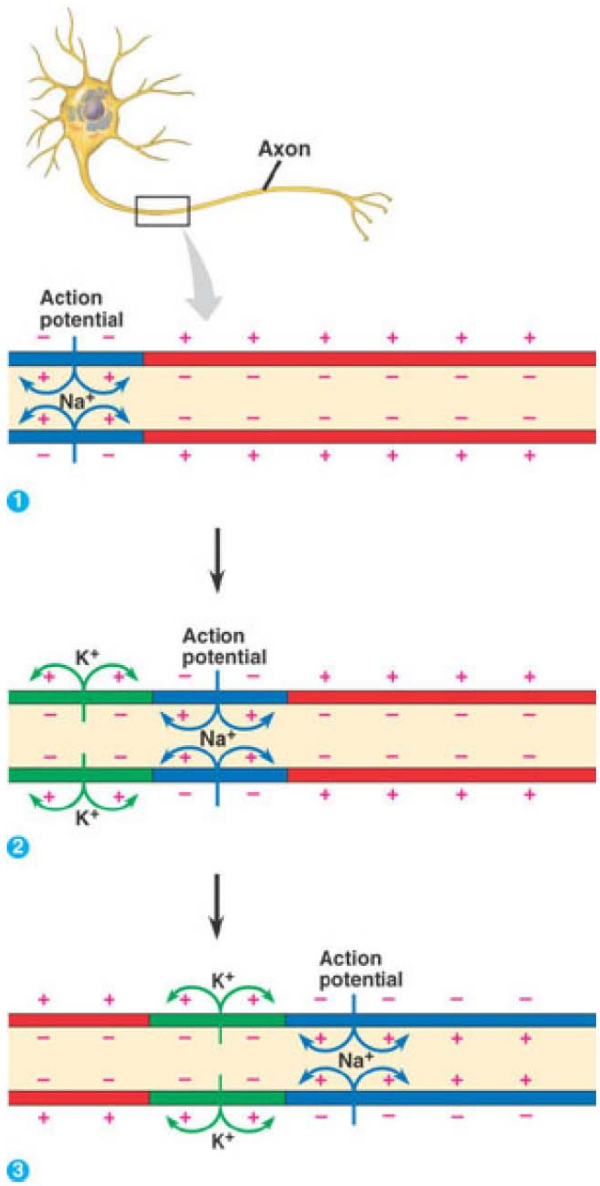


**Figure 1.2** The action potential propagating down an axon. 1) Voltage gated channels open allowing $Na^+$ to flow in along its concentration gradient. The membrane potential shifts to a more positive potential (blue coloration) called depolarization. 2) Behind the region of more positive membrane potential $K^+$ rushes out of voltage gated $K^+$ channels. This leads to a hyperpolarized region of membrane (green coloration). 3) Both the depolarized and hyperpolarized regions move along the axon as voltage gated $Na^+$ and $K^+$ channels open and close. Illustration can be found at kvhs.nbed.nb.ca.

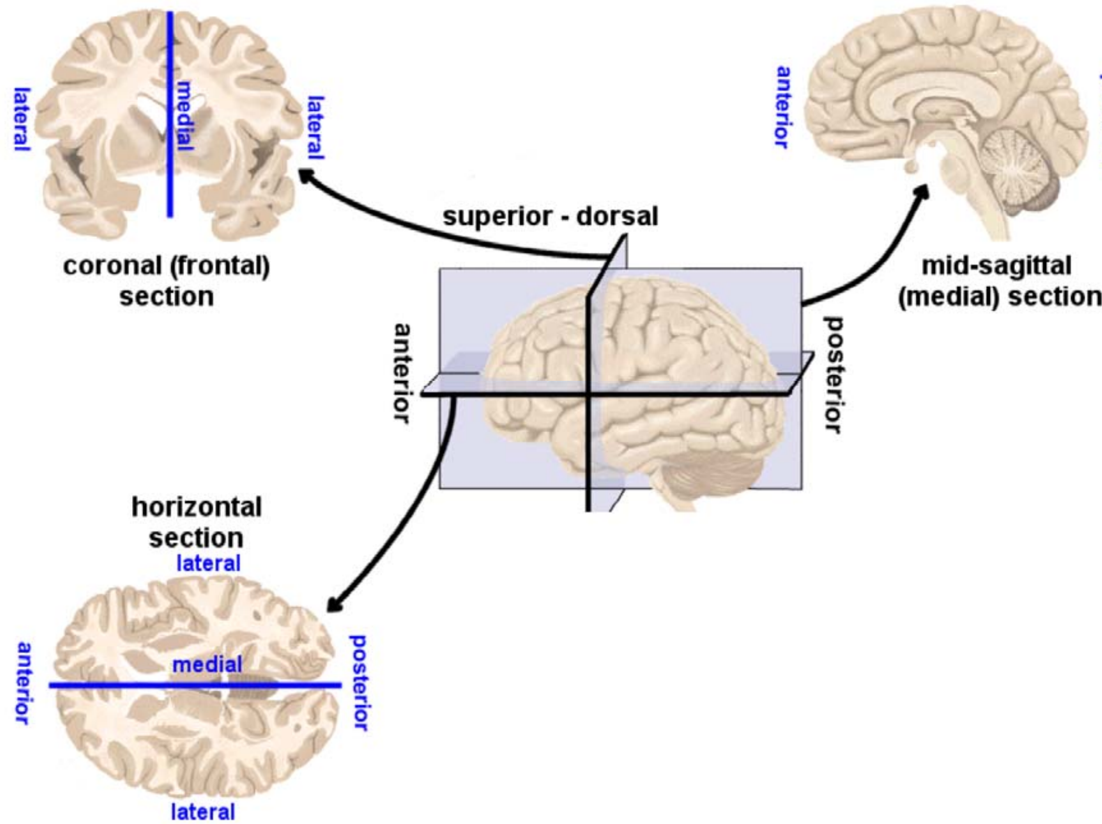


**Figure 1.3** Slicing planes used in the section of the human brain. Center: The three dimensional brain showing the section planes. Top Left: An example coronal slice in which the brain is sliced from dorsal surface to the ventral surface perpendicular to the horizontal plane. Top Right: Sagittal slices are still perpendicular to the horizontal plane but are taken from the anterior to posterior surfaces. Bottom Left: A horizontal slice is taken from the anterior surface to the posterior surface but is perpendicular to the coronal plane. Graphic modified from http://homepage.smc.edu/russell_richard.

isolating and studying midbrain structures which are occluded by the cortex and difficult to visualize and access when the brain remains intact (Kandel, 2008). Slices are prepared according to the structures and anatomical orientation deemed most appropriate to answer the specific question of interest. For example, the isolation of the intact nigrostriatal dopamine pathway is best achieved using a sagittal or horizontal section while isolation of the dopamine terminal region is best done with a coronal section. A brain slice is shown in Figure 1.4 where the nigrostriatal dopamine pathway has been visualized with immunoperoxidase staining of the dopamine transporter (DAT) (Salahpour et al., 2008). Had this slice been maintained in a viable state rather than fixed, it would have been possible to do spatially resolved studies at the cell bodies, terminals, or both.

### Electrochemistry

Electrochemistry is a technique through which redox chemistry can be used to study electroactive species at the surface of an electrode. Direct monitoring of neurotransmitter concentration changes over time is important to properly understand their actions in the brain. This dissertation focuses on the use of two types of electrochemistry to monitor biogenic amines: fast scan cyclic voltammetry (FSCV) and constant potential amperometry (referred to hereafter as amperometry). The analytical sensor used was a carbon fiber microelectrode (CFME) (Cahill et al., 1996).

FSCV at CFMEs is a useful method to evaluate the concentration of biogenic amines and its rapid changes. In FSCV, a linear voltage ramp is used to oxidize and reduce species of interest at an electrode surface. FSCV at CFMEs has the ability to monitor small changes in analyte concentration while in a complex mixture. Monitoring neurotransmitter release in brain tissue is subject to a unique set of analytical problems: closely resolved anatomical structures require a small sensor, nanomolar analyte concentrations require a

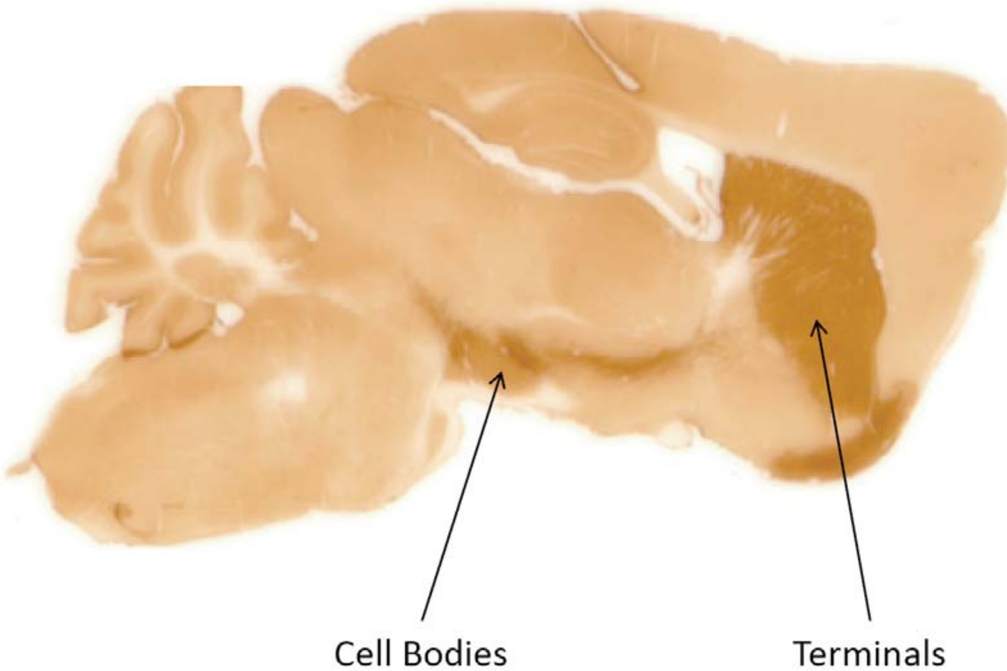


**Figure 1.4** A sagittal section of the mouse brain. This section has been stained with immunoperoxidase to visualize the dopamine transporter (DAT). The DAT is located in high density on dopamine terminals and cell bodies making them appear darker than the surrounding tissue (Salahpour *et al.*, 2008).

sensitive technique, and a host of interfering compounds requires selectivity for the analyte of interest. Also, subsecond time resolution is necessary to effectively monitor real time release and uptake events in biological tissue (Venton et al., 2002). The cylindrical T-650 CFME used in this work is 6 μm in diameter and cut to a length of 50 μm, providing very good spatial resolution (Figure 1.5) (Kawagoe et al., 1993; Cahill et al., 1996). Carbon fibers provide enhanced sensitivity by adsorbing biogenic amines when held at a negative potential (Heien et al., 2003).

The peak faradaic current at a voltammetric electrode can be defined by (Bard and Faulkner, 2001):

$$i_p = (2.69 \times 10^5) n^{3/2} A D_O^{1/2} C_O^* v^{1/2} \qquad (1)$$

where **n** is the number of electrons, **A** is the electrode area, $\mathbf{D_O}$ is the diffusion rate of the oxidant, $\mathbf{C_o}$ is the concentration of the oxidant, and ***v*** is the scan rate. This equation predicts that the peak faradaic current should increase as the square root of the scan rate, but it only applies to a freely diffusing, non-adsorbed oxidant in solution. When an analyte is adsorbed to the electrode surface its peak faradaic current scales proportionally with scan rate, enhancing the analytical signal associated with the same concentration of non-adsorbed analyte at a given scan rate. The adsorption of analyte on the sensor surface enhances the electrochemical signal by preconcentrating the analyte and changing its electrochemical properties.

The selectivity and temporal resolution required to monitor neurotransmission is provided by performing FSCV at the CFME. The use of an ultra-microelectrode such as a CFME permits the use of faster scan rates by reducing the ohmic drop and RC time constant of the electrode (Wightman et al., 1988). Typical scan rates used in this work range from 600 V/s to 1000 V/s applied at 10 Hz or 60 Hz. Therefore, the ultimate time

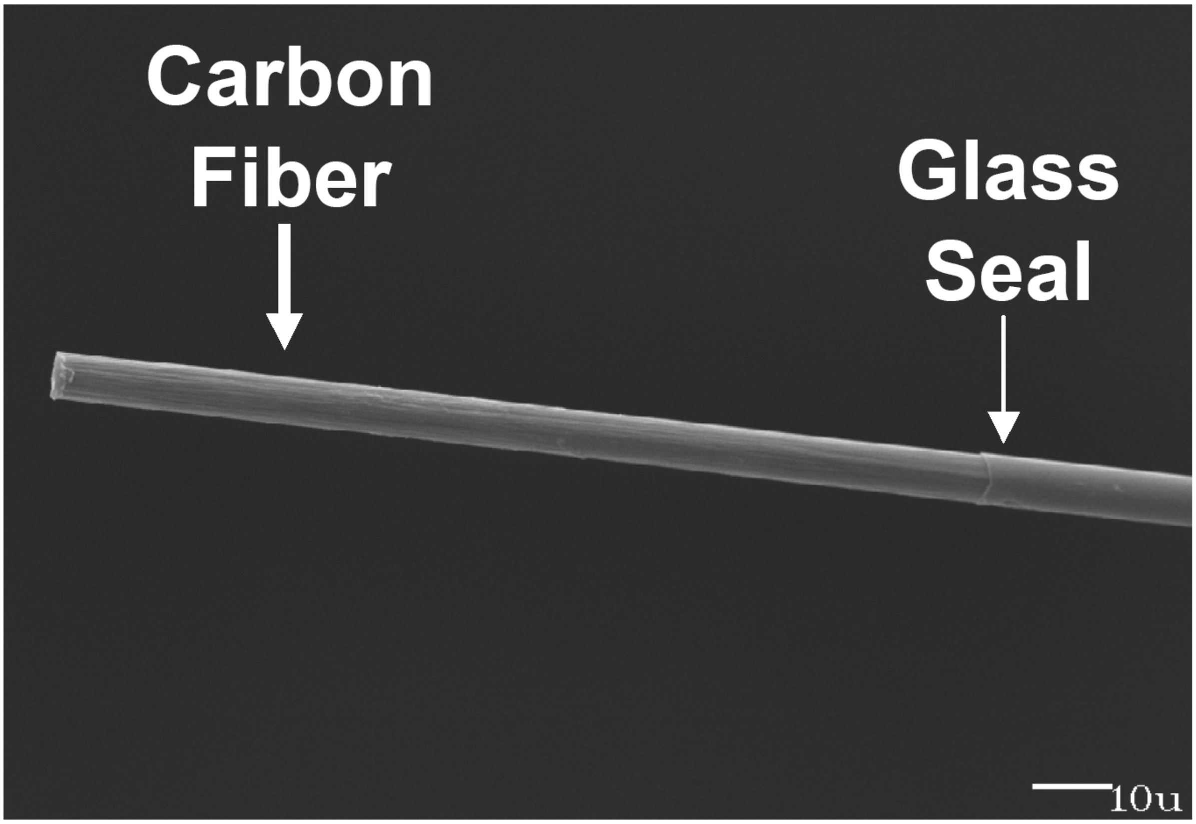


**Figure 1.5** A cylindrical T-650 carbon fiber microelectrode. A T-650 carbon fiber has been sealed in a glass capillary and cut to a length suitable for experimentation. The glass seal can be seen in the right hand portion of the panel. The fiber has a diameter of 6 μm and is typically cut to a length of 50 μm (Cahill *et al.*, 1996). Scale Bar: 10 μm.

resolution of the CFME using FSCV under these conditions would be 100 ms for 10 Hz and 16.7 ms for 60 Hz. Other techniques used to monitor neurotransmission, such as microdialysis, normally operate on the minute time scale. The fastest demonstrated microdialysis measurements were made 15 s apart using stepped flow sampling (Wang et al., 2008).

A second advantage to FSCV is the selectivity achieved using the cyclic voltammogram (CV) for identification of an analyte. Figure 1.6 shows the structures, voltage ramps, and CVs for dopamine and 5-HT. The positive current arises from oxidation of dopamine or 5-HT accumulated on the electrode surface in the time between scans (either 100 ms or 16.7 ms) while the negative current is the reduction of oxidized analyte remaining on the electrode surface. The positive and negative current deflections occur at a characteristic potential for each analyte, allowing the identity and presence of the analyte to be verified in a complex mixture of proteins, lipids, other neurotransmitters, and dissolved gases. Notice that the ramp used for 5-HT is different than that for dopamine (Figure 1.6). The electrochemistry of 5-HT is more complicated than dopamine, requiring a more complex waveform to prevent the accumulation of interfering species that form when 5-HT is oxidized (Jackson et al., 1995). Figure 1.6 also shows that although the voltammetric waveforms are very different, the oxidation of both analytes occurs at a similar potential. This similarity should prevent positive identification of 5-HT over dopamine if both were present in a mixture. However, the ramp provides enhanced sensitivity for 5-HT over dopamine because the electrode rests at a positive potential preventing dopamine adsorption (Jackson et al., 1995). This waveform makes the electrode insensitive to physiological dopamine concentrations and allows for exclusive monitoring of 5-HT in the presence of dopamine. Therefore, the FSCV potential ramp can be used to impart selectivity on the electrode if the CVs of two species do not facilitate positive identification.

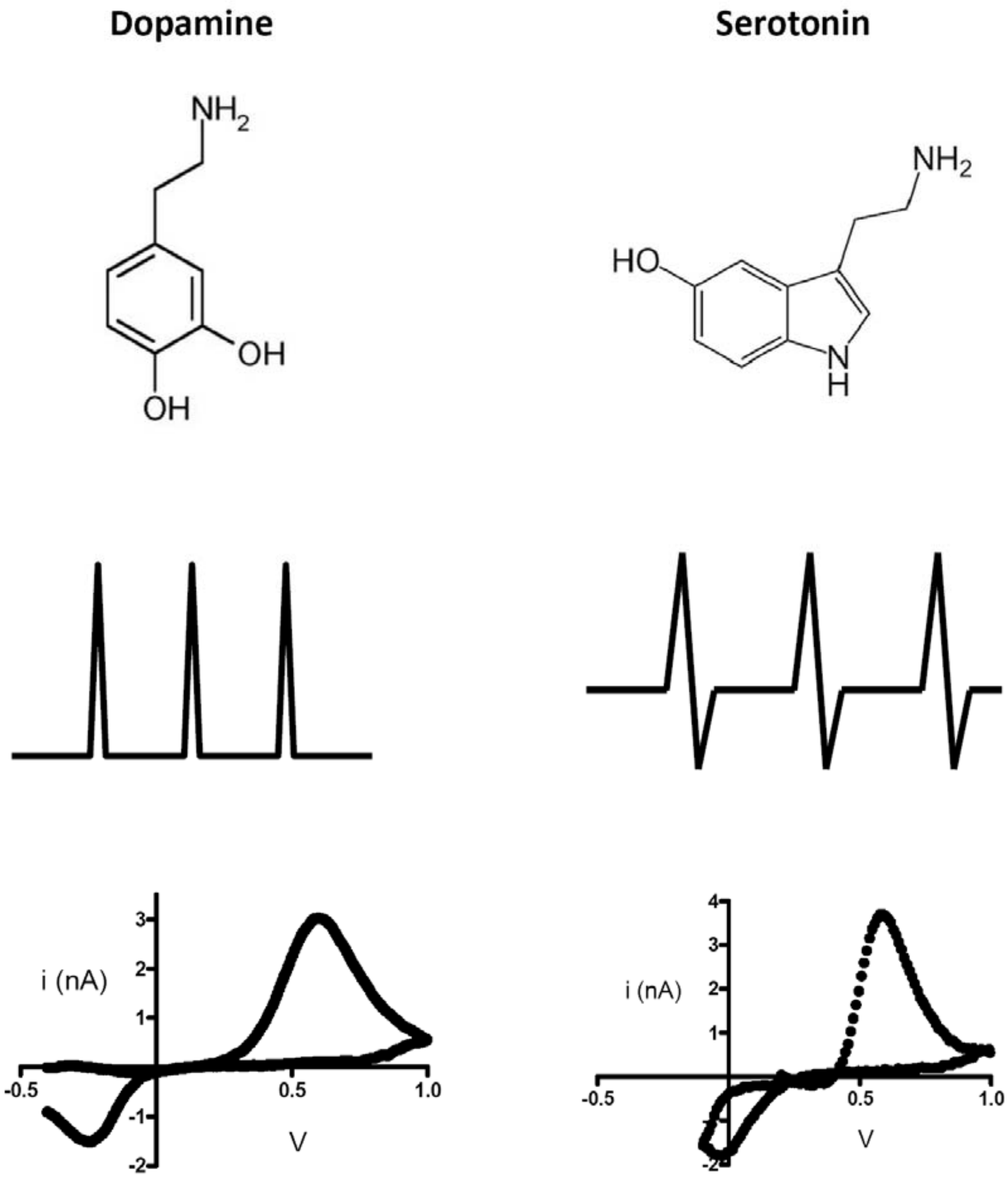


**Figure 1.6** Example voltammograms of two biogenic amines. Left Panels: Dopamine is detected using a linear voltage ramp from -400 mV to 1,000 mV back to -400 mV scanned at 600 V/s. The dopamine CV is characterized by an $i_{p,c}$ at 650 mV and an $i_{p,a}$ at -200 mV. Right Panels: 5-HT detection requires a more complicated waveform where the voltage rests at 200 mV ramps to 1,000 mV and back to -100 mV at 1,000 V/s holding again at 200 mV between scans. This waveform keeps the electrode clear of fouling products. The 5-HT CV is characterized by an $i_{p,c}$ at 600 mV and an $i_{p,a}$ at 0 mV.

An unavoidable effect of scanning a voltammetric electrode quickly is the large background current associated with charging of the double layer capacitance. The background current swamps out the relatively small faradaic current associated with analyte detection. For example, the background of a typical 50 μm cylinder electrode may be as high as 1000 nA while the current due to dopamine oxidation is typically less than 10 nA. To get around this problem, background subtracted FSCV is used (Figure 1.7). The background is stable over the time period of the measurement and can be removed by subtraction leaving only the faradaic current associated with analyte detection.

Amperometry is used when greater temporal response is necessary. In FSCV, there is a time delay associated with the adsorption and desorption of the analyte from the electrode surface (Heien et al., 2003). These events slow the electrode response to changes in analyte concentration (Bath et al., 2000). In amperometry the electrode is held at a constant potential sufficient to oxidize the analyte of interest (700 mV for dopamine). When the analyte encounters the electrode surface it is immediately oxidized and a signal recorded (Hochstetler et al., 2000). The lack of any adsorption or desorption means that the temporal response is only limited by mass transport and electron transfer kinetics. The net result is a faster response time than FSCV (Mundroff and Wightman, 2002). Amperometric measurements are less sensitive (almost 100 fold for dopamine) than FSCV due to a lack of preconcentration; however, similar S/N ratios have been reported for the two techniques (Venton et al., 2002). Unfortunately, the lack of an analyte-specific cyclic voltammogram prevents analyte identification. For this reason amperometry is generally only used once the identity of the electrochemical signal has been established.

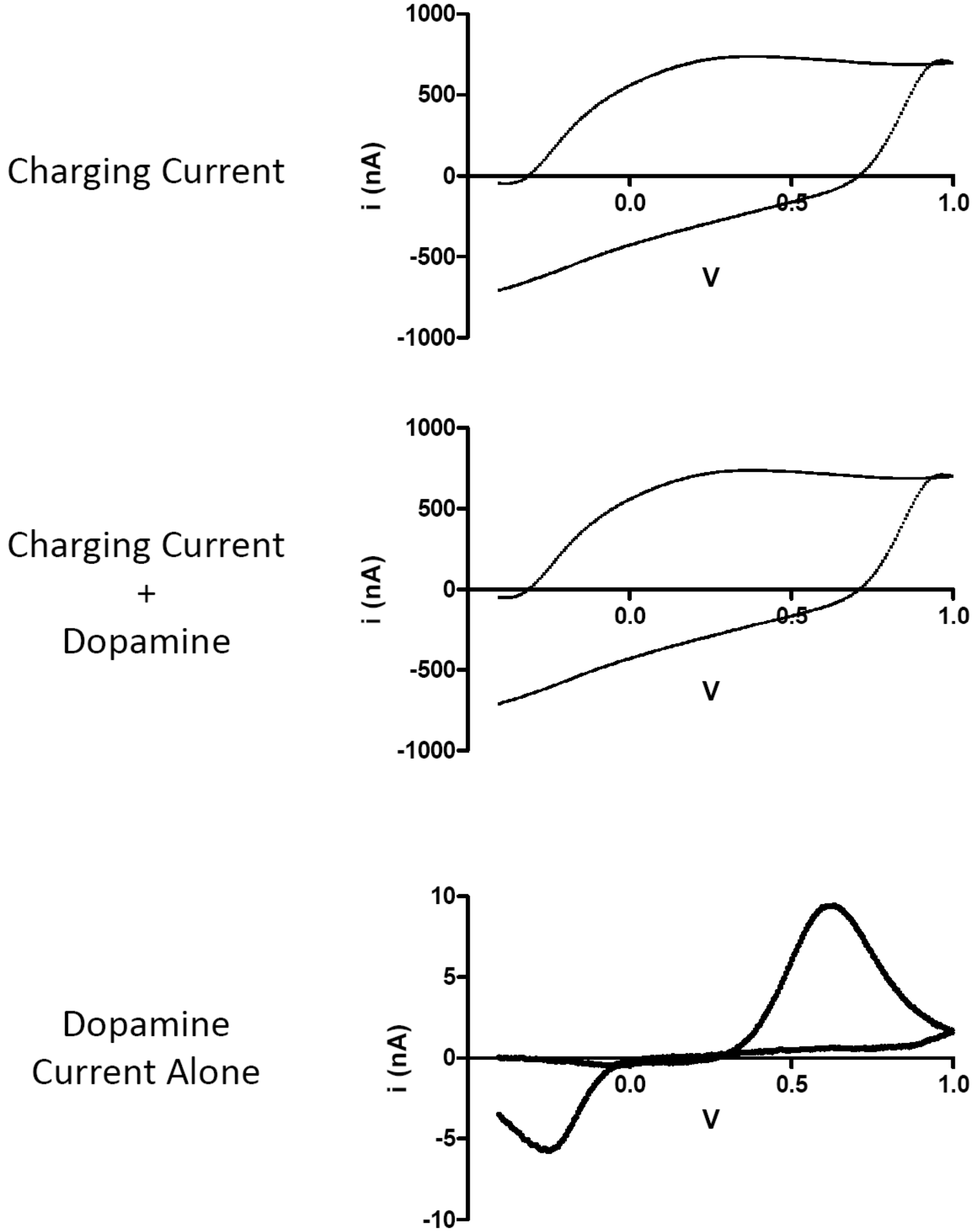


**Figure 1.7** The charging current associated with fast scan rates is large compared to the Faradaic current associated with dopamine detection. The background remains relatively unchanged over the measurement time and can be subtracted out digitally (midddle panel less the top panel) revealing a CV of dopamine alone.

**Brain Slice Measurements**

Brain slices are a robust and reliable tissue preparation to be used in electroanalytical studies. In a brain slice experiment, neurotransmitter release is typically evoked by a current pulse through a bi-polar stimulating electrode and monitored at the working electrode (Figure 1.8). The data from the working electrode is viewed in two ways: the CV (as shown in Figure 1.7), used for substance identification, and the current trace, generated by monitoring the oxidation potential for changes over time (Figure 1.8). The current trace is then translated into a concentration trace by calibrating the electrode against a known concentration of analyte (see chapter 2). The concentration trace has two distinct phases that occur after electrical stimulation. There is an instantaneous rise in amine concentration after stimulation followed by clearance through presynaptic uptake transporters (Figure 1.8). The environment of the slice can be modified by changing ion concentrations, applying drugs, or changing temperature to modify the size and shape of this basic curve.

Brain slice experiments are particularly informative when monitoring uptake kinetics. The uptake of biogenic amines can be effectively modeled using Michaelis-Menten kinetics where the transporter is treated as the enzyme and the neurotransmitter as the substrate. Based on these approximations, the concentration of amine can be expressed as a function of time for a single pulse stimulation:

$$\frac{d[DA]}{dt} = [DA]_{max} - V_{max}\left(1 + \frac{K_m}{[DA]}\right)^{-1} \qquad (2)$$

Based on this equation the uptake parameters $K_m$ (the binding affinity for dopamine at the transporter) and $V_{max}$ (the maximal rate of dopamine uptake) can be calculated for different locations, animal types, and environmental conditions. The Michaelis-Menten model is a

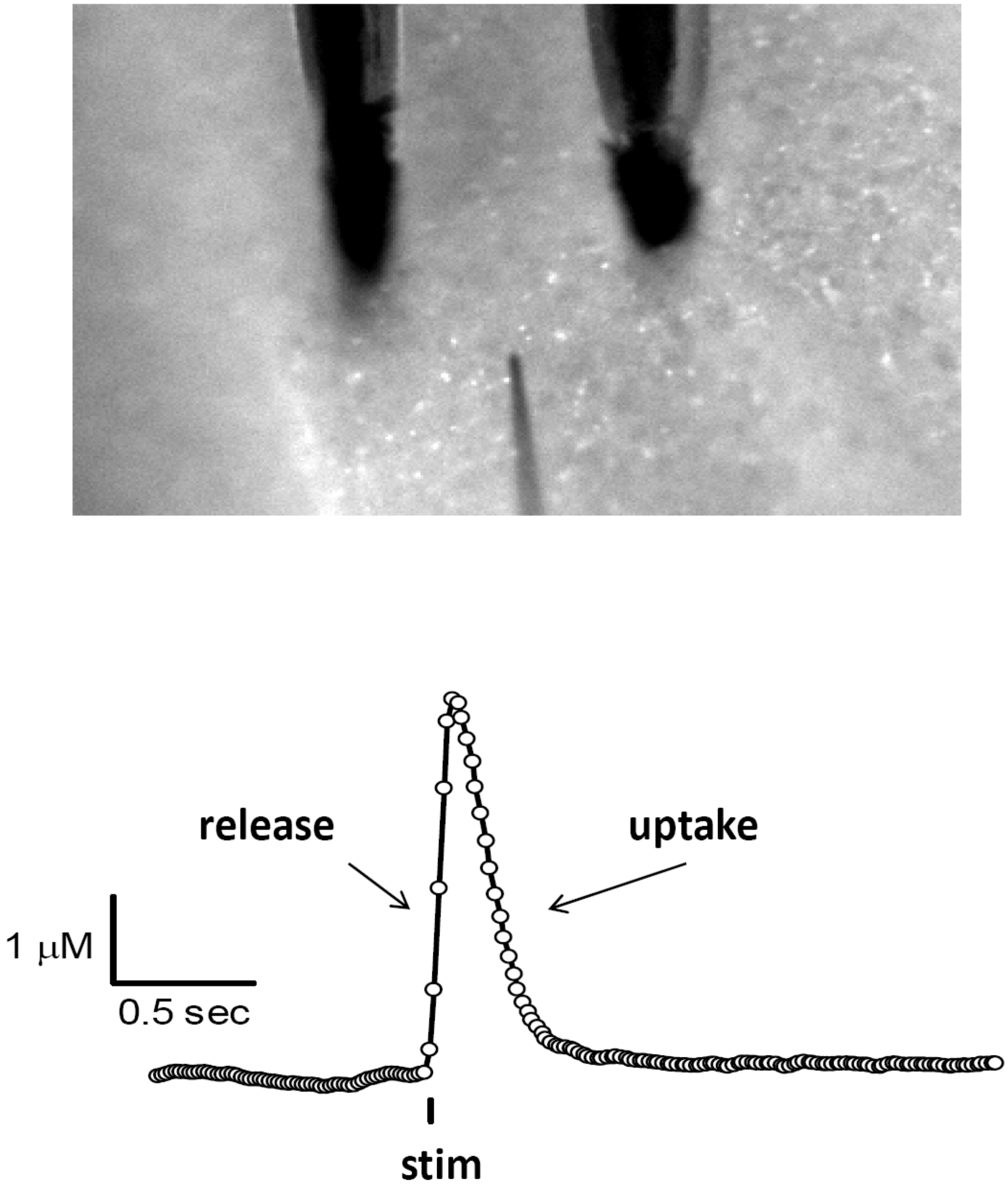


**Figure 1.8** An example of stimulated dopamine release in a striatal brain slice. Top Panel: A brightfield image of the two-pronged tungsten stimulating electrode placed on the slice surface and the CFME placed 100 μm away. The stimulus is provided through the tungsten electrode and dopamine is measured at the working electrode. Bottom Panel: The [DA] as a function of time in response to the stimulus. The stim, release portion, and uptake portion of the curve are marked.

robust and effective way to measure clearance rates (Wightman et al., 1988; Wu et al., 2001). A more detailed explanation of how uptake rates can change in the brain will be explained in later chapters.

### High Performance Liquid Chromatography

High performance liquid chromatography (HPLC) with electrochemical detection is an important technique for the support and validation of electrochemical monitoring of biogenic amines using CFMEs in brain slices. HPLC is most often used as the analytical sensor associated with microdialysis measurements (Umriukhin et al., 2007; Howard et al., 2008; Wang et al., 2008). Chapter 6 focuses on the use of HPLC in support of electrochemical data by providing information about the content of amines in a particular brain region. HPLC is run using an amperometric detector incapable of differentiating between different biogenic amines electrochemically. The selectivity of the HPLC measurement arises from a polarity based separation mechanism which resolves biogenic amines temporally (Figure 1.9). An additional analytical technique like HPLC is often needed because, although powerful, FSCV is unable to determine the total biogenic amine profile for a particular brain region. Total content is also important data to have in cases where the amount of dopamine being released has been altered in some way (Senior et al., 2008). The combination of electrochemical and chromatographic data provides better understanding of the mechanism of the release change by separating changes in dopamine available for release and an increased release probability of dopamine. LC total content measurements are also powerful when looking at regions with interfering substances. The total content measurements can verify or refute the presence of a neurotransmitter that cannot be distinguished from the analyte of interest using FSCV.

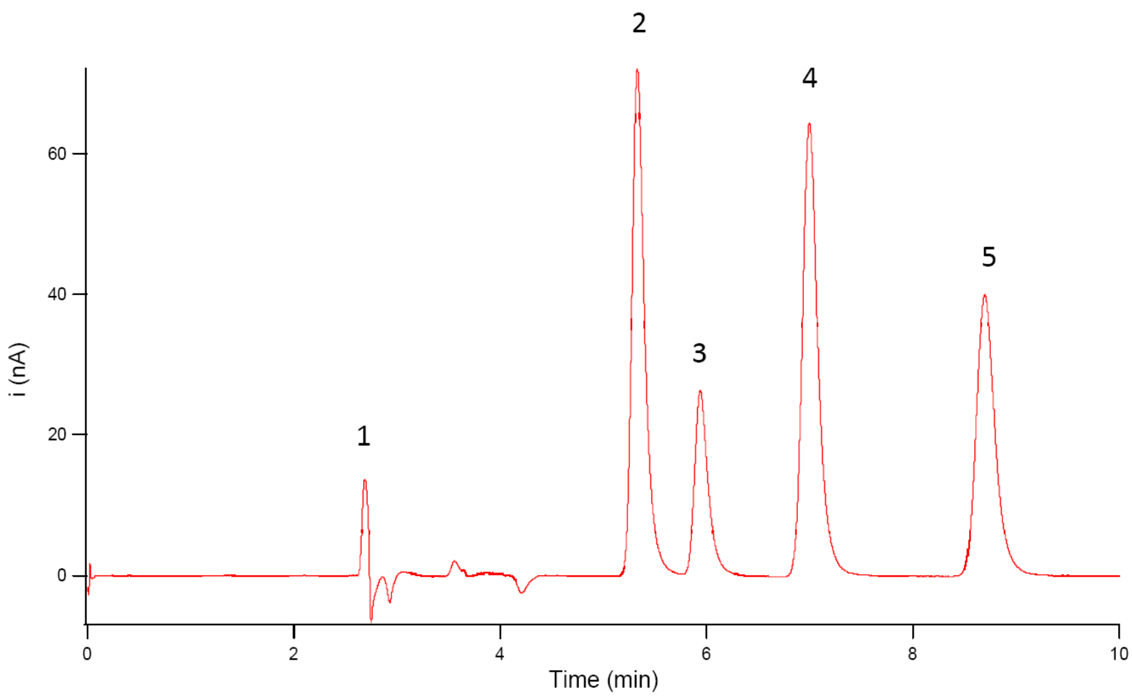


**Figure 1.9** An isocratic reverse phase separation of several biogenic amines using reverse phase HPLC with electrochemical detection. Analytes are separated temporally based on their relative polarity and detected by amperometry. The x-coordinate is the elution time in minutes while the y-coordinate shows the oxidation current of each species. Peak Assignments; 1) Solvent front 2) norephinephrine 3) hydroquinone (quantification standard) 4) l-dopa 5) epinephrine.

## Transgenic Mouse Models

In 2007, Oliver Smithies shared the Nobel Prize in Medicine with Sir Martin Evans and Mario Capecchi for their contributions to the field of transgenic mutagenesis. In particular, their research was central to the development of embryonic stem (ES) cells as vehicles for specific gene mutations. The role of transgenic mice in the development of disease state models cannot be downplayed. Mouse models such as these can be credited with the development of new Alzheimer's treatments, diabetes drugs, and the advancement of heart disease research among other things. A few more examples of the impact made by transgenic mice in the medical field can be found in the following references (Adlard et al., 2008; Bjorkqvist et al., 2008; Choi et al., 2008; Pattison and Robbins, 2008; Seidler et al., 2008). The two most common generation techniques are direct transfection or ES cells transfection of fertilized embryos.

The first technique involves the direct introduction of foreign DNA into a fertilized mouse embryo. The introduction of the foreign DNA can be performed by pronuclear injection, retroviral infection, or adenoviral infection. Pronuclear injection requires the introduction of foreign DNA by micropipette directly into the fertilized egg. Transfected eggs are then implanted into a pseudo-pregnant female who gives birth to a founder animal (a pup that expresses the transgene). Once germline transmission of the transgene is complete, many generations are mated to create homozygous transgenic animals. This technique is more technically controlled than the viral transfection techniques, but requires a longer training period for proficiency and more expensive equipment. Pronuclear injection technique can also yield unreliable transfection results because the number of incorporated transgene copies is unknown, and the expression of the transgene can be affected by its local chromosomal environment.

Viral transfection involves the incubation of a fertilized egg with adeno or retroviruses. These viruses are unable to replicate their own genome because they have had selected genetic deletions preventing it. Even though replication is prevented, the virus is still able to interpolate some foreign DNA into the host egg for replication. Viral transfection of fertilized eggs is more cost effective than pronuclear injection, but does have limitations. Only a small amount of exogenous genetic material can be added to the viral genome (4-7.5 kb) without making the virus non-functional. The relatively small amount of genetic material that is implantable with this technique makes it impractical for large genetic manipulations. In rare cases, the virus can undergo recombination with the host genome activating its replication ability. The entire viral genome will then propagate through the host egg. The problems with viral transfection are often outweighed by a simpler and cheaper technique than would be possible with pronuclear injection.

The development of ES cells as transgene hosts has eliminated many of the problems associated with previous methodologies. ES cells are undifferentiated cells capable of replicating to form any type of physiological tissue, and therefore are capable of carrying a transgenic manipulation to all cell types. Under proper conditions they can be maintained in an undifferentiated state where the addition of exogenous genetic material can occur. ES cells expressing the desired transgene can then be selected for injection into the fertilized egg. The selection of cells is most often done using a selectable marker gene in the transgenic cassette. The integration of the selectable marker gene will convey attributes to the transfected cell such as antibiotic resistance that can be used to isolate it from non transfected cells. There are many different types of selectable markers such as *NEO* or *β-GEO* which impart neomycin resistance or expression of β-galactosidase respectively. Reporter genes can also be added to the cassette so that the degree of gene expression can be monitored in the intact animal.

Gene targeting relies on the naturally occurring process of homologous recombination to impart characteristics on the host animal. The first evidence of homologous recombination was in the early 1980s between two plasmid molecules, and was soon followed by targeting of the first endogenous locus in 1985 (Folger et al., 1982; Smithies et al., 1985). Homologous recombination requires the use of known endogenous sequence markers for targeted transfer of genetic material in ES cells. There are two main types of gene targeting: replacement and insertion. These techniques differ mainly in the design of the DNA vector (both contain homologous sequences, reporter genes, selectable marker genes, and the transgene). In general, two flanking regions of homology (at least 500 bp on the short arm) are used because the length of homology increases the targeting frequency (typically only 1:1,000,000 treated cells undergo targeted recombination). Replacement vectors are structured so that they contain two separate homologous regions separated by non-homologous DNA which is then incorporated into the host DNA replacing the area between the homologues. The vector is cut outside of the region of homology forcing the DNA polymerase to replace the endogenous locus during recombination. The insertion vector is linearized within the region of homology inducing the DNA polymerase to insert the entire cassette between the regions of homology. Either technique can be used to generate gene knockout mice; however, only insertion can be used to generate a gene knock-in animal.

Most targeted transfections require a double selection process during which ES cells that express the gene are selected then screened for proper gene targeting. A common double selection method uses HSVTK (contains *NEO* and *TK* marker genes in the cassette). The *NEO* gene provides resistance to neomycin like drugs while the *TK* gene makes the cell susceptible to ganciclovir. The transgene is created such that homologously transfected cells are $NEO^{+}TK^{-}$ and ES cells transfected by random insertion are $NEO^{+}TK^{+}$. Selection against G418 (a synthetic neomycin derivative) spares all cells expressing the transgene. A second exposure to ganciclovir only spares cells that have undergone homologous recombination because a randomly inserted transgene makes the cell sensitive to ganciclovir. The selected cells are then used to generate a mouse line that has the targeted transgene expressed in the correct genetic location.

The introduction of genetic material by insertion is more complicated than the knockout procedure. The insertion of genetic material is difficult because the reporter gene or selectable marker gene could impede on the expression of the transgene once the transgenic animal has been generated. A method developed to deal with this problem utilizes the Cre-*lox*P system to remove the reporter region after selection (Sunaga et al., 1997). This system is a robust way to snip out small sections of genetic material by flanking that gene(s) with *lox*P binding sites. The enzyme cre recombinase binds and removes the genetic material between two *lox*P binding sites. Cre recombinase exposure can be done while the cells are still *in vitro* or once the animal has been generated. An example insertion paradigm would use a selectable marker that is flanked by *lox*P binding sites. After a positive selection is done using the marker to select for cells expressing the transgene, cre recombinase is used to remove the selectable marker gene preventing interference with the transgene. A similar removal could be done for any reporter genes that are being used to measure transgene expression. This example is by no means the only use of the Cre-*lox*P system. Binding sites for cre recombinase could also be placed around endogenous genetic material. Endogenous material could then be silenced at particular times to study the effect of a particular gene during development or cut out to generate a knockout animal. Performing transgenic manipulations in this way is often referred to as conditional transfections. The use of this system is a more elegant way of transfecting but is not always necessary.

A large amount of literature is available for the study of mouse transgenic techniques. The topics discussed here are only a sampling and are derived mainly from several sources dedicated to the molecular biology of transgenic mouse generation (Scarpelli et al., 1992; Tymms and Kola, 2001; Clarke, 2002; Hofker and Deursen, 2003).

**Thesis Overview**

The following work focuses on the combination of electrochemistry, brain slices, and transgenic mouse models for the evaluation of biogenic amine transmission in the brain. Five distinct transgenic mouse models have been used to better understand the neurotransmission of dopamine and 5-HT. A particular emphasis has been placed on dopaminergic transmission as it applies to movement phenotypes and drugs of addiction (ie. cocaine and methamphetamine). Collaboration with Marc Caron at Duke University has facilitated the study of animals over-expressing the dopamine transporter and how it relates to amphetamine sensitivity and movement initiation. A second transgenic mouse model from the lab of George Augustine at Duke University has been used to study the genetic deletion of the presynaptic protein synapsin and how it relates to the action of cocaine. Two mouse models were used in collaboration with the lab of Brad Lowell at Harvard University. These mice were used to evaluate obesity and ATP utilization and how they apply to movement phenotypes and dopamine release. Finally, dopamine dynamics in *Fmr1* KO mice were studied in collaboration with the University of Illinois at Urbana-Champagne. This dissertation will clearly demonstrate the power of transgenic mouse models for the understanding of neurotransmitter dynamics.

## Literature Cited


Adlard PA, Cherny RA, Finkelstein DI, Gautier E, Robb E, Cortes M, Volitakis I, Liu X, Smith JP, Perez K, Laughton K, Li QX, Charman SA, Nicolazzo JA, Wilkins S, Deleva K, Lynch T, Kok G, Ritchie CW, Tanzi RE, Cappai R, Masters CL, Barnham KJ, Bush AI (2008) Rapid restoration of cognition in Alzheimer's transgenic mice with 8-hydroxy quinoline analogs is associated with decreased interstitial Abeta. Neuron 59:43-55.

Bard AJ, Faulkner LR (2001) Electrochemical methods : fundamentals and applications, 2nd Edition. New York: Wiley.

Barr AM, Lehmann-Masten V, Paulus M, Gainetdinov RR, Caron MG, Geyer MA (2004) The selective serotonin-2A receptor antagonist M100907 reverses behavioral deficits in dopamine transporter knockout mice. Neuropsychopharmacology 29:221-228.

Bath BD, Michael DJ, Trafton BJ, Joseph JD, Runnels PL, Wightman RM (2000) Subsecond adsorption and desorption of dopamine at carbon-fiber microelectrodes. Anal Chem 72:5994-6002.

Bjorkqvist M, Wild EJ, Thiele J, Silvestroni A, Andre R, Lahiri N, Raibon E, Lee RV, Benn CL, Soulet D, Magnusson A, Woodman B, Landles C, Pouladi MA, Hayden MR, Khalili-Shirazi A, Lowdell MW, Brundin P, Bates GP, Leavitt BR, Moller T, Tabrizi SJ (2008) A novel pathogenic pathway of immune activation detectable before clinical onset in Huntington's disease. J Exp Med 205:1869-1877.

Brown AM, Birnbaumer L (1989) Ion channels and G proteins. Hosp Pract (Off Ed) 24:189-193, 198, 202-184.

Cahill PS, Walker QD, Finnegan JM, Mickelson GE, Travis ER, Wightman RM (1996) Microelectrodes for the measurement of catecholamines in biological systems. Anal Chem 68:3180-3186.

Chase TN, Oh JD (2000) Striatal dopamine- and glutamate-mediated dysregulation in experimental parkinsonism. Trends Neurosci 23:S86-91.

Choi CW, Chung YJ, Slape C, Aplan PD (2008) Impaired differentiation and apoptosis of hematopoietic precursors in a mouse model of myelodysplastic syndrome. Haematologica 93:1394-1397.

Clarke AR (2002) Transgenesis techniques : principles and protocols, 2nd Edition. Totowa, NJ: Humana Press.

Cooper JR, Bloom FE, Roth RH (2003) The biochemical basis of neuropharmacology, 8th Edition. Oxford ; New York: Oxford University Press.

Fink KB, Gothert M (2007) 5-HT receptor regulation of neurotransmitter release. Pharmacol Rev 59:360-417.

Folger KR, Wong EA, Wahl G, Capecchi MR (1982) Patterns of integration of DNA microinjected into cultured mammalian cells: evidence for homologous recombination between injected plasmid DNA molecules. Mol Cell Biol 2:1372-1387.

Heien ML, Phillips PE, Stuber GD, Seipel AT, Wightman RM (2003) Overoxidation of carbon-fiber microelectrodes enhances dopamine adsorption and increases sensitivity. Analyst 128:1413-1419.

Heimer L (1995) The human brain and spinal cord : functional neuroanatomy and dissection guide, 2nd Edition. New York: Springer-Verlag.

Hochstetler SE, Puopolo M, Gustincich S, Raviola E, Wightman RM (2000) Real-time amperometric measurements of zeptomole quantities of dopamine released from neurons. Anal Chem 72:489-496.

Hodgkin AL, Huxley AF (1952a) Propagation of electrical signals along giant nerve fibers. Proc R Soc Lond B Biol Sci 140:177-183.

Hodgkin AL, Huxley AF (1952b) Movement of sodium and potassium ions during nervous activity. Cold Spring Harb Symp Quant Biol 17:43-52.

Hofker MH, Deursen Jv (2003) Transgenic mouse methods and protocols. Totowa, N.J.: Humana Press.

Howard EC, Schier CJ, Wetzel JS, Duvauchelle CL, Gonzales RA (2008) The shell of the nucleus accumbens has a higher dopamine response compared with the core after non-contingent intravenous ethanol administration. Neuroscience 154:1042-1053.

Jackson BP, Dietz SM, Wightman RM (1995) Fast-scan cyclic voltammetry of 5-hydroxytryptamine. Anal Chem 67:1115-1120.

Kandel ER (2008) Principles of neural science, 5th Edition. New York: McGraw-Hill.

Kawagoe KT, Zimmerman JB, Wightman RM (1993) Principles of voltammetry and microelectrode surface states. J Neurosci Methods 48:225-240.

Mundroff ML, Wightman RM (2002) Amperometry and cyclic voltammetry with carbon fiber microelectrodes at single cells. Curr Protoc Neurosci Chapter 6:Unit 6 14.

Pattison JS, Robbins J (2008) Protein misfolding and cardiac disease: establishing cause and effect. Autophagy 4:821-823.

Paxinos G, Watson C, Pennisi M, Topple A (1985) Bregma, lambda and the interaural midpoint in stereotaxic surgery with rats of different sex, strain and weight. J Neurosci Methods 13:139-143.

Salahpour A, Ramsey AJ, Medvedev IO, Kile B, Sotnikova TD, Holmstrand E, Ghisi V, Nicholls PJ, Wong L, Murphy K, Sesack SR, Wightman RM, Gainetdinov RR, Caron MG (2008) Increased amphetamine-induced hyperactivity and reward in mice overexpressing the dopamine transporter. Proc Natl Acad Sci U S A 105:4405-4410.

Scarpelli DG, Migaki G, Pletcher JM, Registry of Comparative Pathology. (1992) Transgenic animal models in biomedical research : proceedings of a Symposium held at the National Institutes of Health, Bethesda, Maryland, November 4-5, 1991. Washington, DC: Armed Forces Institute of Pathology.

Seidler B, Schmidt A, Mayr U, Nakhai H, Schmid RM, Schneider G, Saur D (2008) A Cre-loxP-based mouse model for conditional somatic gene expression and knockdown in vivo by using avian retroviral vectors. Proc Natl Acad Sci U S A 105:10137-10142.

Senior SL, Ninkina N, Deacon R, Bannerman D, Buchman VL, Cragg SJ, Wade-Martins R (2008) Increased striatal dopamine release and hyperdopaminergic-like behaviour in mice lacking both alpha-synuclein and gamma-synuclein. Eur J Neurosci 27:947-957.

Smithies O, Gregg RG, Boggs SS, Koralewski MA, Kucherlapati RS (1985) Insertion of DNA sequences into the human chromosomal beta-globin locus by homologous recombination. Nature 317:230-234.

Sunaga S, Maki K, Komagata Y, Ikuta K, Miyazaki JI (1997) Efficient removal of loxP-flanked DNA sequences in a gene-targeted locus by transient expression of Cre recombinase in fertilized eggs. Mol Reprod Dev 46:109-113.

Tymms MJ, Kola I (2001) Gene knockout protocols. Totowa, NJ: Humana Press.

Umriukhin AE, Diukareva EV, Vetrile LA, Trekova NA, Kravtsov AN, Evseev VA, Sudakov KV (2007) Dynamics of dopamine and norepinephrine contents in the dorsal hippocampus of rats during immunization with dopamine conjugate. Bull Exp Biol Med 143:399-402.

Unwin N (1993) Neurotransmitter action: opening of ligand-gated ion channels. Cell 72 Suppl:31-41.

Venton BJ, Troyer KP, Wightman RM (2002) Response times of carbon fiber microelectrodes to dynamic changes in catecholamine concentration. Anal Chem 74:539-546.

Wang M, Roman GT, Schultz K, Jennings C, Kennedy RT (2008) Improved temporal resolution for in vivo microdialysis by using segmented flow. Anal Chem 80:5607-5615.

Wightman RM, Amatore C, Engstrom RC, Hale PD, Kristensen EW, Kuhr WG, May LJ (1988) Real-time characterization of dopamine overflow and uptake in the rat striatum. Neuroscience 25:513-523.

Wu Q, Reith ME, Wightman RM, Kawagoe KT, Garris PA (2001) Determination of release and uptake parameters from electrically evoked dopamine dynamics measured by real-time voltammetry. J Neurosci Methods 112:119-133.

# Chapter 2

Materials and Methods

## Introduction

This chapter explains the primary methods used in the generation of transgenic mouse models and the analysis of mouse brain slices with electrochemistry. The methods described here should were used in subsequent chapters unless otherwise noted.

## Transgenic Mouse Models

Mice used in this study were age and sex matched whenever possible and handled via procedures approved by the Institutional Animal Care and Use Committees (IACUC) of Duke University, Harvard University, the University of Illinois at Urbana Champagne, and the University of North Carolina at Chapel Hill.

The DAT-Tg mouse models used in this study were created in the lab of Dr. Marc Caron at Duke University according to the procedure published in Salahpour *et al.* (2008). A bacterial vector (BAC) containing the mouse DAT locus was obtained from Genome Sciences (Duke University, Durham NC). The topology of the BAC was verified using PCR analysis. A BAC clone was chosen for pronuclear injection containing the DAT locus (40 Kb) flanked by 80 Kb of upstream and downstream genomic homology. The BAC DNA was isolated using a Clonetech BAC preparation kit and re-suspended at 2 ng/μl in injection buffer (0.03mM Spermine, 0.07mM Spermidine). Pro-nuclear injections were carried out by the Duke Transgenic Mouse Facility using C57BL/6J embryos. One transgene positive founder was identified by PCR based genotyping with oligos recognizing BAC vector sequences (Forward: 5'-gcatcagccagcgcagaaatatttcc, Reverse: 5'-gatacttcgttatcgacaccagctgc-3') and bred for characterization of the transgene.

The synapsin triple knockout (TKO) animals were generated at Duke University in the lab of Dr. George Augustine. The following procedure for the generation of synapsin TKO mice and corresponding littermate wild type mice was published in Gitler *et al.* (2004). Synapsin TKO mice were generated by serial breeding of synapsin I knockout (KO) mice (Chin et al., 1995), synapsin II KO mice (Ferreira et al., 1998), and synapsin III KO mice (Feng et al., 2002). Genotyping of bred animals was done by PCR using sense and antisense primers for synapsin I, synapsin I/II, and synapsin III. Western blots were used to confirm the presence or absence of the synapsin proteins. Synapsin TKO mice are on a mixed genetic background.

Leptin deficient (*ob/ob* mice) are available for purchase through Jackson Laboratories (Bar Hardbor, ME.). The *ob/ob* mice used in these studies were on a C57BL/6 background and were discovered by chance in a colony at Jackson Laboratories. Mice lacking UCP2 were also generated on a C57 BL/6 background in the lab of Dr. Brad Lowell at Harvard University using ES cell transfection techniques as previously described (Zhang et al., 2001). Briefly, a targeted replacement of the *Ucp2* gene including a portion of the start codon was performed using a replacement cassette. Properly transfected ES cells were injected into mouse blastocysts generating a germline from which WT, heterozygous UCP2 KOs, and homozygous UCP2 KOs were bred. Successful deletion of UCP2 was confirmed by Southern blot analysis and multiplex PCR.

Mice lacking the Fragile X protein gene *Fmr1* were generated at the University of Illinois by William Greenough. They are commercially available through Jackson Laboratories (Bar Harbor, ME.). A complete discussion of their generation can be found in a paper from the Dutch Consortium (1994). Briefly, a targeted vector was used to disrupt the 5' axon of the *Fmr1* gene in ES cells. Properly targeted ES cells were selected and injected into blastocysts from C57BL/6 mice.

**Electrochemistry**

Cylindrical carbon-fiber microelectrodes (6 µm diameter, Thornel T-650, Amoco, Greenville, SC) were fabricated as previously described (Bath et al., 2000). Carbon fibers were aspirated into glass capillary (1.2 mm X 0.68 mm, 4", AM Systems, Carlsborg, WA.). The electrodes were pulled on a vertical capillary puller (Narishige) and the excess carbon fiber was trimmed to 50 µm. Waveform application, current monitoring, and stimulus application were all controlled by locally written software (Tarheel CV, Labview) through a home built potentiostat (UEI, UNC electronics shop).

For dopamine and NE detection, the carbon-fiber electrode was held at -400 mV vs. a Ag/AgCl reference electrode between voltage scans. Detection in brain slices was achieved by application of a triangular waveform: -400 mV to 1,000 mV to -400 mV at a scan rate of 600 V/s repeated every 16.7 or 100 ms. This waveform provides high temporal resolution while maintaining good sensitivity (Bath et al., 2000). The waveform for *in vivo* use employed the same voltages, but at 300 V/s and repeated every 100 ms; this method provides improved sensitivity but decreased time resolution (Baur et al., 1988). The current at the peak oxidation potential for dopamine (500-700 mV vs. Ag/AgCl) was used to evaluate dopamine concentration changes.

For 5-HT detection the electrode potential between scans was 200 mV vs Ag/AgCl. The cyclic voltammogram was obtained with an initial scan to 1,000 mV, back to -100 mV, and then scanned to 200 mV at 1000 V/s applied every 100 ms. The positive rest potential minimizes electrode fouling from 5-HT reduction products (Jackson et al., 1995). In addition, the rapid scan rate prevents side reactions characteristic of the electrochemical detection of 5-HT from contributing to the current signal (Jackson et al., 1995). The positive potential also decreases the electrode's sensitivity to dopamine by at least 100 fold. For dopamine, NE, and 5-HT, the electrodes were calibrated in a flow injection system with a 1 µM bolus of analyte.

Amperometry experiments were performed using the same equipment as the FSCV measurements or an Axopatch 200B (Axon Instruments). For biogenic amine measurements by amperometry, the electrode was held at a potential sufficient for oxidation (700 mV vs. Ag/AgCl). Ascorbic acid (500 µM) was added to the slice and calibration buffers to enhance the amperometric signal and allow for calibration of the electrode (Venton et al., 2002). Amperometric electrodes were calibrated in a flow injection system against 1 µM dopamine in buffer containing 500 µM ascorbate.

**Slice Experiments**

Mice were anesthetized with ether and decapitated. The brain was rapidly removed and placed on ice. Coronal brain slices (300 µm thick) containing the caudate putamen, substantia nigra pars reticulata (SNr), or the ventral bed nucleus of the stria terminalis (*v*BNST), were prepared in ice cold artificial cerebral spinal fluid (aCSF) using a Lancer Vibratome (World Precision Instruments, Sarasota, Fl.). The aCSF contained (in mM): 20 HEPES, 2.4 $CaCl_2$, 1.2 $MgCl_2$, 1.2 $NaH_2PO_4$, 2.45 KCl, 126 NaCl, 11 glucose, and 25 $NaHCO_3$. The pH was adjusted to pH 7.4 and the aCSF was saturated with 95% $O_2$ / 5%

$CO_2$. Slices were superfused in aCSF at 37 $^oC$ for 35-40 minutes prior to recording. Recordings were performed on a microscope (Nikon FN1, Gibraltar Stage) fitted with a slice perfusion chamber (Warner Instruments, Hamden CT).

Neurotransmitter release was evoked by local electrical stimulation delivered through a tungsten bipolar stimulating electrode placed on the surface of the slice (Frederick Haer Co., Bowdoinham, ME). The stimulation consisted of a computer generated, biphasic (2 ms per phase), constant-current (350 µA) pulse. A single stimulation pulse was used to evoke striatal dopamine release in the caudate putamen (Jones et al., 1995), a 20 pulse 100 Hz stimulation train was used to evoke 5-HT release in the SNr (Bunin et al., 1998), and a 60 pulse 60 Hz stimulation was used to evoke NE release in the vBNST (Miles et al., 2002). The current pulse was optically isolated from the preparation (NL 800, Neurolog, Medical Systems, Great Neck, NY). Stimulations were performed at regular 3-5 intervals to maintain consistent release. Neurotransmitter release was detected at a carbon-fiber microelectrode placed 75-100 µm into the slice at a distance of 100-200 µm from the stimulating electrode. Electrode placements were made with the aid of the microscope.

To determine the amount of dopamine release in transgenic animals, the maximal release at 4 locations in a single slice was recorded over a 20 minute period, and the values were averaged together. The responses from animals of each genotype were pooled. The amount of 5-HT released was determined in a similar fashion to dopamine with the exception that three locations were used. A single release site was used for NE measurements in the vBNST. The number of sites used for each neurotransmitter was determined based on brain region size and release heterogeneity within that brain region. Single site recordings were used anytime an experiment required the manipulation of the slice environment to minimize the contribution of spatial heterogeneity to the measured signal. Slices were given a 35 minute recovery period every time the environment was changed by manipulation of external ion concentrations or by the application of a drug. An additional 35 minutes was given if the concentration of external ion or drug was changed. Some drugs (l-dopa and tetrabenazine) required an incubation time of 1 hour prior to recording. With the exception of l-dopa (1 hour incubation followed by a 35 minute rinse with aCSF), all drugs remained in the perfusion buffer for the entirety of the measurement.

Slice experiments utilized two types of background subtraction to remove the large currents associated with double layer charging that occurs when scanning voltages quickly. Stimulated dopamine release experiments used traditional digital background subtraction techniques (Michael et al., 1999). In cases where basal dopamine concentrations were calculated using principal component regression (reverse transport in Chapter 7), analog background subtraction was used. Analog background subtraction was performed as previously described (Hermans et al., 2008). Unless specified, all data was collected using the traditional digital background subtraction methodology.

**Electrochemical Data Analysis**

Dopamine release profiles from striatal brain slices were used to quantify the maximal dopamine release for different animal genotypes. The maximal dopamine released ($[DA]_{max}$) was determined using an electrode calibration factor and the current recorded at the oxidation potential of dopamine (650 mV vs. Ag/AgCl). These $[DA]_{max}$ values are reported as being the value of dopamine release for a particular area or type of animal. The same technique was used for the neurotransmitters 5-HT and NE whose maximum attained concentrations were determined from calibrated current traces. Changes in basal dopamine levels were determined differently than stimulated release by using principal component regression as described previously (Heien et al., 2004). Briefly, mathematic algorithms were used to divide the current signal into contributing components. In brain slices, these components were generally limited to dopamine concentration changes, background drift, and electrode capacitance changes. Removal of components that are not dopamine related facilitates a more accurate description of dopamine dynamics over long times. This technique was not used for stimulated release experiments because the time course of dopamine concentration changes (< 1 sec) was too short for appreciable signal contributions from factors other than dopamine.

Current responses for a particular animal genotype or brain location were pooled prior to further data analysis. All data shown are written as mean ± standard error in the mean (SEM). The n values are the number of animals used for a specific experiment. In addition to this replicate number, multiple locations and stimulations were used to reduce random error in the electrochemical measurements. Tests of significance included Student's t-test and one way ANOVA where applicable.

**Simplex Modeling**

Simplex modeling was used to extract kinetic constants associated with the uptake of dopamine and 5-HT from the extracellular space. Concentration traces were modeled using a Michaelis-Menten based non-linear regression model (Wightman et al., 1988). For a dopamine trace, modeling extracts dopamine per pulse ($DA_p$), maximal uptake rate ($V_{max}$), and transporter affinity for dopamine or 5-HT ($K_m$) values from the trace. Simplex modeling requires deconvolution of the FSCV signal from the adsorption/desorption time delay by using an electrode time constant (15-50 ms for a 60 Hz sampling rate). Deconvolution of the signal for the adsorptive time delay facilitated more accurate modeling of the uptake kinetics (Venton et al., 2002). When determining $V_{max}$ values, the $K_m$ value was fixed at 200 nM (Near et al., 1988) for dopamine and 170 nM for 5-HT (John et al., 2006). When competitive uptake inhibitors were used such as cocaine, a $V_{max}$ value is determined from simplex using predrug files for the measurement site. Once $V_{max}$ for a particular location was determined, it was fixed and changes in $K_m$ ($K_{m(app)}$) were accurately measured. Simplex modeling facilitated the robust and accurate determintation of Michaelis-Menten uptake kinetics from FSCV measurements (Wu et al., 2001).

### $K_m$ Determination

The binding affinity of dopamine for the DAT was determined using two methods: cocaine inhibition and amperometric modeling. Single site measurements were performed using a 60 Hz collection frequency and a single pulse stimulation in coronal brain slices of the mouse caudate putamen. A stable baseline of 50 minutes was prerequisite to any drug application and used to determine an initial $V_{max}$ value for the study location. Cocaine was applied through the superfusion buffer for 35 minutes prior to drug files being recorded. A linearized curve was generated using ascending concentrations of cocaine (1, 2, 5, 10, 20, and 30 μM). The curve represented the $K_{m(app)}$ as a function of cocaine concentration. The y-intercept of the line is the $K_{m(app)}$ without any inhibitor on board which is equivalent to the original $K_m$. These $K_m$ values could be compared for the genotypes in question.

Amperometry was used to directly evaluate the kinetics of dopamine uptake. In this experiment, $V_{max}$ and $K_m$ were measured at three locations in the caudate. An initial large stimulation was used to evoke 2 μM dopamine; the slope of line taken between $[DA]_{max}$ and ½ $[DA]_{max}$ was estimated to be the $V_{max}$ value for that location. Once $V_{max}$ had been determined, a smaller stimulation current was used to evoke dopamine release at a concentration of 400 nM. The resultant curve was modeled with an exponential decay function which effectively mimics dopamine uptake at low concentrations of dopamine. Using this function, and the $V_{max}$ value obtained for the recording site, a $K_m$ value was calculated.

### High Performance Liquid Chromatography

Tissue samples were dissected from a slice (300-500 µm in thickness) containing the region of interest. The tissue was weighed and homogenized with a wand sonicator (Fisher Scientific) in 200-500 µL 0.1 N perchloric acid spiked with 1 µM hydroquinone (HQ) or 1 µM acetamidophenol (AP). Following centrifugation at 6,000 rpm for 10 min, the supernatant was removed and filtered with a 0.2 µm syringe filter unit (Millex-LG). Iontophoretic studies were done by ejecting analytes into a known volume of 0.1 N perchloric acid (Herr et al., 2008). Injections (10 or 50 µL) were made onto a reverse phase column (C-18, 5 µm, 4.6 x 250 mm, Waters symmetry 300 or Waters Atlantis T3). The mobile phase (prepared in HPLC grade water) contained 0.1 M citric acid, 0.1 mM EDTA, and 1 mM hexyl sodium sulfate, pH 3.5. Methanol was added as the organic modifier at a concentration of 5-10 % to shorten analyte elution times. Catecholamines were detected with a thin-layer radial electrochemical flowcell (BASi, West Lafayette, IN, USA), with the working electrode at 700 mV vs. a Ag/AgCl reference electrode (BASi, West Lafayette, IN, USA). Catecholamine standards were prepared from 10 mM stock solutions in 0.1 N perchloric acid. The HQ or AP (1 µM) was used as an internal standard for analyte quantification and recovery. All analyte response ratios were taken with respect to the internal standard to account for differential electrode responses.

### Chromatographic Data Analysis

The determination of peak areas for HPLC total content measurements was performed using custom written Igor programs. These programs were designed in the Jorgenson lab at UNC-CH. Peak area determination was performed using statistical moments regression theory (Hsieh and Jorgenson, 1996). The peak area of the analyte was taken as a ratio to that of an internal standard at a known concentration, adjusted for differential detector response. The ratio was then used to calculate a mass of analyte in the extraction solution which was normalized by the mass of tissue taken. Again, n dictates the number of animals used; however, replicate extractions and injections were performed to reduce random error in the chromatographic measurements.

**Drugs and Reagents**

All drugs were used as received and dissolved in either doubly deionized water or a mixture of doubly deionized water and ethanol. Cocaine, amphetamine, methamphetamine, CNQX, picrotoxin, and buproprion were purchased from Sigma Aldrich. The dopamine uptake blocker PTT was a gift from Dr. F. Ivy Carroll through Dr. Marc Caron. Reagents for buffers and mobile phases were also purchased from Sigma Aldrich and prepared in doubly deionized water or HPLC grade water respectively.

## Literature Cited


(1994) Fmr1 knockout mice: a model to study fragile X mental retardation. The Dutch-Belgian Fragile X Consortium. Cell 78:23-33.

Bath BD, Michael DJ, Trafton BJ, Joseph JD, Runnels PL, Wightman RM (2000) Subsecond adsorption and desorption of dopamine at carbon-fiber microelectrodes. Anal Chem 72:5994-6002.

Baur JE, Kristensen EW, May LJ, Wiedemann DJ, Wightman RM (1988) Fast-scan voltammetry of biogenic amines. Anal Chem 60:1268-1272.

Bunin MA, Prioleau C, Mailman RB, Wightman RM (1998) Release and uptake rates of 5-hydroxytryptamine in the dorsal raphe and substantia nigra reticulata of the rat brain. J Neurochem 70:1077-1087.

Chin LS, Li L, Ferreira A, Kosik KS, Greengard P (1995) Impairment of axonal development and of synaptogenesis in hippocampal neurons of synapsin I-deficient mice. Proc Natl Acad Sci U S A 92:9230-9234.

Feng J, Chi P, Blanpied TA, Xu Y, Magarinos AM, Ferreira A, Takahashi RH, Kao HT, McEwen BS, Ryan TA, Augustine GJ, Greengard P (2002) Regulation of neurotransmitter release by synapsin III. J Neurosci 22:4372-4380.

Ferreira A, Chin LS, Li L, Lanier LM, Kosik KS, Greengard P (1998) Distinct roles of synapsin I and synapsin II during neuronal development. Mol Med 4:22-28.

Heien ML, Johnson MA, Wightman RM (2004) Resolving neurotransmitters detected by fast-scan cyclic voltammetry. Anal Chem 76:5697-5704.

Hermans A, Keithley RB, Kita JM, Sombers LA, Wightman RM (2008) Dopamine detection with fast-scan cyclic voltammetry used with analog background subtraction. Anal Chem 80:4040-4048.

Herr NR, Kile BM, Carelli RM, Wightman RM (2008) Electroosmotic flow and its contribution to iontophoretic delivery. Anal Chem 80:8635-8641.

Hsieh S, Jorgenson JW (1996) Preparation and evaluation of slurry-packed liquid chromatography microcolumns with inner diameters from 12 to 33 microns. Anal Chem 68:1212-1217.

Jackson BP, Dietz SM, Wightman RM (1995) Fast-scan cyclic voltammetry of 5-hydroxytryptamine. Anal Chem 67:1115-1120.

John CE, Budygin EA, Mateo Y, Jones SR (2006) Neurochemical characterization of the release and uptake of dopamine in ventral tegmental area and serotonin in substantia nigra of the mouse. J Neurochem 96:267-282.

Jones SR, Garris PA, Wightman RM (1995) Different effects of cocaine and nomifensine on dopamine uptake in the caudate-putamen and nucleus accumbens. J Pharmacol Exp Ther 274:396-403.

Michael DJ, Joseph JD, Kilpatrick MR, Travis ER, Wightman RM (1999) Improving data acquisition for fast-scan cyclic voltammetry. Anal Chem 71:3941-3947.

Miles PR, Mundorf ML, Wightman RM (2002) Release and uptake of catecholamines in the bed nucleus of the stria terminalis measured in the mouse brain slice. Synapse 44:188-197.

Near JA, Bigelow JC, Wightman RM (1988) Comparison of uptake of dopamine in rat striatal chopped tissue and synaptosomes. J Pharmacol Exp Ther 245:921-927.

Venton BJ, Troyer KP, Wightman RM (2002) Response times of carbon fiber microelectrodes to dynamic changes in catecholamine concentration. Anal Chem 74:539-546.

Wightman RM, Amatore C, Engstrom RC, Hale PD, Kristensen EW, Kuhr WG, May LJ (1988) Real-time characterization of dopamine overflow and uptake in the rat striatum. Neuroscience 25:513-523.

Wu Q, Reith ME, Wightman RM, Kawagoe KT, Garris PA (2001) Determination of release and uptake parameters from electrically evoked dopamine dynamics measured by real-time voltammetry. J Neurosci Methods 112:119-133.

Zhang CY, Baffy G, Perret P, Krauss S, Peroni O, Grujic D, Hagen T, Vidal-Puig AJ, Boss O, Kim YB, Zheng XX, Wheeler MB, Shulman GI, Chan CB, Lowell BB (2001) Uncoupling protein-2 negatively regulates insulin secretion and is a major link between obesity, beta cell dysfunction, and type 2 diabetes. Cell 105:745-755.

## Chapter 3

Synapsins and Dopamine Release

### Introduction

Synapsins are phosphoproteins that bind to the cytosolic surface of synaptic vesicles and represent almost 10% of the total protein content of synaptic vesicles. There are three synapsins genes (synapsin I, II, and III), with alternative splicing creating 10 known synapsin isoforms. They are differentially expressed in nerve terminals, with synapsins I and II predominant in most areas of the adult brain, although synapsin III is present in some regions including the dorsolateral striatum (Pieribone et al., 2002). Synapsins are thought to play a role in segregating vesicles into a reserve pool that is located away from the active zone, where exocytosis occurs (Greengard et al., 1993). Early evidence supporting this proposal include observations that perturbing synapsins by microinjection disrupts a distal, reserve pool of vesicles, while sparing vesicles in the active zone (Pieribone et al., 1995). It is thought that mobilization of vesicles from the reserve pool is triggered by the elevation of presynaptic calcium resulting in phosphorylation of synapsins (Llinas et al., 1991; Greengard et al., 1993; Chi et al., 2003). More recent evidence has shown that synapsins are also important regulators of exocytosis, vesicle recycling, and vesicle integrity at the active zone; furthermore, these actions differ depending on the type of neurotransmitter terminal (Fdez and Hilfiker, 2006; Evergren et al., 2007).

Synapsin knockout mice have provided insight into the role of synapsins in regulating neurotransmitter release. While deletion of individual synapsin genes (Ferreira et al., 2000; Feng et al., 2002) or genes for both synapsins I and II (Rosahl et al., 1995; Lonart and Simsek-Duran, 2006), affect the reserve pool of synaptic vesicles, interpretation of results from such genotypes are hindered by possible compensation caused by remaining synapsin forms and differential expression of synapsins in different brain regions. These problems are solved in triple knockout mice (TKO) which lack all three known synapsin genes. TKO mice exhibit reduced reserve pools in both glutamatergic and GABAergic nerve terminals, evident both as changes in vesicle distribution, changes in neurotransmitter release during trains of action potentials, and defective release of GABA in response to single action potentials (Gitler et al., 2004).

This chapter extends the discussion of synapsin by examining the release of two other neurotransmitters, dopamine and serotonin (5-HT) in synapsin TKO mice. Prior work showed that the vesicular transporter for both dopamine and 5-HT, VMAT2 (Erickson et al., 1996), is found in terminals devoid of synapsin I and II (Bogen et al., 2006). In contrast, synapsin III expression in the adult brain has been confirmed in the striatum (Pieribone et al., 2002) but not the SNr. To determine whether dopamine release is altered in mice lacking all synapsins we compared striatal dopamine release from synapsin TKO mice and wild-type (WT) mice both in brain slices and *in vivo*. Surprisingly, in both cases, dopamine release was enhanced in the absence of synapsins. In contrast, 5-HT release was identical in the two types of mice. The dependence of dopamine release on extracellular calcium was found to differ in TKO and WT mice, with TKO mice being more sensitive. The ability of cocaine to increase release of dopamine was reduced in synapsin TKO mice, supporting the assertion that synapsins, specifically synapsin III, contribute to the presynaptic actions of cocaine (Venton et al., 2006). In contrast, while cocaine inhibited 5-HT uptake, it did not affect release of 5-HT in either genotype. These findings demonstrate that neurotransmitter release from terminals differs as a function of the specific regulatory role played by the synapsins they contain.

**Materials and Methods**

The experimental procedures used in this chapter have been explained in detail in Chapter 2. The *in vivo* recordings show in Figure 3.3 were performed by Jill Venton while she was a graduate student in our lab and have been included here to improve clarity and completeness.

## Results

*Serotonin Release in Substantia Nigra Brain Slices*

The influence of synapsins on electrically evoked release of 5-HT (Bunin et al., 1998) was evaluated by comparing 5-HT release in TKO and WT mice. Local electrical stimulations were used to evoke 5-HT release in slices containing the SNr. A stimulus train consisting of 20 pulses at 100 Hz was used to evoke 5-HT release and cyclic voltammetry (Figure 3.1A inset) was used to positively identify the released substance as 5-HT (Bunin et al., 1998). 5-HT release evoked under such conditions was stable over several hours if the stimulus trains were separated by intervals of 5 min or longer (Bunin et al., 1998). To minimize the contribution of spatial heterogeneity of 5-HT release sites, measurements were made at 3 different positions of the carbon-fiber electrode within each SNr slice and then averaged together.

In slices from both genotypes, 5-HT release began promptly at the onset of the stimulus and ended as soon as the stimulus stopped, with the concentration of 5-HT returning to prestimulus values over the next 1-2 seconds (Figure 3.1A).

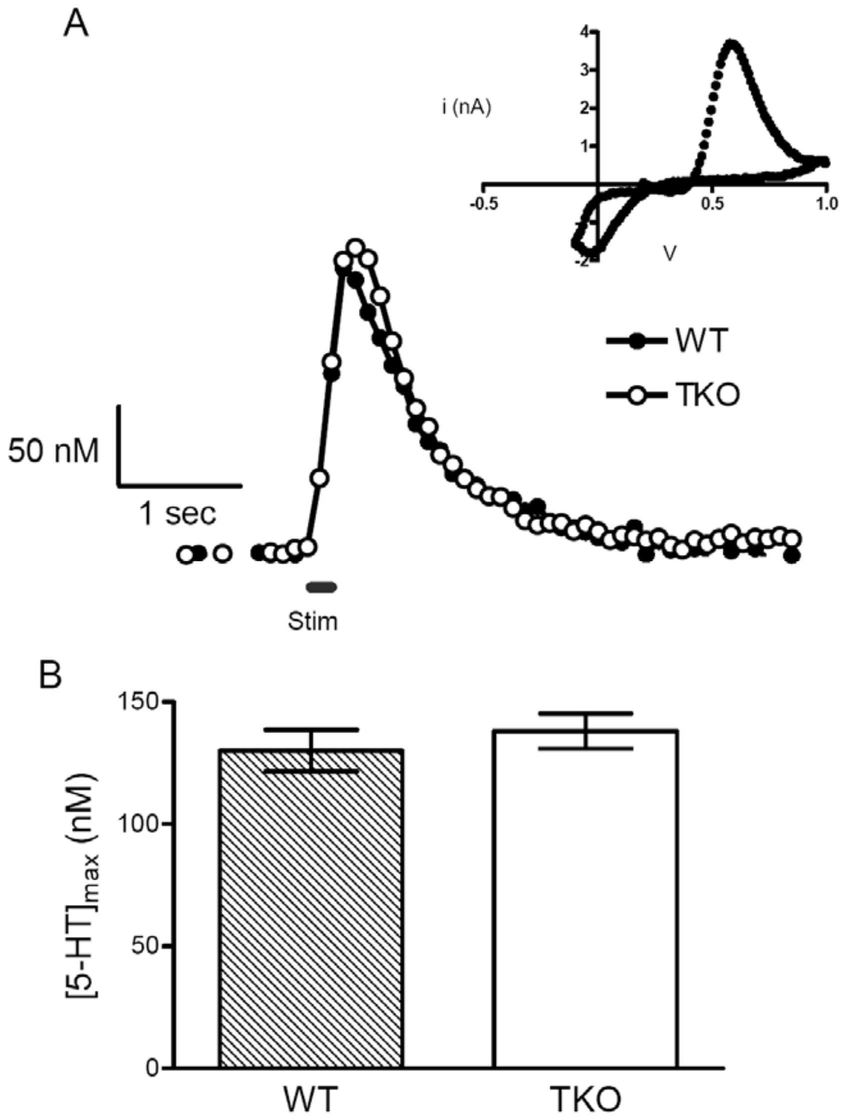


**Figure 3.1** 5-HT release in coronal brain slices containing the SNr of WT and TKO mice evoked by a 20 pulse 100 Hz train (black line). A) Example responses of stimulated 5-HT release; the stimulation was delivered at the time indicated by the horizontal bar. Inset: the cyclic voltammogram used for identification of 5-HT. B) The average release from each genotype (n = 11 animals for each genotype) is not significantly different ($p > 0.05$).

Pooled measurements of the peak concentration of released 5-HT ($[5\text{-HT}]_{max}$) from 10 animals of each genotype showed that mean $[5\text{-HT}]_{max}$ was 130 ± 8 nM in wild-type mice and 140 ± 7 nM in TKO mice (Figure 3.1B). These two values are not significantly different from each other ($p > 0.05$). The maximal rate of 5-HT uptake ($V_{max}$) was compared for WT and TKO animals using nonlinear regression to model the decay component of the traces (Chapter 2). The $V_{max}$ of 5-HT uptake for WT and TKO animals was 450 ± 70 nM/s and 370 ± 80 nM/s respectively; these values were not significantly different from each other ($p > 0.05$). These $V_{max}$ values are similar to those reported previously for measurements made in the SNr (John et al., 2006).

Total 5-HT content in the SNr was also measured by high performance liquid chromatography (HPLC). Tissue punches taken from TKO mice and WT mice (4 animals of each genotype) indicated that the tissue levels of 5-HT were not different between the two genotypes (Chapter 6, Table 6.1). Cortical tissue samples were used as negative controls and 5-HT was undetectable in tissue from either genotype (data not shown).

*Synapsins Affect Dopamine Release in Striatal Brain Slices*

Local electrical stimulation of coronal brain slices was used to evoke dopamine release from terminals in the caudate putamen of synapsin TKO and WT animals. Again, cyclic voltammetry was used to positively identify the signal as dopamine (Figure 3.2A inset). The peak at 600 mV vs Ag/AgCl for the oxidation of dopamine had a potential similar to that of 5-HT. However, the cyclic voltammograms for the two substances differ on the reverse scan, with the peak for reduction of the dopamine-o-quinone occurring at ~ -300 mV with the waveform employed whereas the reduction peak following 5-HT oxidation occurs at a more positive potential (Jackson et al., 1995).

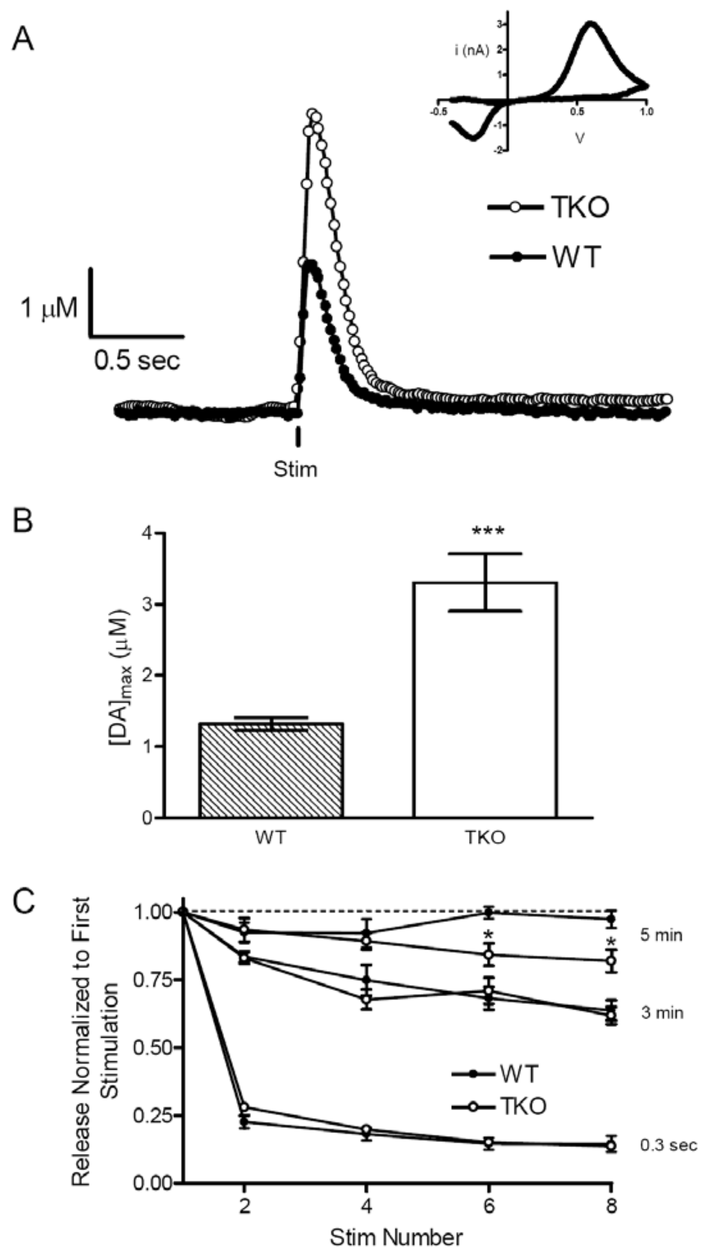


**Figure 3.2** Dopamine release evoked by a single stimulation pulse (vertical black line) in a striatal brain slice from WT or synapsin TKO animals. A) Example responses of stimulated dopamine release. Inset: the cyclic voltammogram used for identification of the neurotransmitter as dopamine. B) Mean $[DA]_{max}$ from multiple locations of each genotype show approximately a two-fold difference in striatal dopamine release ($p < 0.001$, n = 8 TKO, n = 6 WT). C) The rate of releasable vesicle recovery measured in both genotypes at pulse separations of 5 min., 3 min., and 0.3 sec as a ratio of the first stimulation. A 5 minute stimulus separation is sufficient for release recovery in WT animals (n = 5) while a significant reduction ( $p < 0.05$, n = 5) in neurotransmitter release is seen in TKO animals at stimulus numbers six and eight.

Evoked dopamine release was evaluated every 5 min at four different sites per animal, and the values of maximal dopamine release ($[DA]_{max}$) determined at each site were pooled for each genotype. In slices from both genotypes, dopamine release was observed at the onset of stimulation and then declined back to prestimulus values within 1 s after stimulation ceased (Figure 3.2A). $[DA]_{max}$ was significantly greater ($p < 0.01$) in brain slices from TKO mice than in slices prepared from WT mice, being 1.31 ± 0.09 µM (n = 6) for WT and 3.31 ± 0.40 µM (n = 8) for TKO (Figure 3.2B). Dopamine uptake was evaluated with the same procedure described above for 5-HT uptake. The analysis revealed that the $V_{max}$ values for dopamine uptake were not significantly different ($p > 0.05$) between the two genotypes, being 6.00 ± 0.40 µM/s for WT and 6.20 ± 0.50 µM/s for TKO. These values are slightly higher than those reported previously in WT mice (Johnson et al., 2006). To determine how AMPA and $GABA_A$ receptors affect dopamine release, we repeated these measurements in the presence of CNQX, to block AMPA receptors, and picrotoxin, to block $GABA_A$ receptors. CNQX increased dopamine release while picrotoxin depressed it; however, the difference in $[DA]_{max}$ between genotypes remained unchanged (data not shown). Thus, the difference between TKO and WT mice does not arise from differential regulation of dopamine release by AMPA or $GABA_A$ receptors.

The ability of presynaptic terminals to replenish their releasable stores of dopamine after stimulation in WT and TKO animals was evaluated by varying the time interval between stimuli. When single pulse stimulations were repeated at 3 Hz (0.33 s between pulses), the second pulse in the train was 25 % of the first, and release never recovered in subsequent stimulations (Figure 3.2C). When single pulse stimulations were repeated at 3 minute intervals (Figure 3.2C), the response to the second stimulus was only ~70% of that on the first stimulus and dopamine release remained at this reduced level with subsequent stimuli. Responses in the caudate-putamen from TKO and WT mice were indistinguishable with

0.33 s or 3 min between stimulation pulses. In contrast, release in WT animals was statistically identical with each stimulus pulse when they were 5 minutes apart. Release in TKO mice was significantly ($p < 0.05$, $n = 5$) reduced in stimulations with pulses 5 min apart. These experiments reveal that the single pulse stimulations used in this work in slices from both WT and TKO animals require at least 5 minutes before similar release can be evoked. This is consistent with the half life (2.4 min) for the conversion of nonreleasable dopamine, the location of the majority of dopamine stores, to releasable dopamine observed in the striatum of rats (Justice et al., 1988). The other mechanism for refilling of the releasable pool, repackaging of newly synthesized dopamine, has a slightly shorter half life (0.7 minutes) and is presumed to be the same for both genotypes.

To determine whether the increased release of dopamine observed in TKO mice was due to the striatum containing greater amounts of dopamine, HPLC was used to analyze the dopamine content of striatal tissue. No significant difference in the amount of total striatal dopamine was found between the two genotypes (Chapter 6, Table 6.1), indicating that the increased amount of dopamine release found in TKO mice is not due to higher brain dopamine stores. However, knowledge of the tissue content allows estimation of the maximal extracellular concentration that could be achieved if all available dopamine was released by a single pulse stimulation. The molecular weight of dopamine is 153 g/mole and the extracellular volume of the tissue is 20 % (Nicholson and Rice, 1990). Then, the molarity of maximal dopamine release is:

$$(4.97\ \mu\text{g/g tissue}) \times (1/153\ \text{g/mole}) \times (1\ \text{g tissue}/0.2\ \text{mL}) = 162\ \mu\text{M}$$

This calculated value is almost two orders of magnitude greater than found experimentally with single pulse stimulations that cause clear depletion of the releasable store. Thus, consistent with prior studies of release, release in the slice preparation comes from only a fractional amount of the total store (Dobrunz and Stevens, 1997). Furthermore, this store is slowly refilled in tissue from both types of animals. For this reason, vesicles released are termed as part of the readily releasable pool and the remainder the reserve pool from which vesicle replenishment occurs in both animals.

*Synapsins Also Affect Striatal Dopamine Release in vivo*

Synapsins influence the amount of dopamine released *in vivo* as measured in the brains of anesthetized TKO and WT mice. In these experiments, electrical stimulation of the medial forebrain bundle (MFB), rather than local electrical stimulation, was used to evoke dopamine release in the caudate putamen. Again, 5 minute intervals between stimuli were required to observe consistent dopamine release in response to each stimulus. Figure 3.3A shows averaged measurements of dopamine release measured in TKO and WT mice in response to 20 Hz stimuli (0.5 s duration; n = 8 for each genotype). Note that with MFB stimulations, continuous trains release approximately constant amounts of dopamine as is found *in vivo* in rats (Wightman et al., 1988). The amount of dopamine released per stimulus pulse ($[DA]_p$) during these trains was found to be significantly different ($p < 0.05$) in the two genotypes, being 90 ± 14 nM for WT and 150 ± 18 nM for TKO mice.

The loss of synapsins does not affect the frequency dependence of dopamine release. Transmission at dopaminergic synapses is a balance between release and uptake. At low stimulus frequencies, the concentration of dopamine reaches a steady plateau because uptake and release are balanced, while during high-frequency stimulations the dopamine concentration continually increases because the DAT becomes saturated (Wightman et al., 1988). This leads to the different shapes of the release profiles seen in Figure 3.3A where release in WT animals approaches steady state to a greater degree than release in TKO animals.

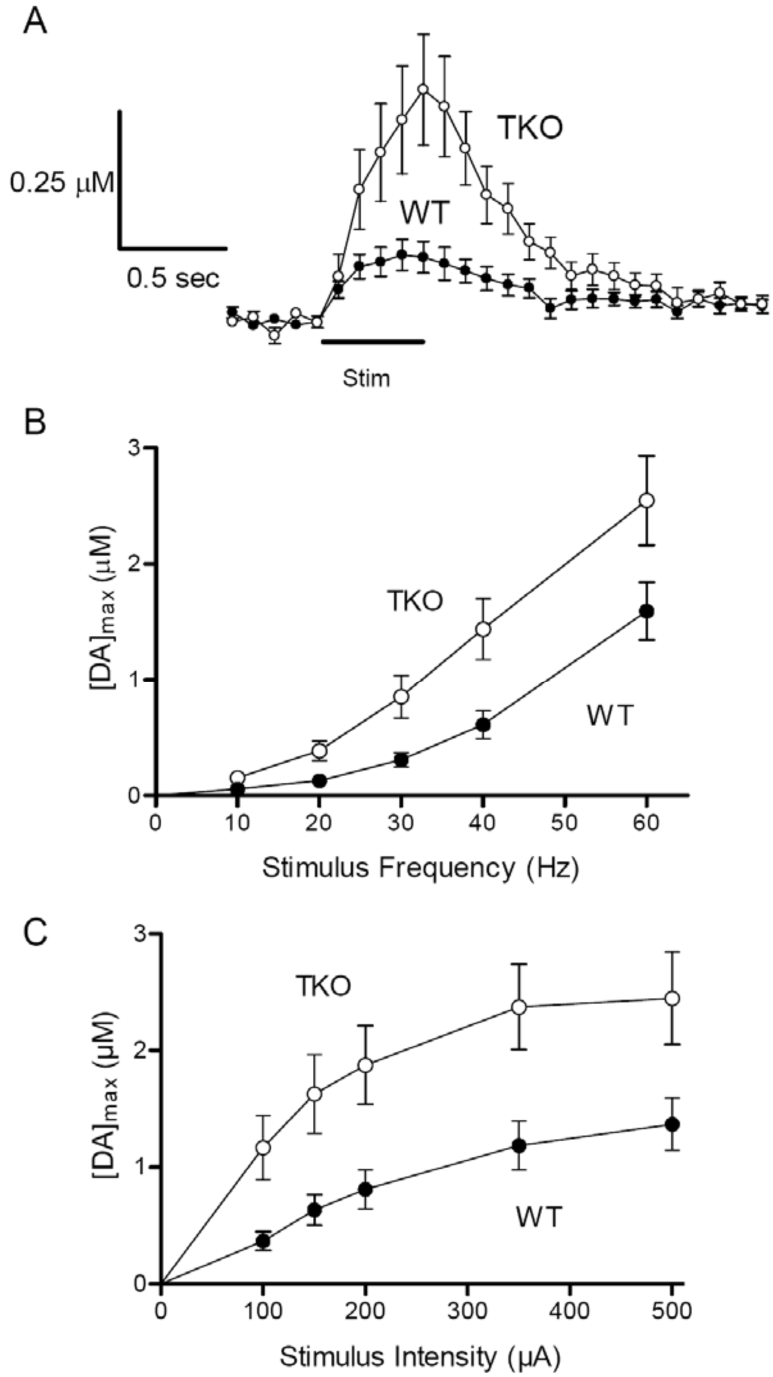


**Figure 3.3** Electrically stimulated dopamine release in the striatum measured *in vivo*. A) Average release profiles measured in WT and TKO mice (n = 8 for each panel) in response to 0.5 s stimulation train at 20 Hz. B) $[DA]_{max}$ values exhibit similar frequency dependencies but release is uniformly greater in TKO animals. C) A similar dependence on stimulus intensity is found in both genotypes although dopamine release is greater in TKO animals.

At higher frequencies, greater release was still observed in TKO animals (Figure 3.3B), but the differences in shape were much less (data not shown). We also examined the relationship between dopamine concentration and stimulus intensity; in rats, this relationship saturates as the stimulation intensity is increased (Wiedemann et al., 1990), due to a restricted amount of dopamine available for immediate release. Although dopamine release from TKO animals reached a plateau at the same stimulus intensity (350 μA) as in WT animals, the amount of dopamine released was higher at all stimulus intensities (Figure 3.3C). This result indicates that TKO mice have a larger immediately releasable pool of dopamine.

*Calcium Dependence of Dopamine Release*

Given the essential role of calcium ions ($Ca^{2+}$) in triggering neurotransmitter release (Augustine and Charlton, 1986; Augustine et al., 1987; Neher, 1998), the effect of synapsin loss on the calcium dependence of dopamine release was evaluated. For this purpose, caudate-putamen slices were equilibrated in conventional aCSF containing 2.4 mM $Ca^{2+}$ and dopamine release produced by electrical stimulation was measured at a single location that was maintained throughout the experiment while the $Ca^{2+}$ concentration was varied. Treatment with aCSF lacking $Ca^{2+}$ was then used to remove $Ca^{2+}$ from the slice and extracellular $Ca^{2+}$ concentration was subsequently increased incrementally from 0.5 mM to 5 mM. At each $Ca^{2+}$ concentration, slices were allowed to equilibrate for 35 min. and then stimulated to evoke dopamine release. To compare the absolute amount of dopamine released between genotypes, the release determined at each $Ca^{2+}$ concentration was scaled by the dopamine release at 2.4 mM $Ca^{2+}$ in WT animals and termed ‘relative dopamine release’.

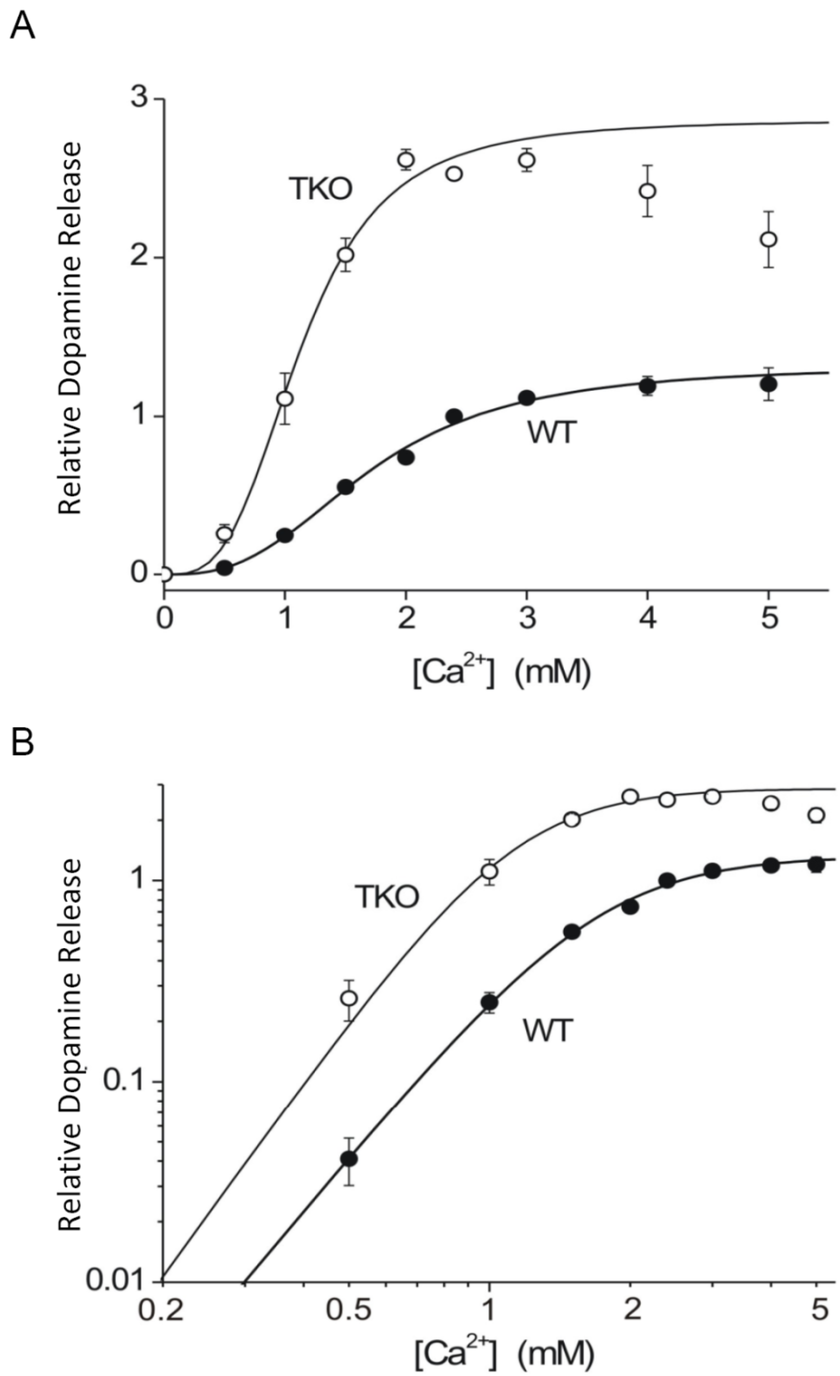


**Figure 3.4** Calcium dependence of dopamine release in striatal slices. A) Relative $[DA]_{max}$ for TKO and WT animals at 0-5 mM extracellular $Ca^{2+}$. TKO animals release more dopamine at all $[Ca^{2+}]$ but experience decreased release at high calcium while WT animals are able to maintain maximal release. B) Log plot used to determine stoichiometric relationship between dopamine release and $Ca^{2+}$ using a fit to the Hill equation.

The $Ca^{2+}$ dependence of dopamine release differed between TKO and WT animals. At all $Ca^{2+}$ concentrations examined, dopamine release was larger in slices from TKO mice than in slices from WT mice. Furthermore, dopamine release in TKO slices saturated at a lower $Ca^{2+}$ concentration than in WT slices, with saturation occurring at approximately 2 mM $Ca^{2+}$ in TKO slices and 4 mM $Ca^{2+}$ in WT slices (Figure 3.4A). The lower saturation level for TKO animals indicates a higher affinity for $Ca^{2+}$ than in WT animals. At the highest $Ca^{2+}$ levels examined, dopamine release in TKO slices decreased somewhat (Figure 3.4A) but such behavior was not observed in slices from WT mice. This may arise from the slow rate of refilling seen for the dopamine readily releasable pool in TKO mice (Figure 3.2C).

To quantify the relationship between the external $Ca^{2+}$ concentration and dopamine release, the data shown in Figure 3.4A were re-plotted on logarithmic coordinates (Dodge and Rahamimoff, 1967; Augustine and Charlton, 1986). In this case, the sigmoidal relationship between $Ca^{2+}$ concentration and dopamine release is linearized, with the slope of the line representing the amount of "cooperativity" in $Ca^{2+}$ triggering of dopamine release and the $Ca^{2+}$ concentration required for half-maximal dopamine release reflecting the apparent $Ca^{2+}$ affinity, $K_{ca}{}^{2+}$ (Dodge and Rahamimoff, 1967). To determine these two parameters, the data was fit using the Hill equation. Although the shape of the logarithmic plots is very similar for dopamine release from both genotypes, we found that the TKO data were shifted toward lower $Ca^{2+}$ concentrations (Figure 3.4B). This leftward shift was due to a difference in the apparent $Ca^{2+}$ affinity, $K_{ca}{}^{2+}$, between the two genotypes, being 1.71 ± 0.01 mM for WT and 1.13 ± 0.11 mM for TKO animals. The Hill coefficient was similar for both genotypes, being 2.80 ± 0.01 for WT animals and 3.22 ± 0.81 for TKO animals. These values of Hill coefficient are similar to that previously reported for depolarization-evoked dopamine release from synaptosomes (Nachshen and Sanchez-Armass, 1987). Thus, the absence of synapsins raises the apparent $Ca^{2+}$ affinity of the dopamine release process without changing the degree of cooperativity.

*Effects of Cocaine on Dopamine and Serotonin Release*

Synapsins are thought to control a reserve pool of dopaminergic synaptic vesicles that is sensitive to cocaine: the ability of cocaine to enhance dopamine release *in vivo* is reduced in synapsin TKO mice (Venton et al., 2006). The effect of cocaine on 5-HT release in SNr brain slices was evaluated by a 35 min application of cocaine (10 μM), a concentration that causes competitive uptake of 5-HT transport (John and Jones, 2007) and thereby increases the apparent value of $K_m$. Cocaine treatment caused dramatic changes in the shape of the 5-HT concentration profile produced by electrical stimulation, mainly prolonging the time course of these signals in slices from both WT and TKO mice (Figure 3.5, left panels). To estimate the apparent $K_m$ for 5-HT uptake (Jones et al., 1995), we used nonlinear regression to evaluate the decaying phase of the 5-HT signal. The apparent $K_m$ values in the presence of cocaine were 0.75 ± 0.06 μM for WT and 0.83 ± 0.09 μM for TKO animals (n = 7 for WT, n = 6 for TKO), values that are significantly larger than the predrug value of 0.17 μM (John et al., 2006). However, the $K_m$ values measured in the presence of cocaine are not significantly different from each other ($p > 0.05$) and are similar to previous measurements made for 5-HT uptake in the presence of 10 μM cocaine (John and Jones, 2007). In addition, cocaine treatment did not significantly alter the amount of 5-HT released by electrical stimulation in slices from either genotype (Figure 3.6).

The influence of synapsins on the ability of cocaine to increase dopamine release was evaluated. The effect of cocaine on dopamine release evoked by electrical stimulation was compared in caudate-putamen slices prepared from the two mouse genotypes. These slices were treated for 35 minutes with 2 μM cocaine, a dose known to inhibit dopamine uptake in mouse brain slices (Jones et al., 1995). Although dopamine uptake is much faster than that of 5-HT (compare traces in left and right columns of Figure 3.5), the presence of cocaine also caused a significant slowing in the time course of the dopamine signal produced by electrical stimulation (Figure 3.5, right panels). This slowing indicates an inhibition of dopamine uptake. The apparent $K_m$ values for dopamine uptake after application of cocaine were 2.60 ± 0.09 μM for WT and 2.60 ± 0.15 TKO μM mice (n = 7 for each genotype). While these values are not significantly different from each other ($p > 0.5$), they are substantially larger than the value of 0.2 μM measured in control conditions. Cocaine treatment also caused an increase in the amount of dopamine released by electrical stimulation, evident as an increase in the peak amplitude of the dopamine signals. This is similar to what is observed in rat brain tissue (Jones et al., 1995). The stimulatory effect of cocaine was much greater in slices from WT mice than in slices from TKO mice (Figure 3.5). On average, cocaine increased electrically evoked dopamine release by 89 ± 4% in slices from WT mice, but only 49 ± 3% in TKO slices (Figure 3.6). This difference between the cocaine responses of the two genotypes is significant ($p < 0.001$; n = 4 for each genotype).

We also examined the influence of external $Ca^{2+}$ on the ability of cocaine to enhance dopamine release. Over the entire range of $Ca^{2+}$ concentrations considered, cocaine caused a greater enhancement of dopamine release from WT slices than from TKO slices. To quantify the effects of cocaine on the $Ca^{2+}$ dependence of dopamine release, the ratio of dopamine release measured in the presence and absence of cocaine was calculated (Figure 3.7A). This ratio was significantly greater than 1 at $Ca^{2+}$ concentrations below 2.4 mM for WT slices ($p < 0.001$, n = 6), while TKO slices only showed significant effects of cocaine at 1 mM or less $Ca^{2+}$ ($p < 0.01$, n = 6). Figure 3.7B shows the relative dopamine release of both gentoypes as a function of the external [$Ca^{2+}$].

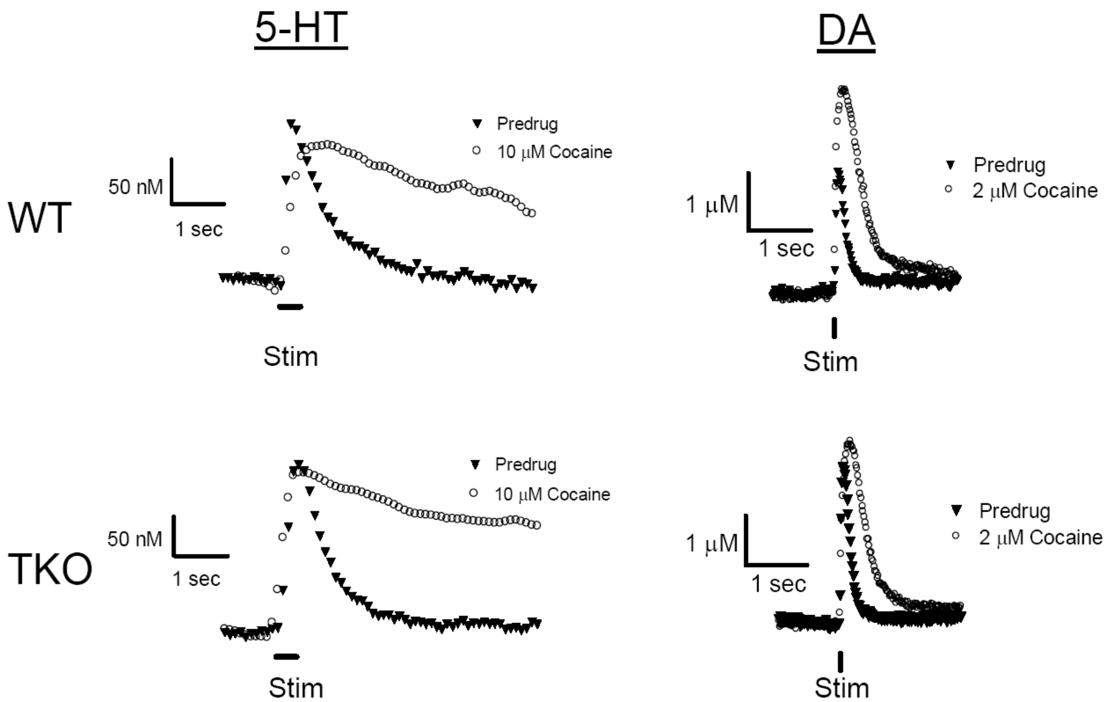


**Figure 3.5** Effects of cocaine on stimulated 5-HT and dopamine release and uptake in brain slices. Left Column: Example responses of 5-HT release in SNr from WT (top) and TKO (bottom) mice in the presence and absence of 10 µM cocaine after 35 minutes. Right Column: Example responses of dopamine in striatal tissue from WT (top) and TKO (bottom) mice in the presence and absence of 2 µM cocaine after 35 minutes.


**Figure 3.6** Dopamine and 5-HT release after 35 minutes of cocaine exposure relative to the predrug value. Relative release of striatal dopamine in WT animals is significantly larger than that in TKO animals ($p < 0.001$, $n = 4$ for each genotype), whereas 5-HT release in SNr tissue ($n = 7$ for each genotype) is not significantly affected by cocaine in either genotype.

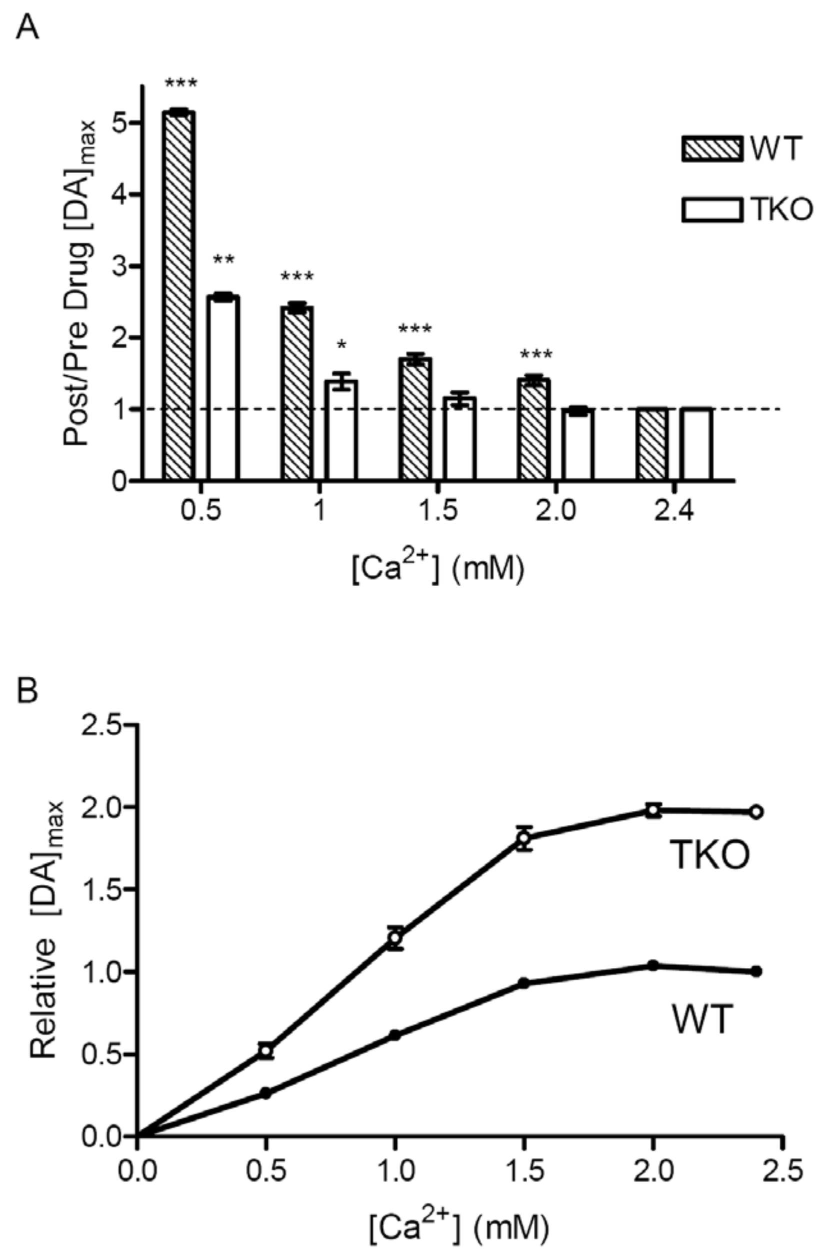


**Figure 3.7** Effect of 2 µM cocaine on the $Ca^{2+}$ dependence of dopamine release (normalized to release at 2.4 mM $Ca^{2+}$) in striatal slices from WT and TKO mice. A) Ratio of release in the presence of cocaine to that in its absence as a function of external $[Ca^{2+}]$ for WT and TKO animals (n = 6, each genotype). In slices from WT mice, cocaine significantly increases electrically stimulated dopamine release at all $[Ca^{2+}]$ below 2.4 mM, however, TKO animals are only facilitated at low levels of $Ca^{2+}$. (* $p < 0.05$, ** $p < 0.01$, *** $p < 0.001$). B) Relative $[DA]_{max}$ in TKO animals and WT animals as a function of extracellular $Ca^{2+}$ in the presence of 2 µM cocaine. Little difference in $Ca^{2+}$ sensitivity is seen between the genotypes when cocaine is present (the curve shapes are similar).

The difference in $Ca^{2+}$ sensitivity between WT and TKO animals shown in Figure 3.4 was abolished by 2 µM cocaine (Figure 3.7B). Therefore, dopamine release from WT animals is preferentially facilitated in response to cocaine by a mechanism that is partially dependent on the extracellular [$Ca^{2+}$].

## Discussion

The comparison of dopamine and 5-HT release from WT mice and mice lacking all three synapsin genes reveals that synapsins play very different roles in nerve terminals employing these two biogenic amine neurotransmitters. First, in the synapsin TKO mice, the release of dopamine evoked by electrical stimulation was almost twice as large as in WT mice. This was true both in brain slices, where a stimulus was used to deplete the readily releasable dopamine pool and *in vivo* where the stimulation was sufficiently mild that continual release during both high and low frequency trains occurred. In contrast, 5-HT release in the SNr was the same in the presence or absence of synapsins. Cocaine blocked uptake of both 5-HT and dopamine, raising the apparent value of $K_m$ in both mouse genotypes, however it was only able to enhance the release of dopamine. In addition, the enhancement of dopamine release was greater in WT animals than in TKO animals. Thus, in the synapsin TKO mouse, dopamine release is larger and more sensitive to external calcium, but less susceptible to enhancement by cocaine.

### *Synapsins Modulate Dopamine Release Dynamics*

Dopamine release was evaluated using intact animals and striatal brain slices. Each preparation offers advantages and disadvantages. The intact animal allows for remote stimulation of dopamine cell bodies using a variety of stimulation intensities and frequencies. However, the release that accompanies stimulus trains causes autoreceptor activation that can diminish dopamine release. The slice preparation is more controlled because intense single pulse stimuli can be used avoiding autoreceptor confounds (Kennedy et al., 1992). The slice preparation also provides an environment where drug and ion concentrations can be manipulated *ad libitum*. Greater dopamine release was observed in both intact TKO mice and in striatal brain slices prepared from these mice confirming that the synapsins effect is mediated at the presynaptic terminal. Although dopamine release was enhanced, its tissue content was the same in TKO and WT mice, clearly showing that deletion of synapsins caused a redistribution of releasable dopamine stores rather than a change in the stores themselves. The increased release was not compensated by an alteration in uptake because the $V_{max}$ values for dopamine uptake were similar for both genotypes.

Loss of synapsins has different effects on release of various transmitters. At GABAergic synapses, loss of synapsins results in a decrease in GABA release evoked by single action potentials (Gitler et al., 2004). Loss of synapsins decreases both the readily releasable vesicles near the active zone and those farther away, in the reserve GABAergic pool. In contrast, synapsin deletion has no effect on glutamate release evoked by single action potentials (Gitler et al., 2004), but it does decrease the number of vesicles in the reserve pool only (Gitler et al., 2004). In contrast, the loss of synapsins increases the release of catecholamines from adrenal chromaffin cells by increasing the number of exocytotic events, while the amount of catecholamine released per vesicle was unchanged, an effect reversed by expression of synapsin IIa (Villanueva et al., 2006).

The greater dopamine release in TKO mice compared to WT mice does not seem to be the consequence of indirect effects mediated by GABA or glutamate activity since dopamine release was unchanged in the presence of CNQX and picrotoxin. Thus, the neurotransmitter specific alterations in release from TKO mice are the result of a unique distribution of the synapsins in the biogenic amine neurotransmitter systems. For example, the functional consequences of synapsin deletion for dopamine release appear similar to the situation in chromaffin cells in that greater dopamine release is obtained (Figures 3.2A and 3.3A); however, unlike chromaffin cells, dopamine terminals lack synapsin IIa (Bogen et al., 2006). Therefore, the most likely candidate for the differences in dopamine release between TKO and WT mice is synapsin III, an isoform that is found in the striatum (Pieribone et al., 2002). Mice with a deletion of synapsin III have an increased recycling pool of hippocampal synaptic vesicles (Feng et al., 2002). Since neurotransmitter release measured in brain slices does not distinguish between the recycling and readily releasable dopamine pool, the same effect may explain our findings.

Release studies done in the SNr show that there are no functional consequences on 5-HT release as a result of synapsin deletion (Figure 3.1). The lack of a synapsin effect in 5-HT neurons is likely related to unique synapsin expression in these neurons. *In situ* hybridization for synapsin I, II, and III mRNA shows that synapsin I is predominantly expressed synapsin gene in the SNr and dorsal raphe nucleus (Allen Institute for Brain Discovery). The expression of synapsin II mRNA in the SNr is low and diffuse while synapsin III is not expressed at detectable levels. The absence in the SNr of two candidates identified as negative regulators of biogenic amine release, synapsin II (Villanueva et al., 2006) or synapsin III (this work), could explain the lack of synapsin regulation of 5-HT release. It remains unclear why synapsin I does not negatively regulate release in 5-HT terminals. Recent reports have indicated that the action of synapsin I on neurotransmitter release from motor synapses is only present at low levels of $Ca^{2+}$ (0.5 mM) (Coleman and Bykhovskaia, 2009). Therefore, it is possible that 5-HT release from these animals is altered but that the alterations were not apparent at the physiological levels of $Ca^{2+}$ used in this experiment. The difference between regulation of 5-HT and dopamine release may also originate from differences in their synaptic vesicles. 5-HT is mainly stored in large dense-core vesicles (Nirenberg et al., 1995) whereas dopamine is primarily stored in small synaptic vesicles (Nirenberg et al., 1997). Accordingly, synapsins appear to associate most heavily with small synaptic vesicles in central nerve terminals (Fdez and Hilfiker, 2006).

*Synapsin Removal Alters Calcium Dynamics*

Calcium entry is required for stimulated dopamine release and may be necessary to liberate synapsin-dependent pool vesicles that supplement depleted releasable stores. This mobilization is a slower process and occurs in the time between stimulations (Justice et al., 1988). Increasing extracellular calcium levels increases $Ca^{2+}$ entry into the presynaptic terminals and subsequent accumulation of $Ca^{2+}$ within the terminal (Nachshen and Sanchez-Armass, 1987) enhancing dopamine release. Release at terminals from TKO mice was more sensitive to external $Ca^{2+}$ than terminals from WT mice. Even in the presence of low external $Ca^{2+}$, dopamine release in the striatum of synapsin TKO animals was greater than in tissue from WT mice. Quantitative analysis showed a higher $K_{Ca}^{2+}$ for WT animals than TKO animals. However, the similar Hill coefficients suggest that the same $Ca^{2+}$-dependent mechanisms that trigger release are operant in both genotypes. The higher saturation value of dopamine release reached by TKO animals also indicates a larger pool of releasable vesicles.

*The Action of Cocaine Requires Synapsins*

Dopamine release in tissue from WT mice undergoes greater enhancement by cocaine relative to TKO tissue. Cocaine increases the extracellular dopamine concentration through at least two mechanisms. The best understood is competitive blockade of the DAT inhibiting dopamine clearance (Jones et al., 1996; Wang et al., 1997; Uhl et al., 2002). However, cocaine also facilitates dopamine release from presynaptic terminals (Lee et al., 2001), an effect that involves synapsin (Venton et al., 2006). The facilitation of dopamine release by cocaine occurs in slices from WT animals and is significantly less in tissue from synapsin TKO animals (Figure 3.6). Since release in slices comes from the readily releasable pool, the facilitated release observed with cocaine in WT animals indicates it has altered the dynamics of this pool through a synapsin dependent pathway. It is unclear at this point whether cocaine is acting directly on synapsin or inducing a cascade in the presynaptic terminal that involves synapsin dependent vesicles. A synapsin independent pathway is necessary to explain the cocaine induced increase in dopamine release from TKO slices (Figure 3.6). Repeated cocaine exposure has been shown to facilitate $Ca^{2+}$ influx through l-type $Ca^{2+}$ channels in the prefrontal cortex of rats (Nasif et al., 2005). However, a simple increase in overall $Ca^{2+}$ influx would not explain the data in Figure 6 because even at 5 mM extracellular $Ca^{2+}$, the dopamine release in WT slices is not enhanced to the same degree as is seen in the presence of cocaine. At low $Ca^{2+}$ concentrations (when much less of the releasable pool is mobilized by the stimulation) cocaine still enhances dopamine release even in tissue devoid of synapsins, although to a lesser extent than seen in WT animals (Figure 3.7A). The application of 2 μM cocaine alleviates the difference in $Ca^{2+}$ sensitivity between TKO and WT animals evident by the similarity in the shape of their $Ca^{2+}$ profiles (Figure 3.7B). A combined effect of cocaine on calcium sensitivity and synapsin modulated dopamine release would explain the findings in both animals. Dopamine release is an indirect measure of $Ca^{2+}$ influx and its subsequent action; therefore, it is unclear how cocaine affects the $Ca^{2+}$ sensitivity of release. However, our findings are consistent with the observation that calcium channel knockout mice do not show an acute locomotor response to cocaine (Han et al., 2002).

Cocaine is also a potent inhibitor of the serotonin transporter (Uhl et al., 2002; Uhl and Lin, 2003). Measurements in the SNr confirm this action of cocaine by showing that the rate of uptake of 5-HT was lowered in the presence of cocaine (Figure 3.5). However, unlike dopamine release, cocaine does not enhance 5-HT release (Figure 3.6).

Furthermore, there is no difference in cocaine sensitivity of 5-HT uptake between WT mice and synapsin TKO mice. These functional differences in the actions of cocaine on dopaminergic and serotonergic neurons may be indicative of the differences in the role of synapsins and their role in vesicular pool dynamics.

The loss of synapsins causes neurotransmitter-specific changes in release from presynaptic terminals. Loss of synapsins leads to a decrease in evoked GABA release, while release of glutamate and 5-HT is unaffected. The release of dopamine is actually enhanced, a result that is likely due to removal of synapsin III. Thus, synapsins appear to have dramatically different functions at presynaptic terminals that employ different neurotransmitters. Future work will probe the molecular underpinnings of these differences in the contributions of synapsins to vesicle trafficking in these different types of presynaptic terminals.

## Literature Cited


Augustine GJ, Charlton MP (1986) Calcium dependence of presynaptic calcium current and post-synaptic response at the squid giant synapse. J Physiol 381:619-640.

Augustine GJ, Charlton MP, Smith SJ (1987) Calcium action in synaptic transmitter release. Annu Rev Neurosci 10:633-693.

Bogen IL, Boulland JL, Mariussen E, Wright MS, Fonnum F, Kao HT, Walaas SI (2006) Absence of synapsin I and II is accompanied by decreases in vesicular transport of specific neurotransmitters. J Neurochem 96:1458-1466.

Bunin MA, Prioleau C, Mailman RB, Wightman RM (1998) Release and uptake rates of 5-hydroxytryptamine in the dorsal raphe and substantia nigra reticulata of the rat brain. J Neurochem 70:1077-1087.

Chi P, Greengard P, Ryan TA (2003) Synaptic vesicle mobilization is regulated by distinct synapsin I phosphorylation pathways at different frequencies. Neuron 38:69-78.

Coleman WL, Bykhovskaia M (2009) Synapsin I accelerates the kinetics of neurotransmitter release in mouse motor terminals. Synapse 63:531-533.

Dobrunz LE, Stevens CF (1997) Heterogeneity of release probability, facilitation, and depletion at central synapses. Neuron 18:995-1008.

Dodge FA, Jr., Rahamimoff R (1967) Co-operative action a calcium ions in transmitter release at the neuromuscular junction. J Physiol 193:419-432.

Erickson JD, Schafer MK, Bonner TI, Eiden LE, Weihe E (1996) Distinct pharmacological properties and distribution in neurons and endocrine cells of two isoforms of the human vesicular monoamine transporter. Proc Natl Acad Sci U S A 93:5166-5171.

Evergren E, Benfenati F, Shupliakov O (2007) The synapsin cycle: a view from the synaptic endocytic zone. J Neurosci Res 85:2648-2656.

Fdez E, Hilfiker S (2006) Vesicle pools and synapsins: new insights into old enigmas. Brain Cell Biol 35:107-115.

Feng J, Chi P, Blanpied TA, Xu Y, Magarinos AM, Ferreira A, Takahashi RH, Kao HT, McEwen BS, Ryan TA, Augustine GJ, Greengard P (2002) Regulation of neurotransmitter release by synapsin III. J Neurosci 22:4372-4380.

Ferreira A, Kao HT, Feng J, Rapoport M, Greengard P (2000) Synapsin III: developmental expression, subcellular localization, and role in axon formation. J Neurosci 20:3736-3744.

Gitler D, Takagishi Y, Feng J, Ren Y, Rodriguiz RM, Wetsel WC, Greengard P, Augustine GJ (2004) Different presynaptic roles of synapsins at excitatory and inhibitory synapses. J Neurosci 24:11368-11380.

Greengard P, Valtorta F, Czernik AJ, Benfenati F (1993) Synaptic vesicle phosphoproteins and regulation of synaptic function. Science 259:780-785.

Han W, Saegusa H, Zong S, Tanabe T (2002) Altered cocaine effects in mice lacking Ca(v)2.3 (alpha(1E)) calcium channel. Biochem Biophys Res Commun 299:299-304.

Jackson BP, Dietz SM, Wightman RM (1995) Fast-scan cyclic voltammetry of 5-hydroxytryptamine. Anal Chem 67:1115-1120.

John CE, Jones SR (2007) Voltammetric characterization of the effect of monoamine uptake inhibitors and releasers on dopamine and serotonin uptake in mouse caudate-putamen and substantia nigra slices. Neuropharmacology 52:1596-1605.

John CE, Budygin EA, Mateo Y, Jones SR (2006) Neurochemical characterization of the release and uptake of dopamine in ventral tegmental area and serotonin in substantia nigra of the mouse. J Neurochem 96:267-282.

Johnson MA, Rajan V, Miller CE, Wightman RM (2006) Dopamine release is severely compromised in the R6/2 mouse model of Huntington's disease. J Neurochem 97:737-746.

Jones SR, Garris PA, Wightman RM (1995) Different effects of cocaine and nomifensine on dopamine uptake in the caudate-putamen and nucleus accumbens. J Pharmacol Exp Ther 274:396-403.

Jones SR, O'Dell SJ, Marshall JF, Wightman RM (1996) Functional and anatomical evidence for different dopamine dynamics in the core and shell of the nucleus accumbens in slices of rat brain. Synapse 23:224-231.

Justice JB, Jr., Nicolaysen LC, Michael AC (1988) Modeling the dopaminergic nerve terminal. J Neurosci Methods 22:239-252.

Kennedy RT, Jones SR, Wightman RM (1992) Dynamic observation of dopamine autoreceptor effects in rat striatal slices. J Neurochem 59:449-455.

Lee TH, Balu R, Davidson C, Ellinwood EH (2001) Differential time-course profiles of dopamine release and uptake changes induced by three dopamine uptake inhibitors. Synapse 41:301-310.

Llinas R, Gruner JA, Sugimori M, McGuinness TL, Greengard P (1991) Regulation by synapsin I and Ca(2+)-calmodulin-dependent protein kinase II of the transmitter release in squid giant synapse. J Physiol 436:257-282.

Lonart G, Simsek-Duran F (2006) Deletion of synapsins I and II genes alters the size of vesicular pools and rabphilin phosphorylation. Brain Res 1107:42-51.

Nachshen DA, Sanchez-Armass S (1987) Co-operative action of calcium ions in dopamine release from rat brain synaptosomes. J Physiol 387:415-423.

Nasif FJ, Hu XT, White FJ (2005) Repeated cocaine administration increases voltage-sensitive calcium currents in response to membrane depolarization in medial prefrontal cortex pyramidal neurons. J Neurosci 25:3674-3679.

Neher E (1998) Vesicle pools and Ca2+ microdomains: new tools for understanding their roles in neurotransmitter release. Neuron 20:389-399.

Nicholson C, Rice ME (1990) Diffusion of ions and transmitters in the brain cell microenvironment. In: Volume transmission in the brain: novel mechanisms for neuronal transmission, Vol. 1 (Fuxe K, Agnati LF, eds), pp 279-294. New York: Raven Press.

Nirenberg MJ, Liu Y, Peter D, Edwards RH, Pickel VM (1995) The vesicular monoamine transporter 2 is present in small synaptic vesicles and preferentially localizes to large dense core vesicles in rat solitary tract nuclei. Proc Natl Acad Sci U S A 92:8773-8777.

Nirenberg MJ, Chan J, Liu Y, Edwards RH, Pickel VM (1997) Vesicular monoamine transporter-2: immunogold localization in striatal axons and terminals. Synapse 26:194-198.

Pieribone VA, Shupliakov O, Brodin L, Hilfiker-Rothenfluh S, Czernik AJ, Greengard P (1995) Distinct pools of synaptic vesicles in neurotransmitter release. Nature 375:493-497.

Pieribone VA, Porton B, Rendon B, Feng J, Greengard P, Kao HT (2002) Expression of synapsin III in nerve terminals and neurogenic regions of the adult brain. J Comp Neurol 454:105-114.

Rosahl TW, Spillane D, Missler M, Herz J, Selig DK, Wolff JR, Hammer RE, Malenka RC, Sudhof TC (1995) Essential functions of synapsins I and II in synaptic vesicle regulation. Nature 375:488-493.

Uhl GR, Lin Z (2003) The top 20 dopamine transporter mutants: structure-function relationships and cocaine actions. Eur J Pharmacol 479:71-82.

Uhl GR, Hall FS, Sora I (2002) Cocaine, reward, movement and monoamine transporters. Mol Psychiatry 7:21-26.

Venton BJ, Seipel AT, Phillips PE, Wetsel WC, Gitler D, Greengard P, Augustine GJ, Wightman RM (2006) Cocaine increases dopamine release by mobilization of a synapsin-dependent reserve pool. J Neurosci 26:3206-3209.

Villanueva M, Thornley K, Augustine GJ, Wightman RM (2006) Synapsin II negatively regulates catecholamine release. Brain Cell Biol 35:125-136.

Wang YM, Gainetdinov RR, Fumagalli F, Xu F, Jones SR, Bock CB, Miller GW, Wightman RM, Caron MG (1997) Knockout of the vesicular monoamine transporter 2 gene results in neonatal death and supersensitivity to cocaine and amphetamine. Neuron 19:1285-1296.

Wiedemann DJ, Basse-Tomusk A, Wilson RL, Rebec GV, Wightman RM (1990) Interference by DOPAC and ascorbate during attempts to measure drug-induced changes in neostriatal dopamine with Nafion-coated, carbon-fiber electrodes. J Neurosci Methods 35:9-18.

Wightman RM, Amatore C, Engstrom RC, Hale PD, Kristensen EW, Kuhr WG, May LJ (1988) Real-time characterization of dopamine overflow and uptake in the rat striatum. Neuroscience 25:513-523.

**Chapter 4**

Dopamine Uptake and Transporter Expression

## Introduction

Dopamine is cleared from the extracellular space by uptake through a membrane bound dopamine transporter (DAT). DAT belongs to a family of transporters including the 5-HT transporter (SERT), and the norepinephrine transporter (NET) (Torres and Amara, 2007). This family of transporters is characterized by 12 transmembrane spanning domains and intracellular C-terminated and N-terminated domains. The DAT co-transports dopamine along with 2 $Na^+$ and 1 $Cl^-$ from the extracellular space into the intracellular compartment. Dopamine is a volume transmitter; therefore, the expression of DAT is not limited to neuronal synapses (Rice and Cragg, 2008).

Extracellular dopamine concentrations are dependent on adequate DAT function; a property that can be altered by disease or drugs of abuse. Several drugs of abuse (eg. cocaine, ampehetamine, methylphenidate, and methamphetamine) interact with the DAT to increase the extracellular dopamine concentration. There is a large body of evidence suggesting that these increased dopamine concentrations are partly responsible for the addictive properties of these drugs (Sora et al., 2001; Uhl et al., 2002; Uhl and Lin, 2003). Dopamine transport blockers tend to reside in one of two categories with regards to their interaction with dopamine terminals. Cocaine and cocaine like drugs increase extracellular dopamine by inhibiting the formation of a dopamine-DAT complex

(Jones et al., 1995; Uhl et al., 2002; Schramm-Sapyta et al., 2006). This inhibition slows the re-uptake of dopamine and increases its extracellular residence time. Cocaine itself has also been implicated as a facilitator of release, presumably by altering calcium sensitivity in dopamine neurons (White et al., 1998; Han et al., 2002; Schramm-Sapyta et al., 2006) (Chapter 3). Amphetamines inhibit vesicular packaging through the vesicle monamine transporter (VMAT2) and invert the DAT, extruding cytosolic dopamine into the extracellular space (Sulzer et al., 2005; Wallace and Connell, 2008; Goodwin et al., 2009). Cocaine actions on dopamine are said to be impulse dependent while amphetamines' actions are not. The study of DAT function is also important for disease state models in which dopamine transmission has been disrupted in some way. The DAT is an attractive target when studying disease states related to hyper or hypo dopaminergia. For example, attention deficit and hyperactivity disorder in humans is believed to be related to altered expression levels of DAT in the brain (Dougherty et al., 1999; Krause et al., 2006; Volkow et al., 2007).

In this chapter, we describe the use of a novel transgenic mouse model to evaluate dopaminergic transmission in the face of altered DAT function. Traditional studies of the dopamine transporter have relied on the presence of pharamacological agents to alter uptake. More recently, transgenic mice expressing less DAT or no DAT at all have been used to elucidate the action of amphetamines, autoreceptor function, and behavioral phenotypes (Giros et al., 1996; Jones et al., 1998; Jones et al., 1999). The novel transgenic mice described here express more DAT than their wild type counterparts, a very intriguing phenotype. These mice were used to achieve a comprehensive understanding of how the amount of expressed DAT relates to dopamine uptake, extracellular dopamine concentrations, autoreceptor function, and amphetamine action at dopamine terminals.

## Materials and Methods

The electrochemical procedures used in this chapter have been explained in detail in Chapter 2. The Southern blot analysis, Western blot analysis, and gold-silver staining have been explained in detail elsewhere (Salahpour et al., 2008). The tissue levels of DA from the striatum of WT or DAT-Tg animals were evaluated using RP-HPLC with ECD as described previously (Wang et al., 1997). Locomotor activity experiments were performed as described previously (Salahpour et al., 2008) using automated locomotor activity monitors (Accuscan Instruments). Briefly, mice were initially placed for 60 min into the activity monitor chamber. After this period of habituation, animals were injected (3 mg/kg of body weight i.p.) with vehicle or the drug, returned to the chamber, and the total distance covered monitored for additional 60 min after injection.

## Results

*Transgenic Modification of DAT Expression*

Pronuclear injection of a DAT locus containing bacterial vector like that shown in Figure 4.1A was used to alter the expression of DAT in C57 BL/6 mice (Salahpour et al., 2008). The transfection of a WT animal containing two endogenous copies of the DAT gene yielded a DAT-Tg animal expressing 6 copies of the DAT gene (DAT-Tg (6)). Southern blot analysis indicated a 3-fold increase in transporter DNA in DAT-Tg (6) animals relative to WT controls corresponding to the four additional gene copies (Figure 4.1B). The increase in DNA was coincident with a 3-fold increase in DAT protein relative to WT animals as determined by Western blot analysis (Figure 4.1C). To test the relationship between increased DAT protein and increased expression of transporters on the cell membrane, immunogold-silver staining was used to visualize DAT localization in electron micrographs (EMs) (Salahpour et al., 2008). A qualitative increase in DAT can be easily seen by

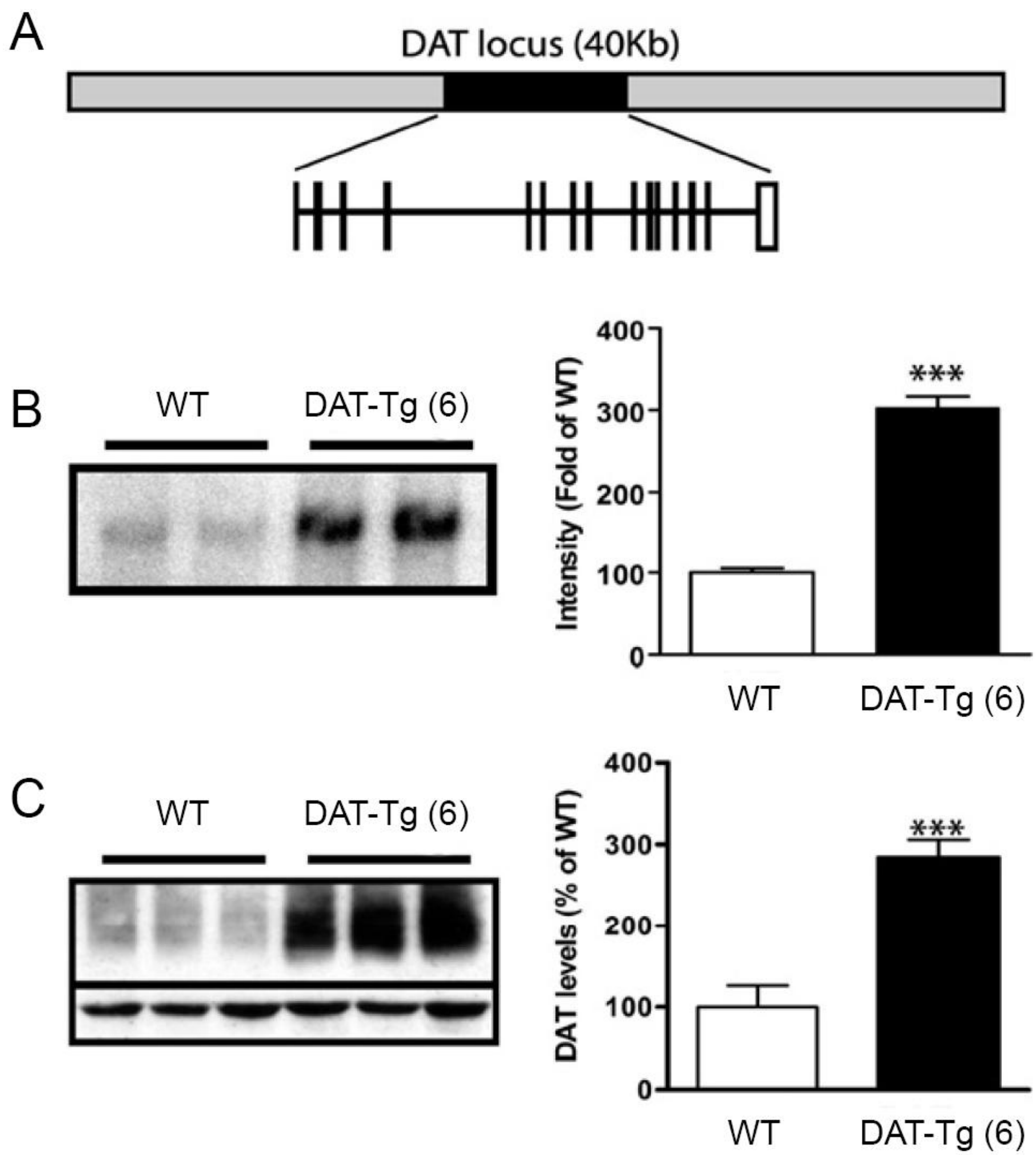


**Figure 4.1** Generation of DAT transgenic animals by pronuclear injection. A) A representation of the bacterial vector used for the transfection. B) Southern blot analysis showing a significant ($p < 0.001$, $n = 4$ both genotypes) increase in DAT DNA, this increase in DNA corresponds to an additional four copies of the DAT gene. C) A Western blot confirming a 300 % increase in DAT protein levels in transgenic animals ($p < 0.001$, $n = 5$ both genotypes). Figure modified from Figure 1 of Salahpour et al. (2008).

comparing EMs from WT animals to those taken from DAT-Tg (6) animals (Figure 4.2). DAT was expressed perisnyaptically on the plasma membrane and within intracellular compartments of dopamine terminals. These data support a successful transfection technique in which the amount of membrane bound DAT can be increased by introducing more copies of the DAT gene.

This work will focus on the comparison of WT control animals with three different transgenic mouse models expressing different amounts of DAT. The HET animal expresses only 1 copy of the DAT gene and was generated during the creation of the DAT KO mouse line (Giros et al., 1996). The transfection of the HET animal using the pronuclear injection procedure described here was used to generate the DAT-Tg (5) animal. Finally, transfection of a WT animal yielded a DAT-Tg animal expressing six copies previously defined as DAT-Tg (6). Therefore, HET animals have 1 DAT copy, WT animals have 2 DAT copies, DAT-Tg (5) animals have 5 DAT copies, and DAT-Tg (6) animals have 6 DAT copies.

*Variation of $V_{max}$ with Transporter Copy Number*

DAT expression changes the profile of stimulated dopamine release in striatal brain slices. The DAT KO animal achieves a steady state dopamine concentration shortly after stimulation that does not change over the course of the recording (Figure 4.3). The absence of appreciable clearance in the DAT KO animal confirms that uptake is the sole clearance mechanism of dopamine over the time course of these experiments as previously reported (Jones et al., 1999). The expression of a single DAT gene creates a bi-phasic dopamine profile in which there is an immediate rise in the dopamine concentration after stimulation followed by dopamine uptake (Figure 4.3). Increased expression of DAT from 1 copy to 5 copies changes this profile by making the peak shorter in time and smaller in size. To evaluate this phenomenon, dopamine uptake in brain slices containing the caudate putamen

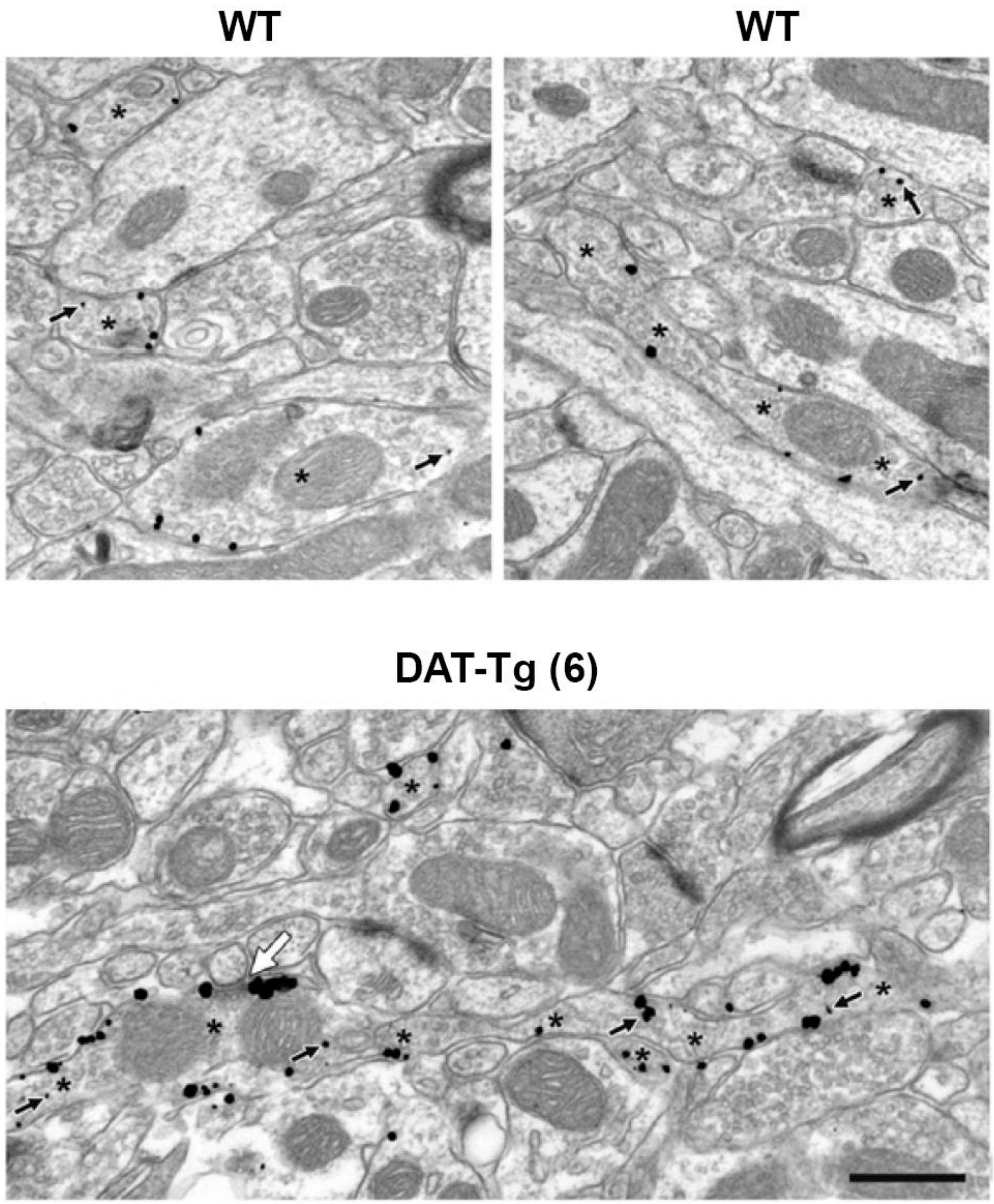


**Figure 4.2** Immunogold-silver staining of the dorosolateral striatum (scale bar: 500 nm). Asterisks denote immunoreactive axons and the white arrow shows a synapse with a medium spiny neuron. Black arrows indicate cytoplasmic gold particles, all other gold particles are associated with the plasma membrane. There is a larger amount of membrane associated DAT in transgenic animals (Bottom Panel) compared to WT animals (Top Panels). Localization indicates perisynaptic DAT reactivity. Figure adapted from Figure 3 in Salahpour et al. (2008).

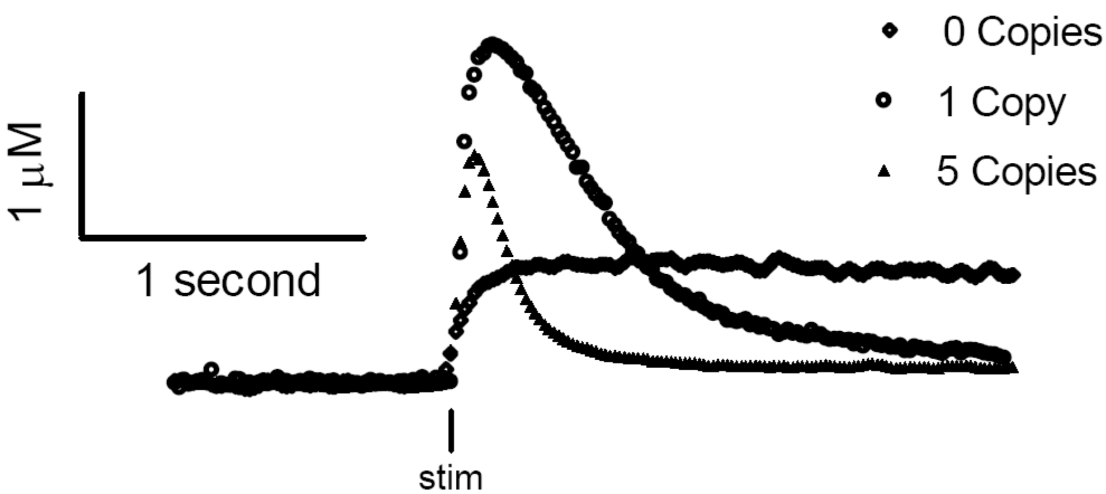


**Figure 4.3** The rate of uptake changes with the expression level of the DAT gene. Stimulated dopamine release in the caudate putamen of mice expressing 0, 1, and 5 copies of the DAT gene. The animal without expressed DAT is unable to clear dopamine after it is released. As more DAT is expressed, the rate of dopamine uptake increases manifested by a thinner and shorter peak in the trace from a 5 copy animal vs. the trace from a 1 copy animal.

of DAT-Tg (6) mice was measured using either FSCV or amperometry and compared to the uptake of WT animals (Figure 4.4).

In constant-potential amperometry, the electrode is held at a fixed potential sufficient to oxidize dopamine when it contacts the electrode surface (Venton et al., 2002). When release is evoked by a single pulse stimulation in tissue from WT animals, there was an almost immediate rise in dopamine followed by a decay to baseline (Figure 4.4A). In striatal tissue from transgenic animals the amplitude of release was smaller and the decay faster than in WT tissue. The initial descending slope taken from $[DA]_{max}$ to ½ $[DA]_{max}$ was used as the $V_{max}$ value. The $V_{max}$ value for WT animals and DAT-Tg (6) animals was compared to quantify the apparent difference in uptake rate. The $V_{max}$ ratio of DAT-Tg (6) to WT (n = 5, each genotype) was found to be 1.62 for amperometry (Figure 4.4A).

Dopamine release and uptake was also evaluated with FSCV in which voltage scans sufficient to oxidize dopamine were recorded at periodic intervals, every 16.7 ms in this case. The current at the peak potential for dopamine oxidation is taken as a measure of the dopamine concentration (Baur et al., 1988). Again, a single pulse electrical stimulation was used to evoke dopamine release in striatal brain slices from WT animals and DAT-Tg (6) animals. Release measured by FSCV was lower and the disappearance was faster in DAT-Tg (6) striatal brain slices than WT striatal brain slices (Figure 4.4B). The responses are qualitatively similar to the amperometry data (compare Figures 4.4A and 4.4B).

To evaluate the kinetics of dopamine uptake using FSCV measurements, traces were deconvoluted to account for the temporal distortion due to dopamine adsorption and evaluated with a using simplex non-linear regression model (Figure 4.4B, solid traces). The $V_{max}$ values obtained from the examples in Figure 4.4B were 5.0 μM/s for WT and 7.2 μM/s for DAT-Tg (6); the overlays clearly indicate a reasonable fit. The $V_{max}$ ratio of DAT-Tg (6) to

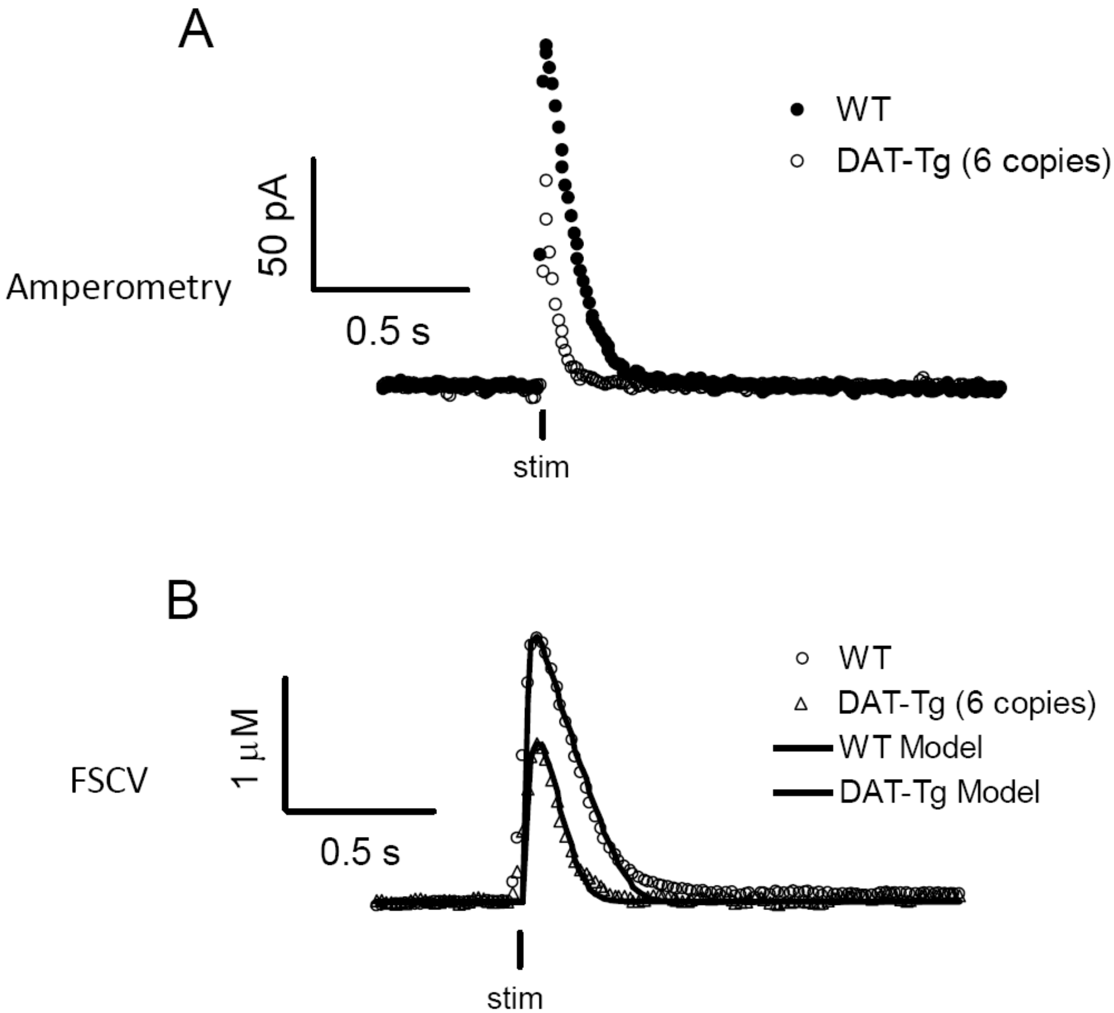


**Figure 4.4** The rate of uptake in WT and DAT-Tg (6) animals measured with amperometry and FSCV. A) Amperometric recordings of stimulated dopamine release in WT and DAT-Tg (6) animal. The slope of the curve was taken from $[DA]_{max}$ to ½ $[DA]_{max}$ and compared for both gentoypes, the DAT-Tg (6) / WT ratio was determined to be 1.62 (n = 5 each genotype). B) Stimulated dopamine release as measured by FSCV in striatal brain slices from WT and DAT-Tg (6) animals. The solid line is the non-linear model used to determine $V_{max}$ values from FSCV data. Based on the model curve, the $V_{max}$ values for these traces were 5.0 μM/s for WT and 7.2 μM/s for DAT-Tg (6), a ratio of 1.44.

WT was found to be 1.44 for FSCV modeling (n = 5, each genotype), quite similar to the ratio obtained by amperometry. The similarity in the $V_{max}$ ratio between amperometric recordings and FSCV recordings indicates that FSCV with deconvolution has sufficient temporal resolution to monitor uptake in animals overexpressing the dopamine transporter. A more complete discussion of how adsorptive delay affects dopamine uptake measurements can be found in Chapter 8.

The $V_{max}$ of dopamine uptake was measured using simplex non-linear regression of stimulated dopamine release for HET, WT, DAT-Tg (5), and DAT-Tg (6) animals (Figure 4.5A, n = 5 for all four genotypes). An increase in the expression level of DAT led to a significant ($p < 0.001$ for DAT-Tg (5) and DAT-Tg (6)) increase in maximal uptake rate while a reduction in DAT expression significantly ($p < 0.01$) decreased uptake in HET animals. The increase in uptake rate seen in DAT-Tg (6) animals was independent of a change in the binding affinity of dopamine for the transporter as indicated by the $K_m$ value (Figure 4.5B). The maximal uptake rate does not scale proportionally with number of transporter copies indicating that there is not a direct relationship between the number of gene copies and the amount of transporter participating in dopamine uptake (Salahpour et al., 2008).

*Increased Uptake Reduces Extracellular Dopamine Levels*

Electrically evoked dopamine release was monitored using FSCV in striatal brain slices to determine the relationship between the number of transporters and maximal dopamine release (Figure 4.6). Changing the expression of DAT significantly alters the $[DA]_{max}$ achieved by local electrical stimulation in striatal brain slices. HET animals release significantly ($p < 0.01$, n= 5) more dopamine than WT animals while DAT-Tg (5) and DAT-Tg (6) animals each release significantly less dopamine ($p < 0.001$, n = 5 both genotypes) than WT animals (Figure 4.6). To assess if these release differences were due to differences in

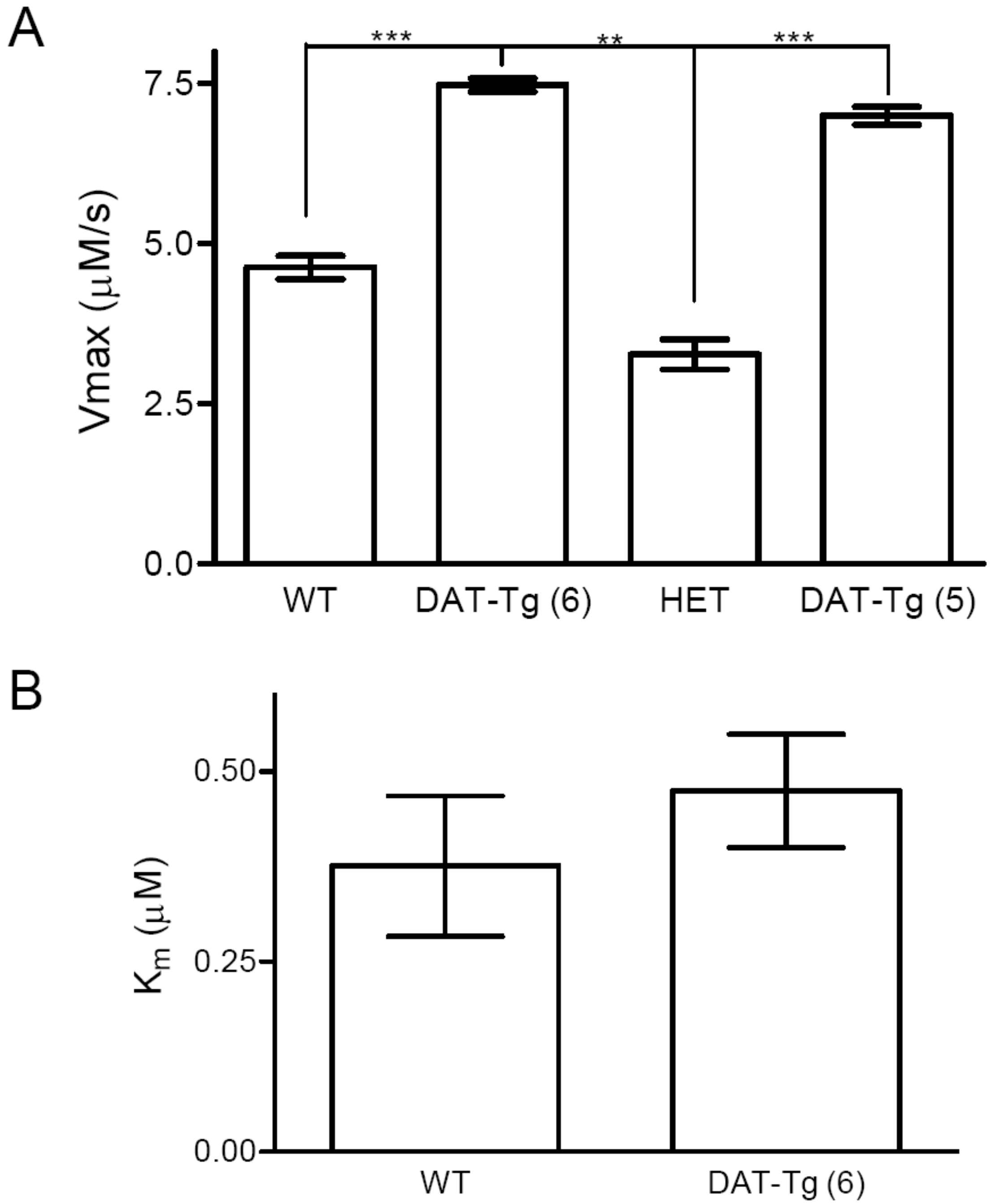


**Figure 4.5** Uptake rate constants measured in WT and DAT-Tg animals. A) There is a significant (*** $p < 0.001$, n = 5, one way anova) increase in $V_{max}$ when additional copies of the dopamine transporter are expressed (DAT-Tg animals) when compared to WT animals. A decrease in the expression of the DAT significantly (** $p < 0.01$, n = 5, one way anova) decreases $V_{max}$ in HET animals. B) There is no difference in the equilibrium binding affinity ($K_m$) of dopamine at the transporter ($p > 0.05$, n = 5) in DAT-Tg (6) animals compared to WT animals.

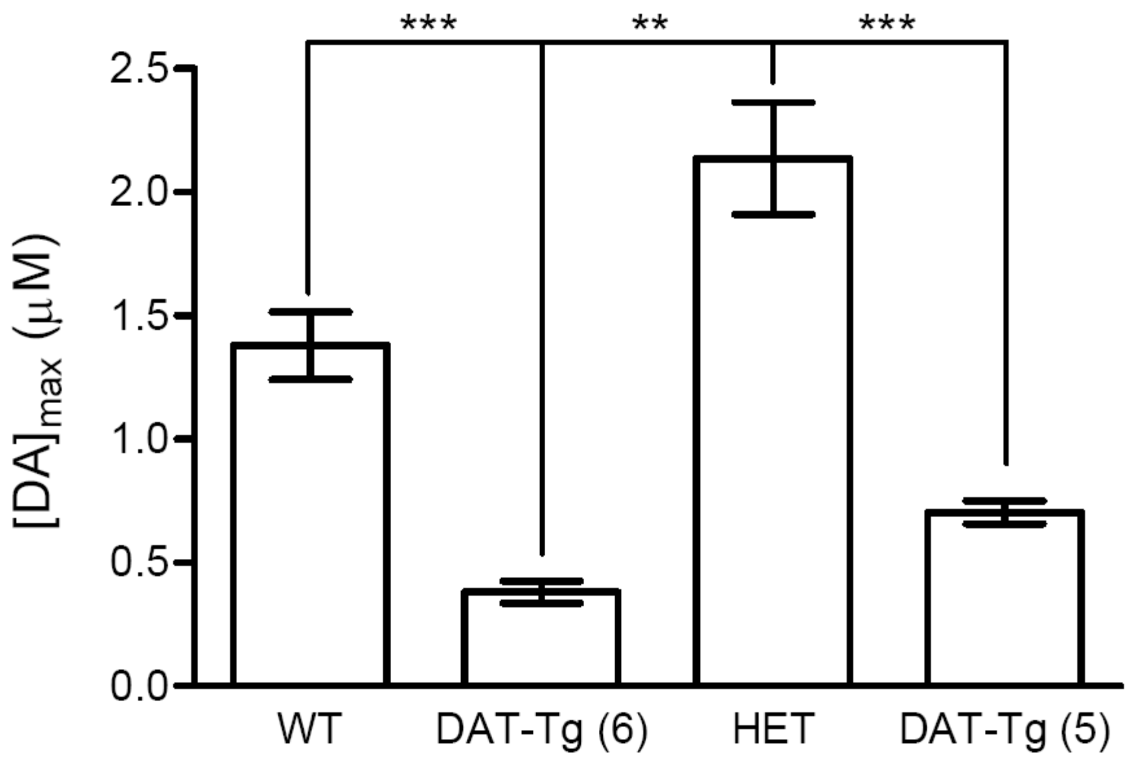


**Figure 4.6** The $[DA]_{max}$ measured at the electrode is altered in mice over expressing the DAT. When compared to WT animals, DAT-Tg (6) and DAT-Tg (5) animals have a significantly lower $[DA]_{max}$ (*** $p < 0.001$, $n = 5$, one way anova) and HET animals have a significantly higher $[DA]_{max}$ (** $p < 0.01$, $n = 5$, one way anova).

uptake rate, release in HET, WT, and DAT-Tg (5) animals was compared in the presence and absence of uptake blockade (Figure 4.7, n = 4 all genotypes). In the absence of uptake blockade, the measured maximal dopamine signal decreased from 2.13 μM for HET to 0.67 μM for DAT-Tg (5) animals (Figure 4.7A). However, in the presence of the uptake inhibitor PTT the electrically evoked dopamine signal was approximately 3.50 μM for all three animal genotypes (Figure 4.7B). The data shown in the presence of uptake blockade agrees with the total content analysis which shows that the three genotypes studied have the same amount of total dopamine in striatal tissue, about 12 μg/g (n = 12, each phenotype). Taken together, these data clearly demonstrate that the DAT expression level is critical for spatiotemporal control of dopamine.

*DAT Overexpression Does Not Affect Autoreceptor Efficacy*

The efficacy of $D_2$-autoreceptors on dopamine release in the caudate putamen of mice overexpressing the dopamine transporter was compared to WT mice by application of the $D_2$-agonist, quinelorane. Measurements were taken in striatal brain slices in response to a single pulse electrical stimulation. The effect of autoreceptor agonism on the maximal dopamine release of WT mice and DAT-Tg (5) was evaluated using FSCV. A dose response curve to ascending concentrations of quinelorane (0.5, 1, 2.5, 5, 10, 25, 50, 100, and 250 nM) was generated for WT animals and DAT-Tg (5) animals. The maximal dopamine release at each drug concentration was normalized to the predrug release value and plotted against the log of the drug concentration (Figure 4.8). There is no statistical difference ($p > 0.05$) in the response to quinelorane for DAT-Tg (5) animals compared to WT animals at any concentration of the $D_2$-autoreceptor agonist (n = 5, each phenotype). The dose response curves were also fit to a sigmoidal (variable slope) regression to calculate $EC_{50}$ values for quinelorane for each genotype. The $EC_{50}$ values for quinelorane in WT and DAT-Tg (5) animals were 4.9 ± 1.1 nM and 4.3 ± 1.1 nM respectively, not statistically

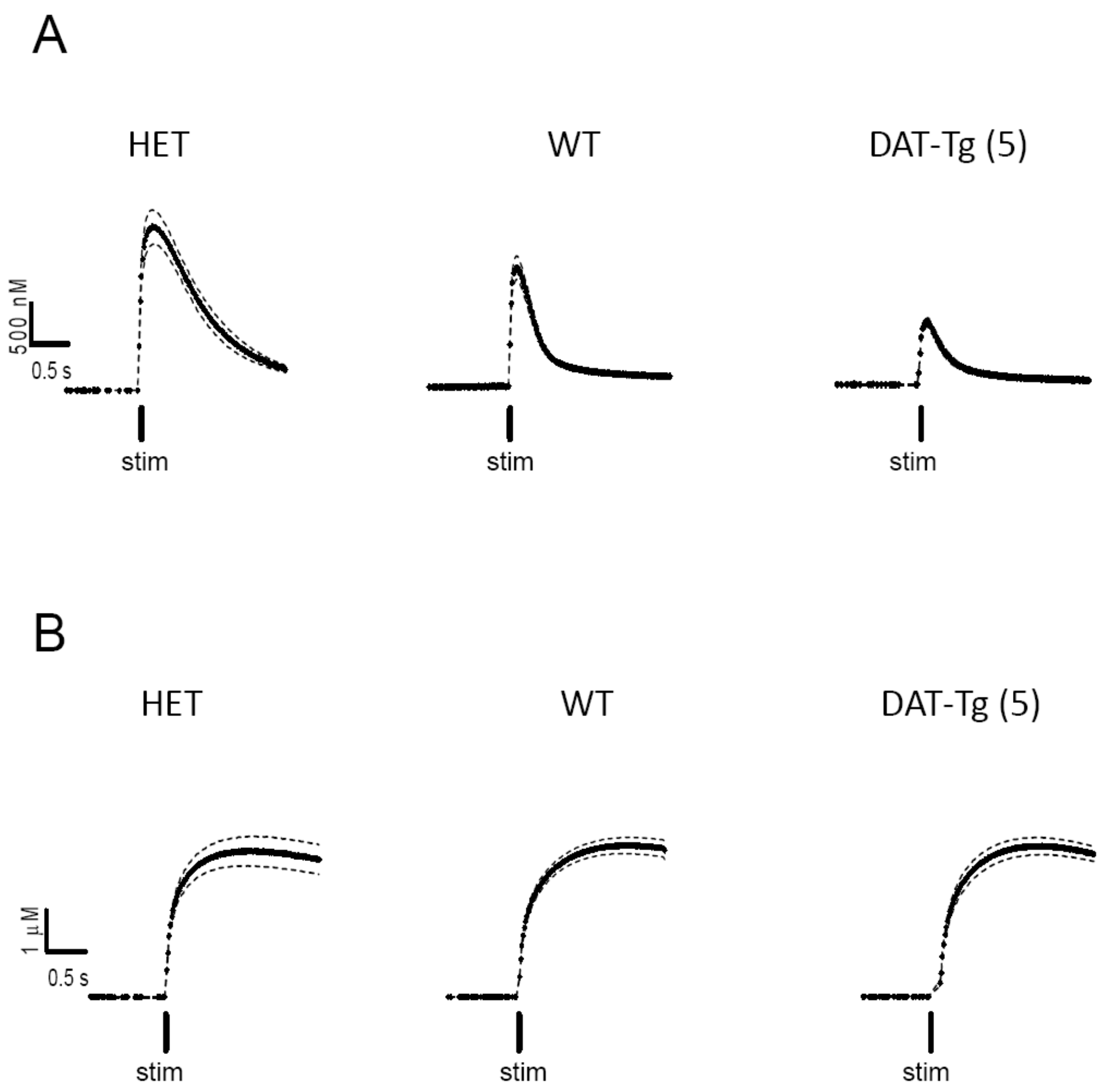


**Figure 4.7** Release differences are abolished by uptake blockade. A) The amount of dopamine released (as measured at the electrode) for a single pulse stimulation (n = 4, each genotype) decreases with increasing DAT expression. B) The application of DAT inhibitor PTT abolishes the perceived difference in dopamine release (n = 4, each gentoype) when evoked by the same single pulse stimulation.

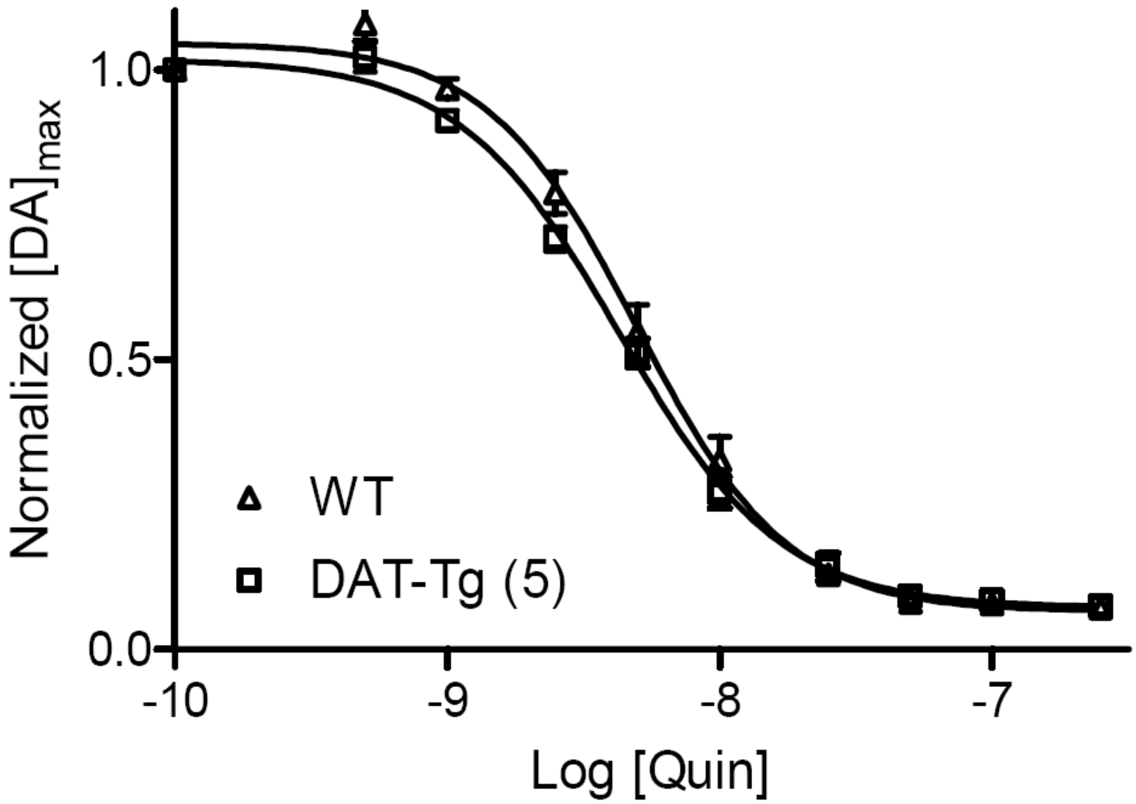


**Figure 4.8** Autoreceptor efficacy in DAT-Tg (5) animals. Application of ascending concentrations of $D_2$-agonist quinelorane causes a decrease in stimulated dopamine release. There is no significant difference ($p > 0.05$, $n = 5$) in the efficacy of quinelorane in DAT-Tg (5) animals compared to WT animals. The $EC_{50}$ of quinelorane in WT and DAT-Tg animals were $4.9 \pm 1.1$ nM and $4.3 \pm 1.1$ nM respectively.

different ($p > 0.05$). These values are similar to values found in the literature for quinelorane at $D_2$-autoreceptors but much higher than the $EC_{50}$ of the $D_2$ agonist quinpirole (Bates et al., 1991; Mercier et al., 2001).

*Behavioral Phenotypes of DAT Transgenic Animals*

Injection of 3 mg/kg amphetamine to WT animals and DAT-Tg (5) animals has a dramatically different effect on locomotion (Figure 4.9). The basal movement level taken for 60 minutes prior to injection was the same for WT mice and DAT-Tg (5) animals (Figure 4.9). Upon injection of 3 mg/kg amphetamine *i.p.* the DAT-Tg (5) animals undergo greater behavioral activation than WT animals for the first 30 minutes after drug. After 30 minutes, both genotypes show a similar increase in behavioral activation over baseline.

The behavioral activation seen in DAT-Tg animals is not due to a difference in dopamine reverse transport caused by amphetamine. The ability of amphetamine to induce reverse transport in WT animals and DAT-Tg (5) animals was evaluated using FSCV in striatal brain slices. Vesicular dopamine was first depleted by application of 10 µM tetrabenazine, a VMAT2 inhibitor that does not cause reverse transport alone (Jones et al., 1998). The application of tetrabenazine eliminates stimulated dopamine release after 1 hour. During this time period, presynaptic dopamine was protected from breakdown by monamine oxidase (MAO) using 20 µM pargyline, an MAO inhibitor (Rice et al., 1997). Application of 20 µM amphetamine to the superfusion buffer after vesicular depletion results in a dramatic rise in the amount of basal dopamine as measured by a shift in the FSCV background current (Figure 4.10). The baseline rise seen after depletion mimics that seen with direct application of amphetamine to striatal brain slices (Jones et al., 1998). Cyclic voltammograms taken at the ½ $[DA]_{max}$ for WT and DAT-Tg (5) slices confirm that the measured signal increase is dopamine. The rate of reverse transport is the same in WT and

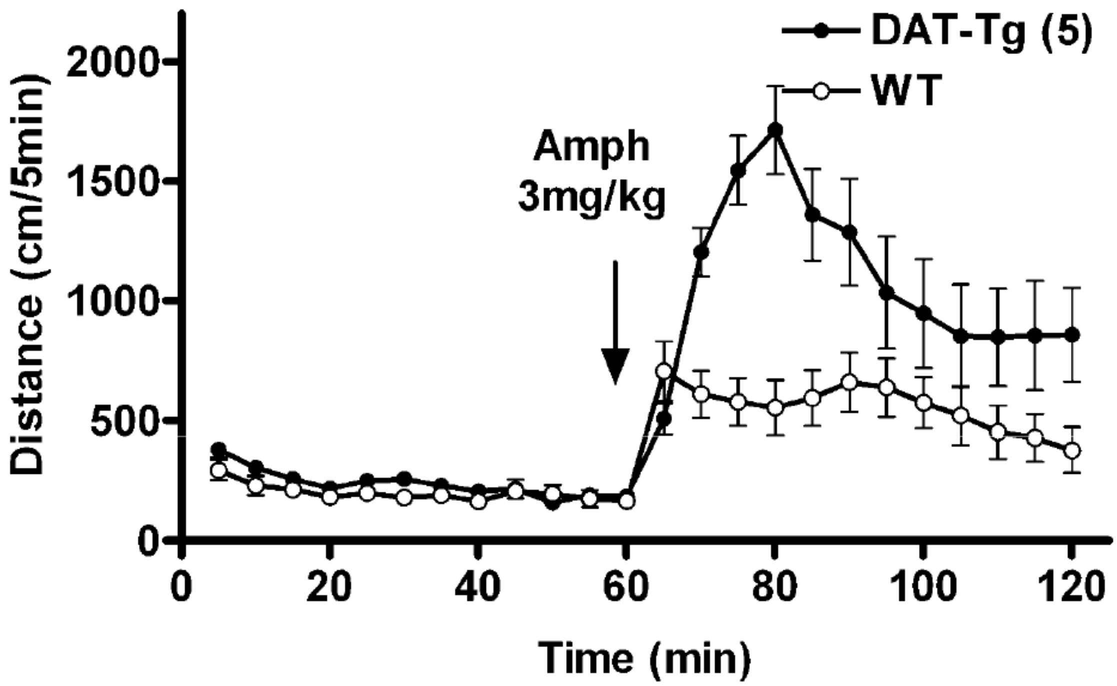


**Figure 4.9** Behavioral activation induced by amphetamine injection. The distance traveled shown per 5 minute interval for WT and DAT-Tg (5) mice, there is no difference in locomotion prior to amphetamine injection. An ip injection of 3 mg/kg amphetamine causes greater behavioral activation in DAT-Tg (5) animals compared to WT control animals for the first 30 minutes. After 30 minutes, DAT-Tg (5) animals are still facilitated to a greater extent than WT animals, a level above baseline.

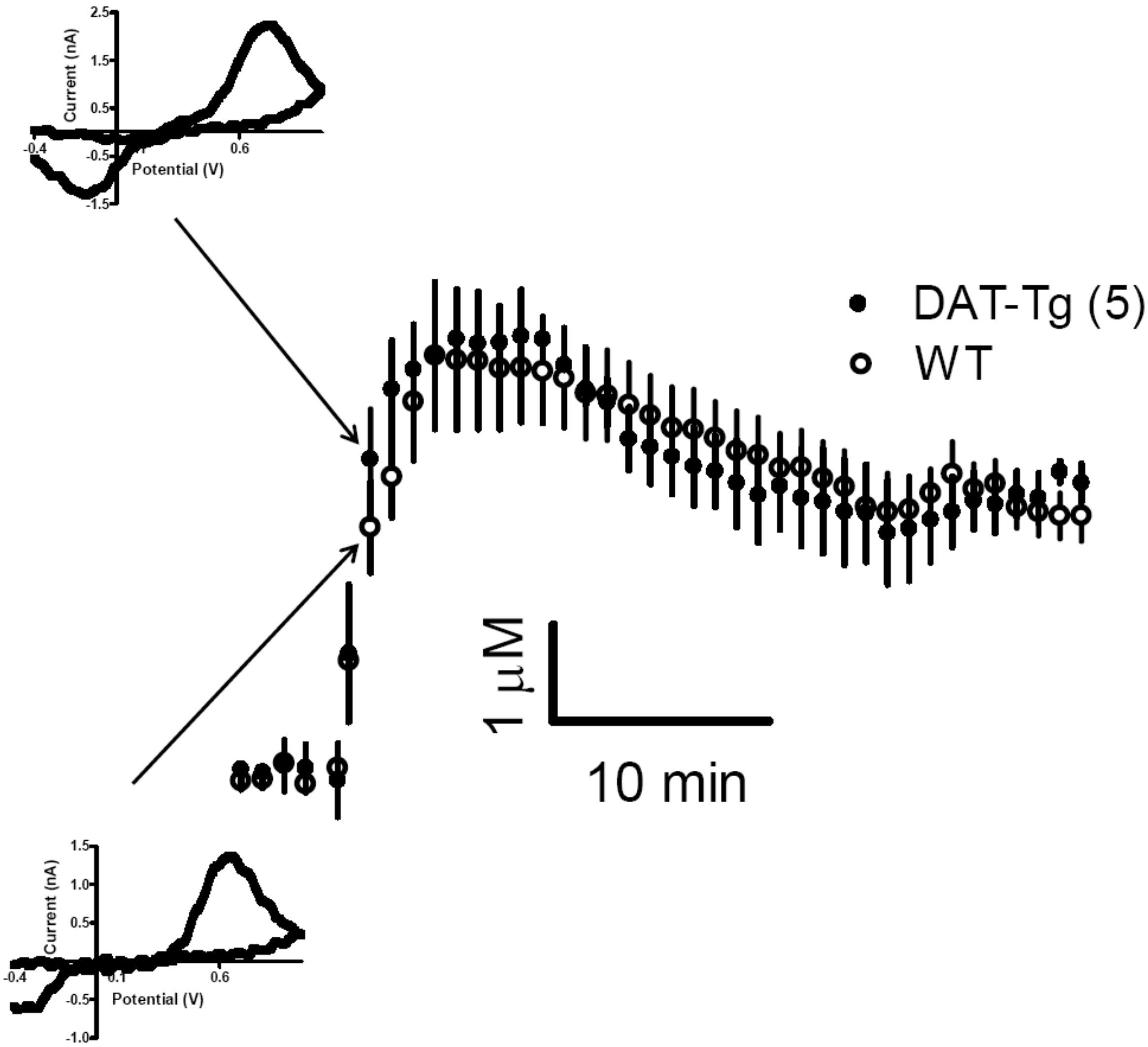


**Figure 4.10** Basal dopamine concentration changes due to amphetamine application. Vesicular dopamine stores were depleted by application of VMAT2 inhibitor tetrabenazine (10 µM) and protected by enzymatic degradation by 20 µM pargyline (an MAOI). Application of 20 µM amphetamine facilitated a rise in the basal dopamine concentrations to 4.5 µM dopamine for both genotypes with 50 % $[DA]_{max}$ reached 2 ½ minutes after onset (data reduced to 10 second intervals for clarity). Cyclic voltammograms taken at the 50 % of $[DA]_{max}$ confirm the measured substance is dopamine. No differences (n = 5, both gentoypes) were seen in the rise time or $[DA]_{max}$ between DAT-Tg (5) and WT animals.

DAT-Tg animals with the ½ $[DA]_{max}$ occurring ~2 minutes after onset (which is approximately 5 ½ minutes after drug application). In addition, the amount of dopamine released is not significantly different ($p > 0.05$) in slices from WT and DAT-Tg animals being 4.4 ± 0.77 μM and 4.6 ± 0.49 μM respectively. The magnitude and time course of the shifts in the basal dopamine concentration as a result of amphetamine application does not depend on the number of dopamine transporters on the membrane surface when tetrabenazine has been used to deplete vesicular stores.

## Discussion

### *DAT Expression and Dopamine Uptake*

The relationship between the amount of expressed dopamine transporter and the rate of dopamine uptake has been described using transgenic mouse models. The pronuclear injection of the DAT locus facilitates the integration of four additional DAT gene copies and a 300 % increase in DAT protein (Figure 4.1). Increased protein expression does not linearly translate to increased membrane bound transporter; therefore, immunogold-silver staining was used to asses the compartmentalized expression of DAT in striatal tissue (Figure 4.2). DAT expression was shown to be increased on the membrane as well as within intracellular compartments in DAT-Tg (6) animals.

Stimulated dopamine release in the caudate putamen is bi-phasic consisting of an immediate rise in dopamine concentration followed by clearance of dopamine through DAT. As Figure 4.3 shows, the shape of stimulated dopamine release in striatal brain slices is dependent on the amount of transporter available. Of particular interest is the lack of any clearance in a DAT KO animal supporting the assertion that DAT is the primary clearance mechanism for dopamine (Garris and Wightman, 1995; Giros et al., 1996). Increased expression of DAT in WT animals increases the rate of dopamine uptake in striatal brain slices after stimulated release as indicated by two electrochemical techniques: FSCV and amperometry (Figure 4.4). Simplex modeling of FSCV traces collected from three different transgenic models supports the assertion made by Michaelis-Menten kinetic theory: $V_{max}$ scales with the amount of expressed dopamine transporter. Figure 4.5A shows compiled $V_{max}$ values from animals expressing a range of transporter amounts. Increased transporter causes a significant increase in $V_{max}$ while a decrease in transporter causes as significant decrease in the $V_{max}$ for dopamine uptake. The increased maximal uptake rate documented in DAT-Tg (6) animals (Salahpour et al., 2008) is independent of a change in the binding affinity of dopamine for DAT with both animals showing $K_m$ (Figure 4.5B)(Salahpour et al., 2008) values similar to those reported previously in rats (Near et al., 1988). The increased $V_{max}$ for DAT-Tg animals (about 60 %) is not proportional to the 250 % increase in membrane associated DAT protein reported by Salahpour et al. (2008). It is much closer to the reported 30 % enhancement in synaptic plasma membrane associated DAT in these animals (Salahpour et al., 2008). These data indicate that there is a component of DAT trafficking that limits the amount of membrane associated protein available to participate in uptake. A multitude of proteins have been shown to interact with the DAT (Torres, 2006) some of which may have altered expression levels in DAT-Tg animals. Increasing the expression of proteins designed to limit DAT surface expression would decrease the impact of such a drastic change in transporter protein levels during development. This ceiling effect on DAT membrane expression may also explain why there is little difference in the uptake rates of DAT-Tg (5) and DAT-Tg (6) animals even though a very large difference in uptake is seen between HET and WT animals (Figure 4.5A).

*DAT Expression and Dopamine Levels*

The amount of dopamine incident on synaptic targets is a balance between release and uptake events. Dopamine is thought to act through volume transmission (Rice and

Cragg, 2008); an assertion supported by perisynaptic expression of DAT in the dorsolateral striatum (Figure 4.2). We show a significant decrease in stimulated dopamine release from striatal brain slices of DAT-Tg (5) and DAT-Tg (6) animals compared to WT animals; a reduction coincident with lower extracellular dopamine levels as determined by *in vivo* microdialysis (Salahpour et al., 2008). Conversely, an increase in $[DA]_{max}$ is seen in HET animals similar to the signal increase characteristic of pharmacological uptake inhibition (Jones et al., 1995; Lee et al., 2001). There is no clear indication whether the differences in $[DA]_{max}$ found in DAT-Tg animals are due solely to differences in uptake or if they have a release component. The DAT-Tg (6) animals have neurodegeneration indicated by a lower striatal dopamine total content value relative to WT animals (6 µg/g for DAT-Tg (6) vs. 12 µg/g for WT). However, there must be some contribution from uptake to the differences in stimulated $[DA]_{max}$ because no total content abnormalities were documented between WT, HET, and DAT-Tg (5) animals. The ability of the uptake blocker PTT to normalize the release of WT, HET, and DAT-Tg (5) animals supports the hypothesis that the uptake rate in part controls the amount of dopamine able to contact the electrode. Unfortunately, the PTT data does not prove this effect because it is a cocaine analog and cocaine has been shown to alter dopamine release properties (Chapter 3) (Venton et al., 2006). These data clearly demonstrate how intertwined dopamine release and uptake events are when it relates to extracellular dopamine concentrations.

The presynaptic $D_2$ autoreceptor is coupled to and a modulator of the DAT (Ralph et al., 2001; Bertolino et al., 2009). Mice lacking the $D_2$ autoreceptor show decreased DAT function in the dorsolateral striatum (Dickinson et al., 1999). Conversely, mice lacking the DAT lack $D_2$ modulation of stimulated dopamine release (Jones et al., 1999). We investigated any release regulating autoreceptor changes in mice that overexpress the DAT using the $D_2$ agonist quinelorane to modulate stimulated dopamine release. Dopamine release is an indirect measure of autoreceptor function; however, it is the most pertinent in the context of a study on release and uptake in these animals. No difference in autoreceptor efficacy was documented in DAT-Tg (5) animals relative to WT animals. The hypodopaminergic state of DAT-Tg animals has been shown to affect the expression and efficacy of post-synaptic $D_2$ receptors in the striatum (Ghisi et al., 2009). Our data suggests that the receptor change does not translate to the presynaptic terminal or that presynaptic $D_2$ receptor modifications are not affecting stimulated dopamine release to a different degree than WT mice.

*Amphetamine Action on Dopamine Terminals*

Behavioral activation due to amphetamine is altered in mice overexpressing the dopamine transporter. Salahpour et al. (2008) found DAT-Tg (6) mice experienced greater behavioral activation when exposed to amphetamine; a result not duplicated with cocaine, GBR-12909, or methylphenidate. Amphetamine caused a 400 % increase over basal dopamine levels in DAT-Tg (6) animals compared with a 200 % increase in WT animals (Salahpour et al., 2008). These data are consistent with the theory that many amphetamine effects are dependent on the expression level of DAT. Accordingly, amphetamine is unable to facilitate dopamine reverse transport in DAT KO animals (Jones et al., 1998). A second behavioral study was done in DAT-Tg (5) and WT animals to rule out the contribution of neuronal degeneration on the behavioral activation in DAT-Tg (6) animals. After a 60 minute habituation period, the introduction of 3 mg/kg amphetamine causes a drastic increase in the movement of DAT-Tg (5) animals over that seen in WT animals (Figure 4.9). This behavioral activation is independent of a change in the rate or magnitude of reverse transport in DAT-Tg (5) when cytosolic dopamine levels have first been increased by tetrabenazine (Figure 4.10). Therefore, a pathway independent of reverse transport but related to DAT expression is causing the increase in basal dopamine levels. A possible mechanism may be related to the accumulation of presynaptic amphetamine through DAT. Increased transporter expression would facilitate greater amphetamine accumulation within the presynaptic terminal because amphetamine can utilize the transporter to enter the presynaptic terminal (Jones et al., 1998). Increased amphetamine accumulation will enhance VMAT2 blockade and end point inhibition of tyrosine hydroxylase (Kehr et al., 1977; Wallace and Connell, 2008) in DAT-Tg (5) animals without altering the rate of reverse transport.

Our experiments do not rule out a post-synaptic component to the amphetamine effect; $D_1$ and $D_2$ receptors are upregulated in DAT-Tg mice (Ghisi et al., 2009). A postsynaptic pathway would be affected equally by increased extracellular dopamine levels. Traditional uptake blockers are able to increase extracellular dopamine but not to a level high enough to cause preferential activation in DAT-Tg animals. Amphetamine must be able to increase extracellular dopamine tone to a greater extent than these drugs. Cocaine, GBR, and methylphenidate are impulse dependent drugs meaning they require continued vesicular release to have an effect. As these drugs begin to act, they increase extracellular dopamine which inhibits further dopamine release by acting on autoreceptors (Kita et al., 2007). The negative feed back loop of the autoreceptors would put a ceiling on the effectiveness of these drugs at increasing dopamine tone. Amphetamine is able to increase dopamine tone to a greater extent by utilizing reverse transport through the DAT, an impulse flow independent pathway unaffected by autoreceptor modulation. It is hypothesized that amphetamine would be able to induce a larger increase in dopamine tone in both animals. Increased dopamine tone would act on the increased number of $D_1$ and $D_2$ receptors in DAT-Tg (5) animals causing behavioral activation.

## Literature Cited


Bates MD, Senogles SE, Bunzow JR, Liggett SB, Civelli O, Caron MG (1991) Regulation of responsiveness at D2 dopamine receptors by receptor desensitization and adenylyl cyclase sensitization. Mol Pharmacol 39:55-63.

Baur JE, Kristensen EW, May LJ, Wiedemann DJ, Wightman RM (1988) Fast-scan voltammetry of biogenic amines. Anal Chem 60:1268-1272.

Bertolino A, Fazio L, Di Giorgio A, Blasi G, Romano R, Taurisano P, Caforio G, Sinibaldi L, Ursini G, Popolizio T, Tirotta E, Papp A, Dallapiccola B, Borrelli E, Sadee W (2009) Genetically determined interaction between the dopamine transporter and the D2 receptor on prefronto-striatal activity and volume in humans. J Neurosci 29:1224-1234.

Dickinson SD, Sabeti J, Larson GA, Giardina K, Rubinstein M, Kelly MA, Grandy DK, Low MJ, Gerhardt GA, Zahniser NR (1999) Dopamine D2 receptor-deficient mice exhibit decreased dopamine transporter function but no changes in dopamine release in dorsal striatum. J Neurochem 72:148-156.

Dougherty DD, Bonab AA, Spencer TJ, Rauch SL, Madras BK, Fischman AJ (1999) Dopamine transporter density in patients with attention deficit hyperactivity disorder. Lancet 354:2132-2133.

Garris PA, Wightman RM (1995) Distinct pharmacological regulation of evoked dopamine efflux in the amygdala and striatum of the rat in vivo. Synapse 20:269-279.

Ghisi V, Ramsey AJ, Masri B, Gainetdinov RR, Caron MG, Salahpour A (2009) Reduced D2-mediated signaling activity and trans-synaptic upregulation of D1 and D2 dopamine receptors in mice overexpressing the dopamine transporter. Cell Signal 21:87-94.

Giros B, Jaber M, Jones SR, Wightman RM, Caron MG (1996) Hyperlocomotion and indifference to cocaine and amphetamine in mice lacking the dopamine transporter. Nature 379:606-612.

Goodwin JS, Larson GA, Swant J, Sen N, Javitch JA, Zahniser NR, De Felice LJ, Khoshbouei H (2009) Amphetamine and methamphetamine differentially affect dopamine transporters in vitro and in vivo. J Biol Chem 284:2978-2989.

Han W, Saegusa H, Zong S, Tanabe T (2002) Altered cocaine effects in mice lacking Ca(v)2.3 (alpha(1E)) calcium channel. Biochem Biophys Res Commun 299:299-304.

Jones SR, Garris PA, Wightman RM (1995) Different effects of cocaine and nomifensine on dopamine uptake in the caudate-putamen and nucleus accumbens. J Pharmacol Exp Ther 274:396-403.

Jones SR, Gainetdinov RR, Wightman RM, Caron MG (1998) Mechanisms of amphetamine action revealed in mice lacking the dopamine transporter. J Neurosci 18:1979-1986.

Jones SR, Gainetdinov RR, Hu XT, Cooper DC, Wightman RM, White FJ, Caron MG (1999) Loss of autoreceptor functions in mice lacking the dopamine transporter. Nat Neurosci 2:649-655.

Kehr W, Speckenbach W, Zimmermann R (1977) Interaction of haloperidol and gamma-butyrolactone with (+)-amphetamine-induced changes in monoamine synthesis and metabolism in rat brain. J Neural Transm 40:129-147.

Kita JM, Parker LE, Phillips PE, Garris PA, Wightman RM (2007) Paradoxical modulation of short-term facilitation of dopamine release by dopamine autoreceptors. J Neurochem 102:1115-1124.

Krause J, Krause KH, Dresel SH, la Fougere C, Ackenheil M (2006) ADHD in adolescence and adulthood, with a special focus on the dopamine transporter and nicotine. Dialogues Clin Neurosci 8:29-36.

Lee TH, Balu R, Davidson C, Ellinwood EH (2001) Differential time-course profiles of dopamine release and uptake changes induced by three dopamine uptake inhibitors. Synapse 41:301-310.

Mercier D, Falardeau P, Levesque D (2001) Autoreceptor preference of dopamine D2 receptor agonists correlates with preferential coupling to cyclic AMP. Neuroreport 12:1473-1479.

Near JA, Bigelow JC, Wightman RM (1988) Comparison of uptake of dopamine in rat striatal chopped tissue and synaptosomes. J Pharmacol Exp Ther 245:921-927.

Ralph RJ, Paulus MP, Fumagalli F, Caron MG, Geyer MA (2001) Prepulse inhibition deficits and perseverative motor patterns in dopamine transporter knock-out mice: differential effects of D1 and D2 receptor antagonists. J Neurosci 21:305-313.

Rice ME, Cragg SJ (2008) Dopamine spillover after quantal release: rethinking dopamine transmission in the nigrostriatal pathway. Brain Res Rev 58:303-313.

Rice ME, Cragg SJ, Greenfield SA (1997) Characteristics of electrically evoked somatodendritic dopamine release in substantia nigra and ventral tegmental area in vitro. J Neurophysiol 77:853-862.

Salahpour A, Ramsey AJ, Medvedev IO, Kile B, Sotnikova TD, Holmstrand E, Ghisi V, Nicholls PJ, Wong L, Murphy K, Sesack SR, Wightman RM, Gainetdinov RR, Caron MG (2008) Increased amphetamine-induced hyperactivity and reward in mice overexpressing the dopamine transporter. Proc Natl Acad Sci U S A 105:4405-4410.

Schramm-Sapyta NL, Olsen CM, Winder DG (2006) Cocaine self-administration reduces excitatory responses in the mouse nucleus accumbens shell. Neuropsychopharmacology 31:1444-1451.

Sora I, Hall FS, Andrews AM, Itokawa M, Li XF, Wei HB, Wichems C, Lesch KP, Murphy DL, Uhl GR (2001) Molecular mechanisms of cocaine reward: combined dopamine and serotonin transporter knockouts eliminate cocaine place preference. Proc Natl Acad Sci U S A 98:5300-5305.

Sulzer D, Sonders MS, Poulsen NW, Galli A (2005) Mechanisms of neurotransmitter release by amphetamines: a review. Prog Neurobiol 75:406-433.

Torres GE (2006) The dopamine transporter proteome. J Neurochem 97 Suppl 1:3-10.

Torres GE, Amara SG (2007) Glutamate and monoamine transporters: new visions of form and function. Curr Opin Neurobiol 17:304-312.

Uhl GR, Lin Z (2003) The top 20 dopamine transporter mutants: structure-function relationships and cocaine actions. Eur J Pharmacol 479:71-82.

Uhl GR, Hall FS, Sora I (2002) Cocaine, reward, movement and monoamine transporters. Mol Psychiatry 7:21-26.

Venton BJ, Troyer KP, Wightman RM (2002) Response times of carbon fiber microelectrodes to dynamic changes in catecholamine concentration. Anal Chem 74:539-546.

Venton BJ, Seipel AT, Phillips PE, Wetsel WC, Gitler D, Greengard P, Augustine GJ, Wightman RM (2006) Cocaine increases dopamine release by mobilization of a synapsin-dependent reserve pool. J Neurosci 26:3206-3209.

Volkow ND, Wang GJ, Newcorn J, Fowler JS, Telang F, Solanto MV, Logan J, Wong C, Ma Y, Swanson JM, Schulz K, Pradhan K (2007) Brain dopamine transporter levels in treatment and drug naive adults with ADHD. Neuroimage 34:1182-1190.

Wallace LJ, Connell LE (2008) Mechanisms by which amphetamine redistributes dopamine out of vesicles: a computational study. Synapse 62:370-378.

Wang YM, Gainetdinov RR, Fumagalli F, Xu F, Jones SR, Bock CB, Miller GW, Wightman RM, Caron MG (1997) Knockout of the vesicular monoamine transporter 2 gene results in neonatal death and supersensitivity to cocaine and amphetamine. Neuron 19:1285-1296.

White IM, Doubles L, Rebec GV (1998) Cocaine-induced activation of striatal neurons during focused stereotypy in rats. Brain Res 810:146-152.

# Chapter 5

Mitochondrial Proteins and Dopamine Release

## Introduction

Uncoupling protein 2 (UCP2) belongs to a family of five mitochondrial uncoupling proteins believed to regulate adenosine triphosphate (ATP) formation. UCPs are believed to differ substantially in location and function in comparison with UCP1 (expressed solely in brown adipose tissue), the best understood uncoupling protein. UCP2 is expressed at relatively low levels in the brain when compared to other UCPs such as UCP4 (Alan et al., 2009), however it is believed to play a vital role in local thermogenesis, $Ca^{2+}$ regulation, ATP formation, and superoxide protection within nerve terminals (Zhang et al., 2001; Horvath et al., 2003). Figure 5.1 shows the inner mitochondrial membrane through which ATP is generated in nerve terminals. Protons generated by the electron-transport chain accumulate in the intermembrane space, altering the inner membrane potential. As protons build up in this space they can move back across the inner mitochondrial membrane through ATP synthase (Figure 5.1), a process that generates ATP. UCP2 is believed to provide an alternate route that allows protons to pass into the inner mitochondrial space and bypass ATP synthase, effectively uncoupling the electron-transport chain from ATP synthesis (Figure 5.1) (Horvath et al., 2003). A byproduct of this uncoupling is a decrease in formation of radical oxygen species that are generated when electrons leak from the electron-transport chain (Negre-Salvayre et al., 1997), a natural but undesirable process. Some believe that

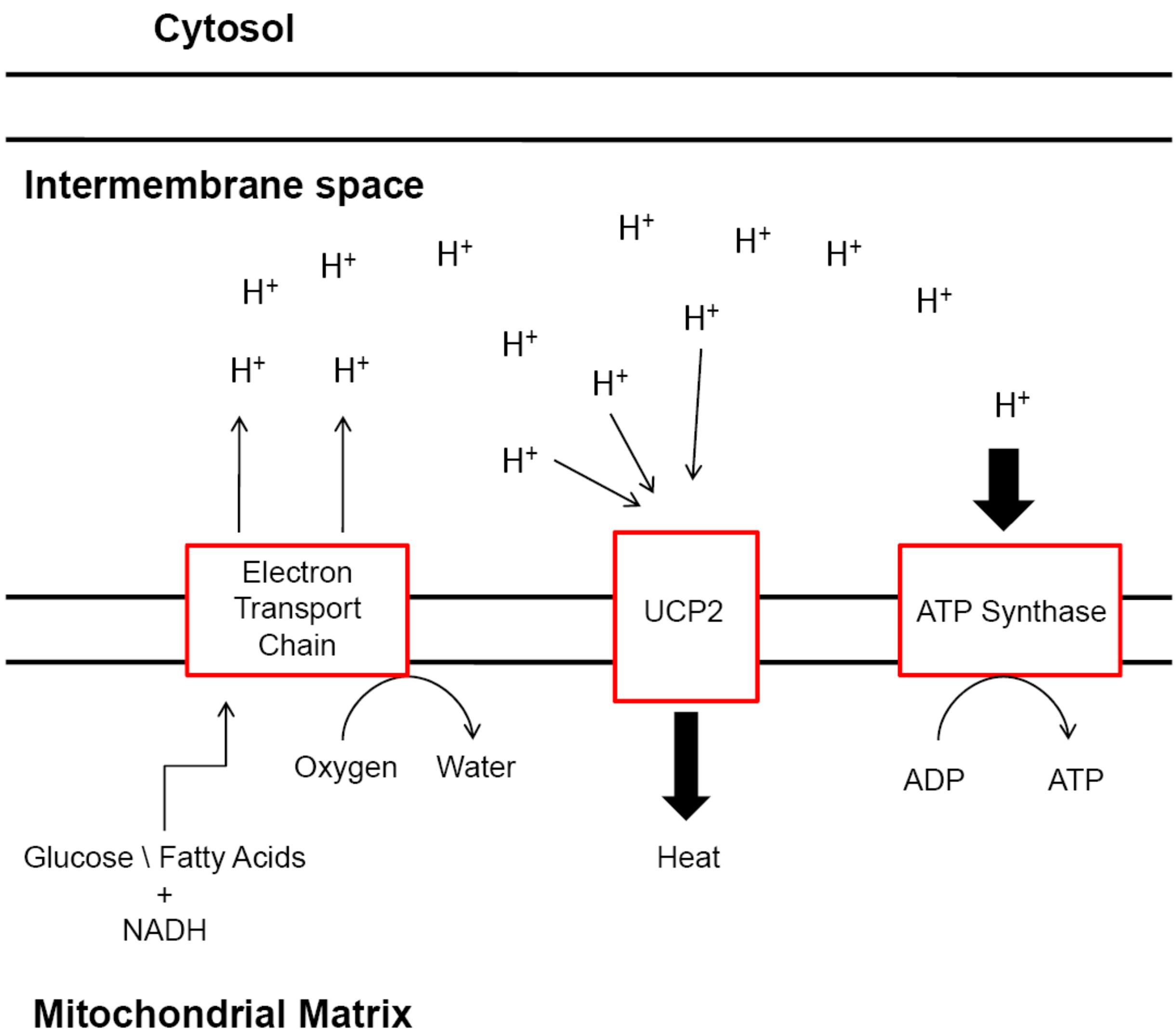


**Figure 5.1** Uncoupling Protein 2 (UCP2) is expressed on the inner mitochondrial membrane. The electron transport chain establishes a proton ($H^+$) gradient within the mitochondria. Protons travel along their concentration gradient through ATP synthase generating ATP. UCP2 allows protons to flow into the mitochondrial matrix without generating ATP.

UCP2 regulation of ATP generation only occurs in response to oxidative stress to help limit cell damage from radical oxygen species (Echtay, 2007). However, other studies have shown that UCP2 accounts for 50 % of the nominal proton leak in resting cells and that animals lacking UCP2 have increased ATP levels compared to WT animals (Krauss et al., 2002).

A large number of processes in the nerve terminal are dependent on the energy state of the neuron. For example, vesicle packaging and recycling, calcium buffering, and vesicle mobility are all ATP-dependent processes (Burgoyne and Morgan, 2003; Chen et al., 2003; Stokes and Green, 2003). No firm hypothesis has been generated as to which aspects of neuronal transmission will be affected by knocking out UCP2 (Horvath et al., 2003). However, clues come from 1-methyl-4-phenyl-1,2,3,6-tetrahydropyridine (MPTP), an agent that specifically causes mitochondrial disruption in dopaminergic neurons. MPTP enters dopamine terminals by uptake through the dopamine transporter (DAT) where it is metabolized to 1-methyl-4-phenylpyridinium (MPP+) by monoamine oxidase B (MAOB). MPP+ passes through the mitochondrial membrane where it interferes with complex I in the electron-transport chain enhancing electron leakage and formation of radical oxygen species (Sayre, 1989; Mizuno et al., 1990). Accumulated free radical oxygen species cause oxidative damage, eventually leading to cell death. It remains unclear exactly how UCP2, endogenously expressed in nigrostriatal dopamine cell bodies (Figure 5.2) (Conti et al., 2005), may be related to this toxicity. However, overexpression of UCP2 and UCP4 have been shown to decrease MPTP induced neurotoxicity in dopamine neurons (Conti et al., 2005; Chu et al., 2009), presumably by alleviating the free radical buildup associated with MPP+ action in mitochondria. The question remains: How does the deletion of UCP2 affect the normal function of the nigrostriatal dopamine pathway?

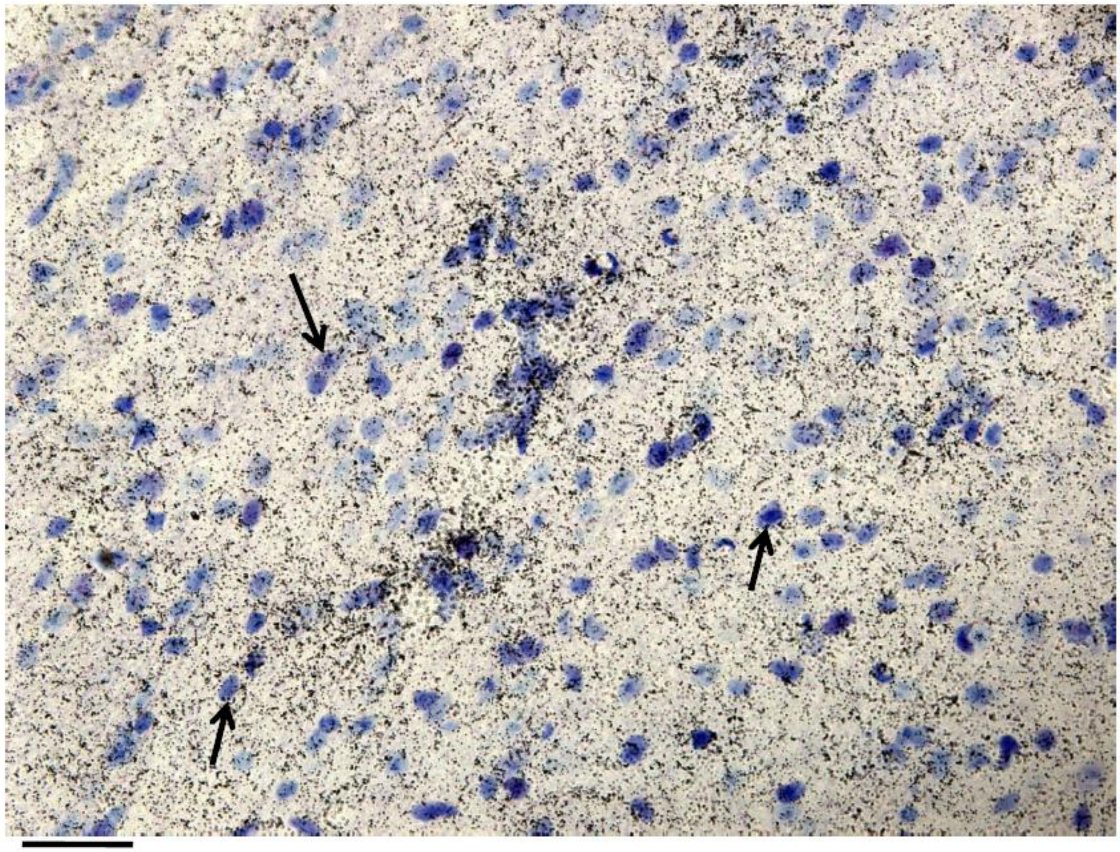

**Figure 5.2** *In situ* hydridization in the substantia nigra pars compacta. Slices (25 µm in thickness) were labeled using a nuclear stain and a ribosomal probe. Cell bodies are visualized in blue (black arrows). A $^{35}$S-labeled riboprobe as described in Parton *et al.* (2007) was used to visualize locations of UCP2 expression (black dots). There is co-localization between dopamine neuron cell bodies and UCP2. Additionally, UCP2 appears to be expressed in some of the terminal regions surrounding the cell bodies. The terminals innervating dopamine cell bodies in the compacta are primarily glutamate, GABA, and 5-HT. Scale bar 20 µm.

This chapter focuses on the role played by UCP2 in the modulation of dopamine release in caudate putamen brain slices. Electrically stimulated dopamine release in striatal brain slices of UCP2 KO animals was found to be enhanced compared to WT animals and coincided with an increase in the maximal rate of dopamine uptake ($V_{max}$). Application of the UCP2 cross-linker genipin was used to show that the effects of knocking out UCP2 are not acute (less than 2 hours), but are most likely due to adaptive changes within the terminal.

**Materials and Methods**

A full description of techniques used in this chapter can be found in Chapter 2. *In situ* hybridization of dopaminergic neurons in the substantia nigra compacta was performed as previously described (Parton et al., 2007).

**Disclaimer**

This chapter shows data taken as part of a collaboration with the lab of Dr. Brad Lowell at Beth Israel Deaconess Hospital in Boston, Massachusetts. My direct contact person at that lab provided me with the genetic identities of all mice used in this study. This contact was recently removed from his/her position due to academic misconduct in regards to the study on UCP2 and how its expression is altered in obese animals. The genetic identities of the animals provided to me have in one form or another been confirmed by the Lowell lab as being correct. Therefore, I stand behind the results shown here and the conclusions drawn from them. Unfortunately, many of the hypotheses tested in this chapter were based on data that is now in question. To this end, this chapter will only show data that has been confirmed to be accurate and will serve as a preliminary discussion of possible mechanisms.

## Results

*UCP2 Expression in the Substantia Nigra pars Compacta*

To verify literature reports that UCP2 is present in the mitochondrial membrane of dopamine neurons, *in situ* hydridization was used. *In situ* hybridization of UCP2 mRNA was performed on brain slices containing the substantia nigra pars compacta. Slices (25 µm thickness) were taken containing dopamine midbrain neurons and stained to visualize cell bodies in blue, several of which are denoted by black arrows (Figure 5.2). The location of UCP2 mRNA was visualized using $^{35}$S-labeled riboprobes (black dots). There is UCP2 mRNA expression in the dopamine cell bodies of the zona compacta of the substantia nigra.

*Stimulated Neurotransmitter Release in Mouse Brain Slices*

Release and uptake of dopamine was evaluated in striatal brain slices containing the caudate putamen. Stimulated dopamine release was measured at several locations within the caudate putamen using FSCV. Dopamine release evoked by a single stimulus pulse in UCP2 KO animals was significantly larger ($p < 0.01$) than evoked dopamine release from WT slices (Figure 5.3A, n = 10 both genotypes). To determine if there was also a change in dopamine uptake, deconvolution and simplex modeling of the dopamine concentration traces were used. The $V_{max}$ of dopamine uptake in the striatum of UCP2 KO animals is significantly larger ($p < 0.01$, n =10 both genotypes) than that found in WT animals (Figure 5.4).

5-HT release in brain slices containing the substantia nigra pars reticulata was also evaluated using electrical stimulation and FSCV. The 5-HT released in response to a 20 pulse 100 Hz stimulation was not significantly altered in UCP2 KO mice compared to WT mice (Figure 5.3B) ($p > 0.05$, n = 10 both gentoypes). Uptake rates were also unchanged in this preparation (data not shown).

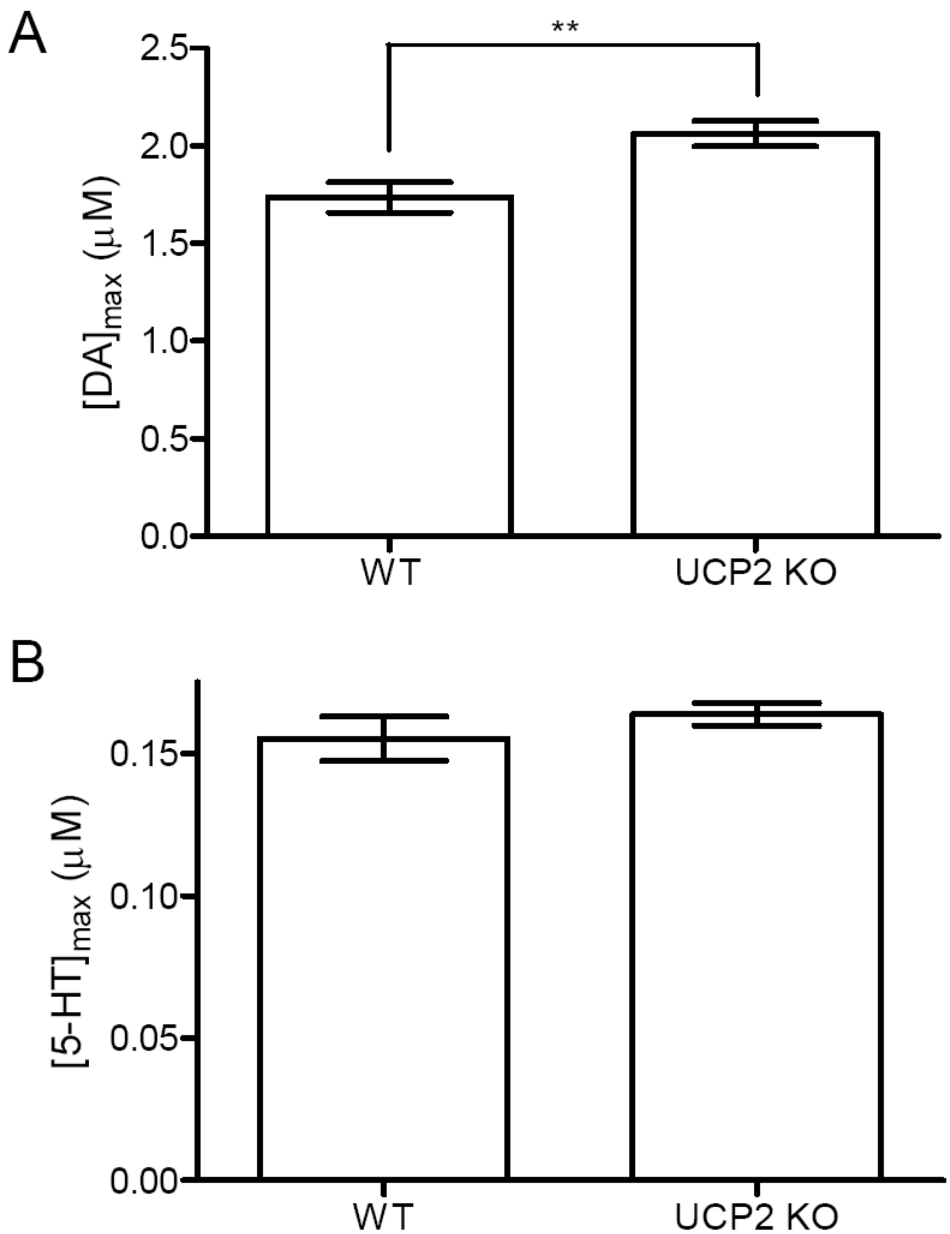


**Figure 5.3** UCP2 deficiency affects striatal dopamine release but not stimulated 5-HT release in the substantia nigra. A) Stimulated dopamine release in the caudate putamen of UCP2 KO mice is significantly enhanced relative to WT animals (** $p < 0.01$, one-way anova, $n = 10$ both genotypes). B) There is no significant difference in stimulated 5-HT release between WT animals or UCP2 KO animals ($p > 0.05$, $n \geq 9$, both genotypes).

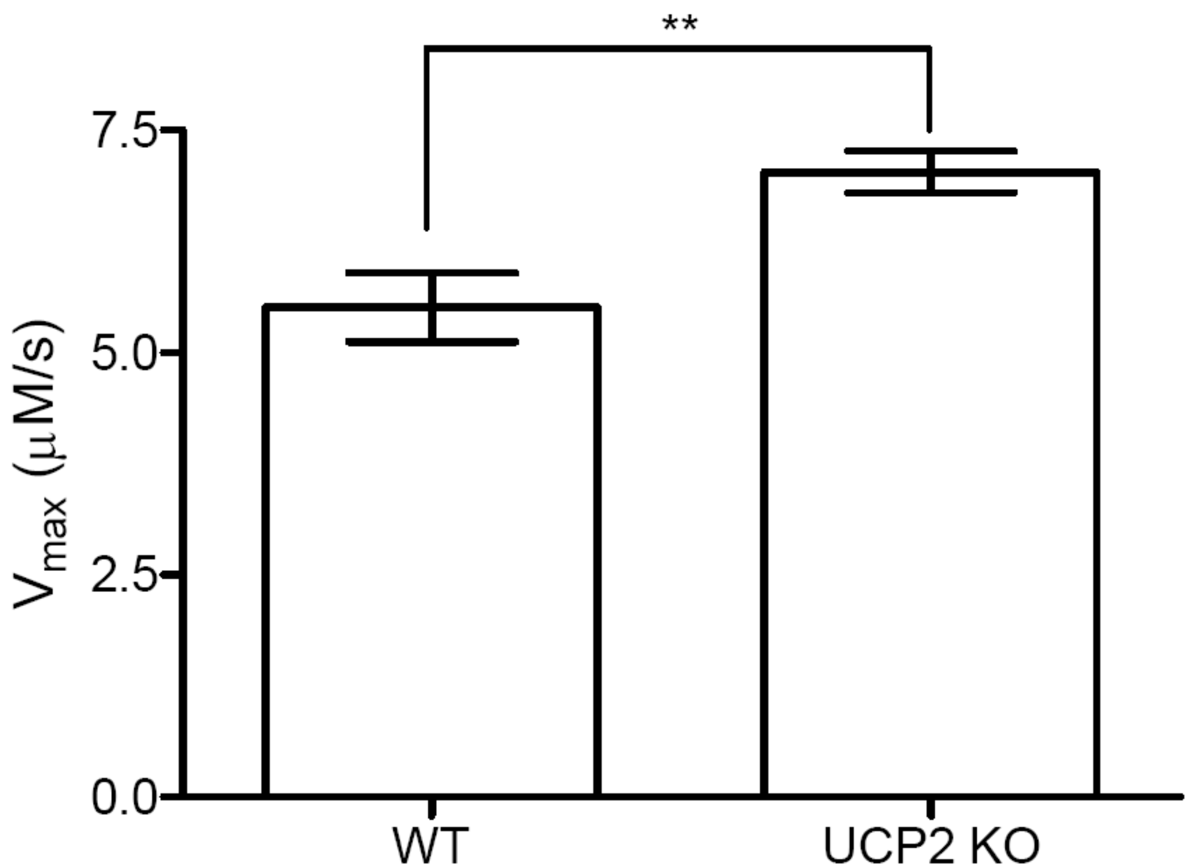


**Figure 5.4** The maximal rate of dopamine clearance is altered in UCP2 KO mice. Temporal deconvolution and simplex modeling were used to extract a $V_{max}$ value from the dopamine traces taken in the caudate putamen. As seen with dopamine release, the $V_{max}$ of dopamine uptake is significantly enhanced in UCP2 KO mice compared to WT animals (**, $p < 0.01$, one-way anova, $n = 5$ both genotypes).

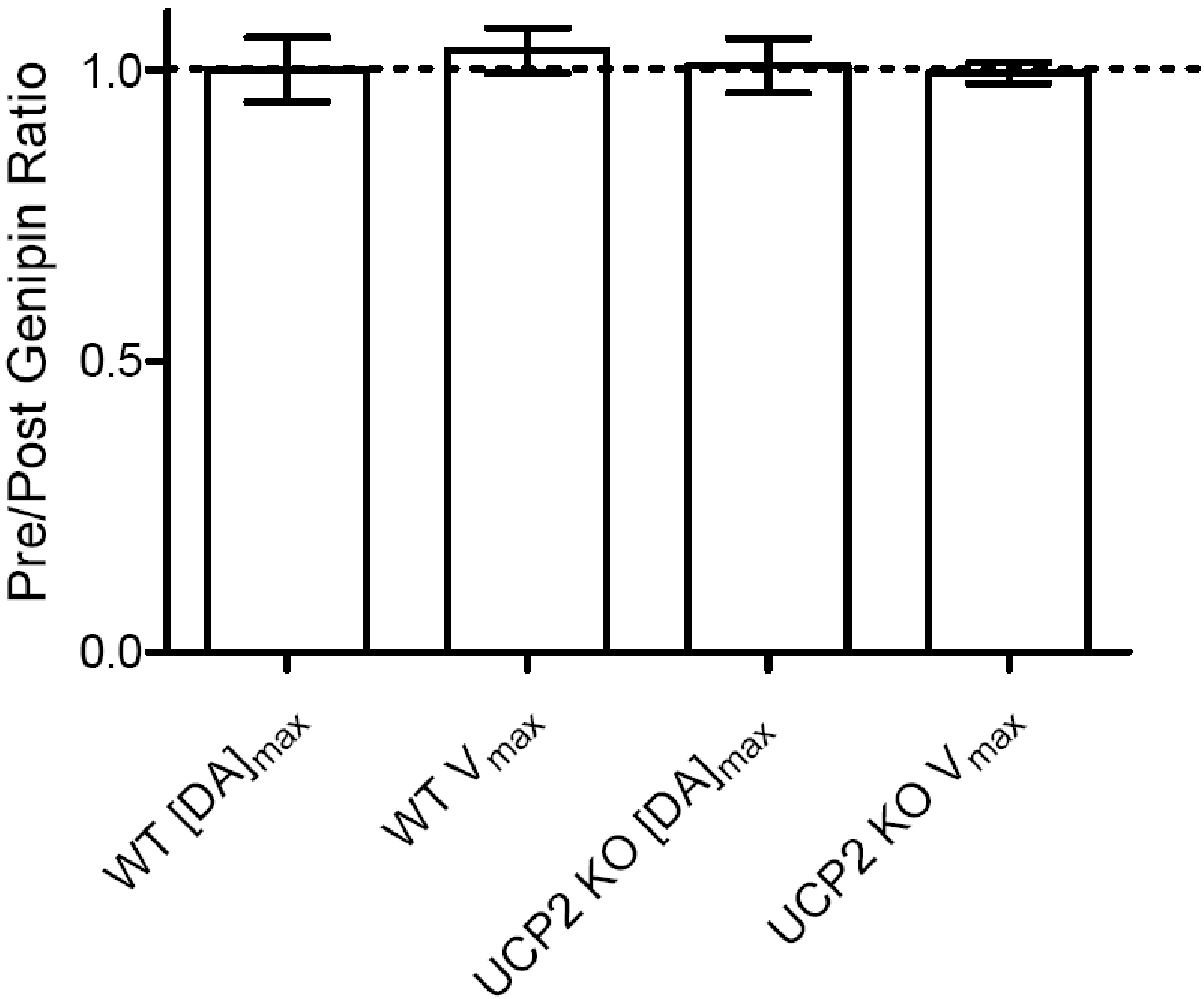


**Figure 5.5** Genipin modulation of dopamine release and uptake in mouse brain slices. The addition of 20 µM genipin to striatal brain slices for 35 minutes does not significantly ($p > 0.05$, $n = 5$ both genotypes) alter $[DA]_{max}$ or $V_{max}$ in WT mice when compared to UCP2 KO mice. In this experiment, the UCP2 KO mouse is the control animal because UCP2 KO mice are insensitive to genipin.

*Genipin Modulation of Dopamine Release*

Genipin, a UCP2 cross-linker (Zhou et al., 2009), was used in an attempt to acutely modulate dopamine release in striatal brain slices. A 20 µM dose of genipin was applied to striatal brain slices for 35 minutes, and then stimulated dopamine release was measured at three locations within the caudate. The dose and time frame used was previously shown to be sufficient to alter ATP levels in striatal synaptosomes (Lowell Lab, unpublished) and alter glucose sensing in pancreatic slices (Parton et al., 2007). Figure 5.5 shows the ratiometric change in $[DA]_{max}$ and $V_{max}$ for WT animals and UCP2 KO animals ($n = 5$, both genotypes). For these experiments, the UCP2 KO animal was used as a negative control because it should be insensitive to the effects of genipin. The application of 20 µM genipin did not significantly alter ($p > 0.05$, single value t-test) stimulated release or uptake of striatal dopamine in brain slices.

**Discussion**

The family of uncoupling proteins to which UCP2 belongs has numerous functions including $Ca^{2+}$ modulation, mediation of reactive oxygen species (ROS), and regulation of ATP formation. It is difficult to predict what effect, if any, the total removal of UCP2 will have on dopamine dynamics.

The hypothesis that UCP2 is primarily protective by diminishing ROS-induced damage in dopamine cell bodies would imply that UCP2 KO mice should experience dopamine cell degeneration over time. In fact, UCP2 has been shown to decrease the oxidative stress in different types of murine tissue during the aging process (Andrews and Horvath, 2009). Damage-induced cell loss in the substantia nigra should lead to decreased dopamine release in the caudate putamen. However, the literature relating UCP2 expression to dopamine cell death is minimal. Several studies have shown that the overexpression of UCP2 allows dopamine neurons to better resist MPTP toxicity (Conti et al., 2005; Chu et al., 2009). Overexpression of UCP2 decreased ROS formation in the substantia nigra, while the removal of UCP2 had the opposite effect. Larger MPTP toxicity was documented in UCP2 KO animals compared to WT animals and was coincident with decreased mitochondrial number in substantia nigra cell bodies (Andrews et al., 2005). These studies indicate quite strongly that a primary function of UCP2 is the protection of dopamine neurons from oxidative stress (Horvath et al., 2003). However, their conclusions rely heavily on a drug-induced Parkinsonian model. These MPTP-induced toxicity studies are problematic because the rate of MPP+ (the metabolite responsible for cell death in this model) uptake into the mitochondria is related to the mitochondrial membrane potential (Scotcher et al., 1991; Chen et al., 2005; Kim et al., 2006). UCP2 negatively modulates inner membrane potential (Horvath et al., 2003). UCP2 KO animals should uptake more MPP+ than WT animals causing more damage and presumably greater cell death. Therefore, the relationship between cell viability and UCP2 cannot be accurately tested using MPTP and cannot be considered an indicator of UCP2 function during nominal dopamine action.

The transgenic removal of UCP2 causes an increase in stimulated dopamine release as measured by FSCV in brain slices (Figure 5.3A). Release facilitation is preferential to dopamine neurons, as stimulated 5-HT release in substantia nigra brain slices remains unaffected (Figure 5.3B). Increased dopamine release is not modulated acutely by altering UCP2 function over short times (2-3 hours), implying that a long term or adaptive mechanism is most likely. Total dopamine content analysis by HPLC showed no difference in the amount of striatal dopamine between WT and UCP2 KO animals (Table 6.1), and no changes in DAT binding have been realized between genotypes (data not shown) (Andrews et al., 2006). These data would support the hypothesis that the increase in release and uptake seen in brain slices is not due to increased nerve innervation in this region but an alteration in terminal dynamics. Increased dopamine release could be the result of improved vesicle packaging, upregulated dopamine synthesis or altered $Ca^{2+}$ dynamics, all ATP-dependent neuronal processes (Burgoyne and Morgan, 2003; Chen et al., 2003; Stokes and Green, 2003). The relationship between UCP2 and DAT function is less clear because the transport of dopamine into the presynaptic terminal is a passive process (Justice et al., 1988; Torres, 2006). However, dopamine is co-transported with $Na^{+}$ along its concentrations gradient (Kandel, 2008). The $Na^{+}$ gradient is established in part by an ATP dependent $Na^{+}/K^{+}$ pump (Hodgkin and Huxley, 1952). The efficiency of this pump could have an effect on the efficiency of dopamine uptake through DAT, altering the $V_{max}$ measurement. As stated previously, the slice results represent a departure from the current hypothesis positively relating UCP2 to dopamine cell viability. One report showed decreased dopamine turnover in the caudate putamen of UCP2 KO animals as measured by the DA/DOPAC ratio (Andrews et al., 2006). The electrochemical measurements (a direct measurement of actual dopamine concentrations) described here would argue against a decrease in dopamine release. It is quite possible that the improved energetic state of the presynaptic terminal increased the efficiency of the monoamine oxidase enzyme responsible for breaking down dopamine into DOPAC. The DA/DOPAC ratio would still be altered in UCP2 KO animals but would no longer represent a decrease in dopamine activity.

The role of UCP2 in the modulation of dopamine release remains controversial. Divergent theories as to the exact function of UCP2 in brain mitochondria prevent the development of a focused hypothesis. It is unlikely that such a large disruption would have a singular effect on neurotransmitter dynamics. Therefore, a mixture of effects in UCP2 KO animals is likely. Future work has begun to focus on the selective removal of UCP2 in dopamine neurons only as well as a more complete characterization of how protein levels are altered in the striatum of these animals. Much more work is necessary before a solid mechanism of UCP2 action can be devised.

## Literature Cited


Alan L, Smolkova K, Kronusova E, Santorova J, Jezek P (2009) Absolute levels of transcripts for mitochondrial uncoupling proteins UCP2, UCP3, UCP4, and UCP5 show different patterns in rat and mice tissues. J Bioenerg Biomembr 41:71-78.

Andrews ZB, Horvath TL (2009) Uncoupling protein-2 regulates lifespan in mice. Am J Physiol Endocrinol Metab 296:E621-627.

Andrews ZB, Horvath B, Barnstable CJ, Elsworth J, Yang L, Beal MF, Roth RH, Matthews RT, Horvath TL (2005) Uncoupling protein-2 is critical for nigral dopamine cell survival in a mouse model of Parkinson's disease. J Neurosci 25:184-191.

Andrews ZB, Rivera A, Elsworth JD, Roth RH, Agnati L, Gago B, Abizaid A, Schwartz M, Fuxe K, Horvath TL (2006) Uncoupling protein-2 promotes nigrostriatal dopamine neuronal function. Eur J Neurosci 24:32-36.

Burgoyne RD, Morgan A (2003) Secretory granule exocytosis. Physiol Rev 83:581-632.

Chen LJ, Gao YQ, Li XJ, Shen DH, Sun FY (2005) Melatonin protects against MPTP/MPP+ -induced mitochondrial DNA oxidative damage in vivo and in vitro. J Pineal Res 39:34-42.

Chen R, Wei J, Fowler SC, Wu JY (2003) Demonstration of functional coupling between dopamine synthesis and its packaging into synaptic vesicles. J Biomed Sci 10:774-781.

Chu AC, Ho PW, Kwok KH, Ho JW, Chan KH, Liu HF, Kung MH, Ramsden DB, Ho SL (2009) Mitochondrial UCP4 attenuates MPP+ - and dopamine-induced oxidative stress, mitochondrial depolarization, and ATP deficiency in neurons and is interlinked with UCP2 expression. Free Radic Biol Med 46:810-820.

Conti B, Sugama S, Lucero J, Winsky-Sommerer R, Wirz SA, Maher P, Andrews Z, Barr AM, Morale MC, Paneda C, Pemberton J, Gaidarova S, Behrens MM, Beal F, Sanna PP, Horvath T, Bartfai T (2005) Uncoupling protein 2 protects dopaminergic neurons from acute 1,2,3,6-methyl-phenyl-tetrahydropyridine toxicity. J Neurochem 93:493-501.

Echtay KS (2007) Mitochondrial uncoupling proteins--what is their physiological role? Free Radic Biol Med 43:1351-1371.

Hodgkin AL, Huxley AF (1952) Movement of sodium and potassium ions during nervous activity. Cold Spring Harb Symp Quant Biol 17:43-52.

Horvath TL, Diano S, Barnstable C (2003) Mitochondrial uncoupling protein 2 in the central nervous system: neuromodulator and neuroprotector. Biochem Pharmacol 65:1917-1921.

Justice JB, Jr., Nicolaysen LC, Michael AC (1988) Modeling the dopaminergic nerve terminal. J Neurosci Methods 22:239-252.

Kandel ER (2008) Principles of neural science, 5th Edition. New York: McGraw-Hill.

Kim YJ, Han JH, Han ES, Lee CS (2006) 7-Ketocholesterol enhances 1-methyl-4-phenylpyridinium-induced mitochondrial dysfunction and cell death in PC12 cells. J Neural Transm 113:1877-1885.

Krauss S, Zhang CY, Lowell BB (2002) A significant portion of mitochondrial proton leak in intact thymocytes depends on expression of UCP2. Proc Natl Acad Sci U S A 99:118-122.

Mizuno Y, Suzuki K, Sone N (1990) Inhibition of ATP synthesis by 1-methyl-4-phenylpyridinium ion (MPP+) in mouse brain in vitro and in vivo. Adv Neurol 53:197-200.

Negre-Salvayre A, Hirtz C, Carrera G, Cazenave R, Troly M, Salvayre R, Penicaud L, Casteilla L (1997) A role for uncoupling protein-2 as a regulator of mitochondrial hydrogen peroxide generation. Faseb J 11:809-815.

Parton LE, Ye CP, Coppari R, Enriori PJ, Choi B, Zhang CY, Xu C, Vianna CR, Balthasar N, Lee CE, Elmquist JK, Cowley MA, Lowell BB (2007) Glucose sensing by POMC neurons regulates glucose homeostasis and is impaired in obesity. Nature 449:228-232.

Sayre LM (1989) Biochemical mechanism of action of the dopaminergic neurotoxin 1-methyl-4-phenyl-1,2,3,6-tetrahydropyridine (MPTP). Toxicol Lett 48:121-149.

Scotcher KP, Irwin I, DeLanney LE, Langston JW, Di Monte D (1991) Mechanism of accumulation of the 1-methyl-4-phenylpyridinium species into mouse brain synaptosomes. J Neurochem 56:1602-1607.

Stokes DL, Green NM (2003) Structure and function of the calcium pump. Annu Rev Biophys Biomol Struct 32:445-468.

Torres GE (2006) The dopamine transporter proteome. J Neurochem 97 Suppl 1:3-10.

Zhang CY, Baffy G, Perret P, Krauss S, Peroni O, Grujic D, Hagen T, Vidal-Puig AJ, Boss O, Kim YB, Zheng XX, Wheeler MB, Shulman GI, Chan CB, Lowell BB (2001) Uncoupling protein-2 negatively regulates insulin secretion and is a major link between obesity, beta cell dysfunction, and type 2 diabetes. Cell 105:745-755.

Zhou H, Zhao J, Zhang X (2009) Inhibition of uncoupling protein 2 by genipin reduces insulin-stimulated glucose uptake in 3T3-L1 adipocytes. Arch Biochem Biophys.

## Chapter 6

Content Analysis by High Performance Liquid Chromatography

### Introduction

Mikhail Tsvet is often credited with performing the first chromatographic separation in 1901 when he resolved plant components on calcium carbonate using ethanol/ether mobile phases (Hadden, 1971). It's been a little over 100 years since that 'first' separation and liquid chromatography has become one of the more prolific analytical tools for the modern day chemist. This chapter will focus solely on the use of reversed phase high performance liquid chromatography (RP-HPLC) for the separation and quantification of biogenic amines in complex samples.

Liquid chromatography separates analytes based on their polarity. In RP-HPLC, the stationary phase is non-polar while the mobile phase is of varying polarity. The stationary phase is bonded to a silica support, usually a spherical particle. The most traditional stationary phases for reversed phase chromatography are straight chain n-alkanes (C5-C30), although more elegant stationary phases (ie. bonded phenyl) are made for a variety of applications. Analytes partition between the bonded stationary phase and the flowing mobile phase; the amount of time spent by the analyte in either phase will dictate the time it takes to elute from the column. The time taken by an analyte to elute from the column is called the retention time ($t_R$), a species dependent property that can be manipulated by changing the separation parameters. On a reversed phase column, non-polar analytes spend more time in the stationary phase than polar analytes thus eluting from the column at a later time. The stationary phase is the primary site of separation; therefore, reversed phase chromatography is best suited for the separation of non-polar compounds.

Mobile phase compositions are critical for the efficient separation of analytes via liquid chromatography. The relative polarity between the mobile phase and the stationary phase affects the partitioning coefficient (a term that expresses a molecule's affinity for either phase) for a given analyte. As the mobile phase increases in polarity, the analyte will spend more time in the stationary phase and elute later. As the polarity of the two phases become similar, retention times will decrease because the analyte will spend more time in the mobile phase. The power of reversed phase separations for biological applications is in the ability to use aqueous based solvents as the mobile phase. Water based mobile phases make separations simpler, cleaner, and more easily connected to tandem separation methods like capillary electrophoresis or electrospray ionization for mass spectrometry (Zhang et al., 2008; Zhao and Suo, 2008). Typically, a small amount of organic solvent (10-20 %) is added to the mobile phase to decrease analyte retention by increasing the organic character of the aqueous mobile phase. For an isocratic elution, the composition of the mobile phase does not change during the analysis time while in a gradient elution the mobile phase composition is altered over the course of the run. Isocratic elutions suffer from poor resolution at low retention times and peak broadening at longer retention times. Gradient elutions circumvent these problems by increasing the separation of less retained analytes while forcing heavily retained analytes off of the column, preserving their shape and decreasing analysis time.

Electrochemical detectors (ECDs) are used to monitor analytes by measuring the current that arises from their oxidation or reduction on an electrode surface placed at the column outlet. ECDs used for the analysis of brain lysates have an advantage over other detector technologies such as UV-Vis or mass spectrometry because they are insensitive to the brain matrix, consisting mostly of small peptides and lipids (Ramstrom et al., 2009). The lack of sensitivity for these matrix components provides simpler chromatograms that are more easily interpreted. This simplicity has made RP-HPLC with ECD desirable for researchers looking into the distribution of biogenic amines in response to environmental stimuli or pharmacological manipulation (Vriend and Dreger, 2006; Filipov et al., 2007).

This chapter focuses on the use of RP-HPLC to support electrochemical measurements of biogenic amines in the brain. RP-HPLC with ECD was used to quantify total content of dopamine and 5-HT in transgenic animals that have disruptions in stimulated neurotransmitter release measured by electrochemistry. Chromatography was also necessary to determine the relative amounts of two biogenic amines, dopamine and norepinephrine (NE), in the ventral bed nucleus of stria terminalis (*v*BNST) in support of mixed electrochemical signals. RP-HPLC with ECD was used to measure biogenic amine total content in non-neuronal tissue samples. The presence of dopamine, NE, and epinephrine (E) in the mouse adrenal gland was confirmed by RP-HPLC with ECD. Finally, chromatography was used to help quantify the component of electroosmotic flow (EOF) in the barrel of an iontophoresis probe in an attempt to better quantify iontophoretic ejections (Herr et al., 2008).

**Materials and Methods**

A full description of all techniques used in this chapter can be found in Chapter 2.

**Results**

Five compounds most commonly found in the parts of the brain related to dopaminergic transmission were separated using isocratic elution reversed phase RP-HPLC, which is shown in Figure 6.1. The following compounds were injected as standards at a concentration of 1 μM in 0.1 N perchloric acid: NE, E, dopamine, l-dopa, and DOPAC. The mobile phase for this elution consisted of citric acid, hexyl sodium sulfate, EDTA, and 5 % methanol. All of the compounds were baseline resolved from one another and from the internal standard HQ, used for quantification. The most closely eluting peaks are E and NE which are also the earliest eluting peaks with a $t_R$ only 2.5 minutes after the dead time marker (Figure 6.1). Less separation between these analytes is not surprising as they are virtually un-retained on the analytical column and differ in structure only by a methyl group on the primary amine. DOPAC is the most retained peak eluting at a $t_R$ of 22 minutes, ~3 minutes after dopamine. The chromatogram in Figure 6.1 clearly demonstrates that even with an isocratic elution most analytes of interest can be separated by RP-HPLC.

*Total Content Analysis of Transgenic Animals*

The analysis of tissue homogenate by RP-HPLC was used to determine total neurotransmitter content in transgenic mouse models. Homogenate taken from the caudate putamen of a WT animal indicates the presence of only dopamine (Figure 6.2). There is no indication that the dopamine precursors or metabolites are present in this sample. An additional peak, ascorbate, not present in the standard injection (Figure 6.1) is present in the tissue homogenate. Ascorbate is not retained on an RP-HPLC column; therefore, it elutes on top of the perchloric acid solvent front that marks the column dead time (Figure 6.2, peak 2). The presence of an overwhelming ascorbate peak is characteristic of all tissue containing samples and serves as a reliable injection quality marker. The chromatograms from the caudate putamen of transgenic mice are qualitatively similar to that shown for WT animals.

The total content of four different transgenic mice was measured ($n \geq 4$, all genotypes) with RP-HPLC (Table 6.1). Dopamine measurements were made in the caudate

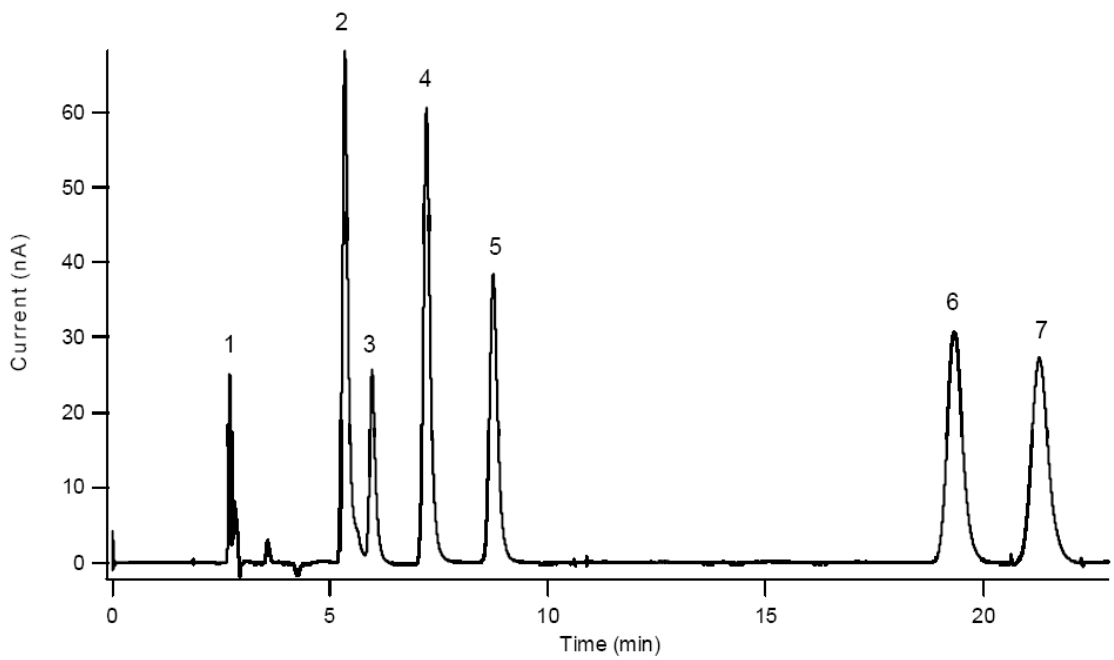


**Figure 6.1** Isocratic separation of biogenic amines using RP-HPLC. Separations were performed on a Waters® Symmetry column (4.6 mm X 250 mm, C18 5 µm bonded particles) in a citric acid mobile phase ( 0.1 M citric acid, 1 mM hexyl sodium sulfate, and 0.1 mM EDTA, pH 3, 5 % methanol). Electroactive species were detected using a thin-layer radial flow cell held at a constant +700 mV. Peak identifications: 1- dead time marker (perchloric acid), 2- NE, 3- E, 4- l-dopa, 5- hydroquinone (HQ) (Std.), 6- dopamine, and 7- DOPAC.

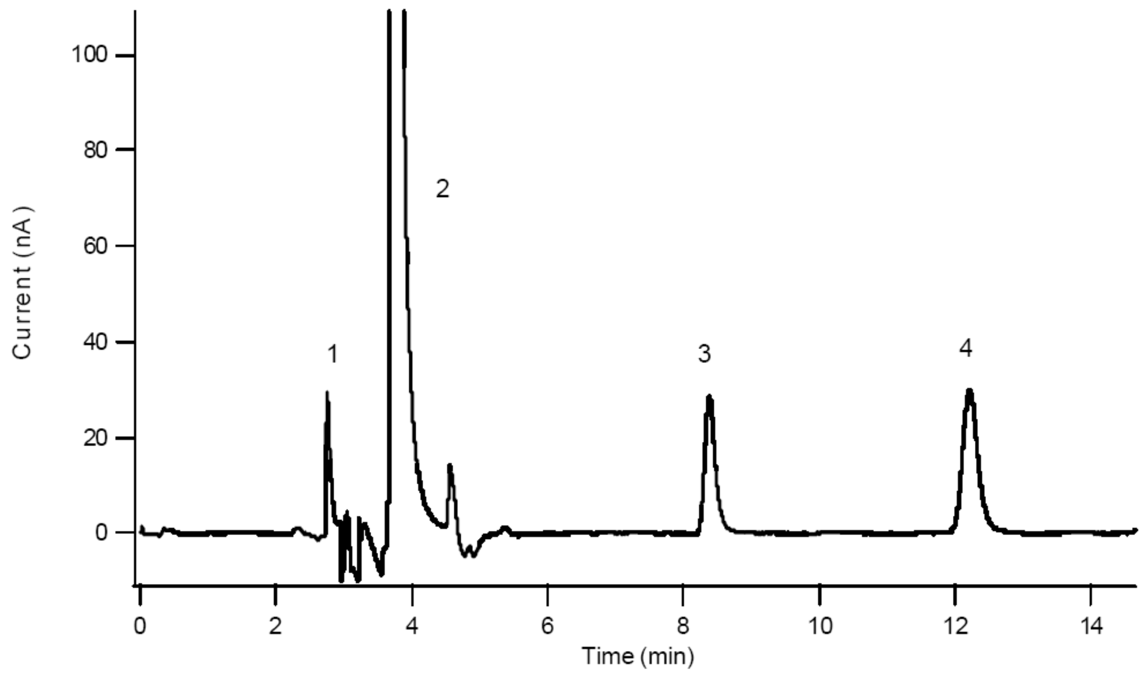


**Figure 6.2** Total content analysis of caudate putamen tissue samples taken from mouse brain slices. HQ is in the extraction buffer at 1 μM to allow for quantification of identified analytes in the tissue sample. Peak identifications: 1- solvent front, 2- ascorbic acid, 3- HQ, 4- dopamine. In caudate putamen tissue, dopamine is the only detectable catecholamine.

putamen and the ventral tegmental area (VTA). 5-HT measurements were made in substantia nigra pars reticulate (SNr) and the VTA. These animals show a 3-fold range of dopamine content values in the caudate, but a very similar amount of 5-HT in the VTA and SNr. Mice expressing enhanced green fluorescent protein (eGFP) do not exhibit a change in dopamine total content in the caudate putamen nor the VTA when compared to WT mice (Table 6.1). This trend is also seen in transgenic mice lacking the presynaptic protein synapsin (synapsin TKO) which show no change in striatal dopamine. Mice insensitive to leptin exhibit a significant ($p < 0.05$) decrease in their striatal dopamine content compared to WT mice. However, mice lacking uncoupling protein 2 (UCP2) did not show a significant ($p > 0.05$) change in striatal dopamine content compared to WT mice (Table 6.1).

*Total Content Changes in Brain Regions of the Rat*

Measurements by RP-HPLC were used to demonstrate a gradient in neurotransmitter content in the *v*BNST of the rat brain. Electrochemical measurements in this area indicate a signal comprised of both dopamine and NE. Brain tissue homogenate taken from this area was analyzed by RP-HPLC to determine the relative amounts of dopamine and NE in parts of this brain region (Figure 6.3). Total content analysis indicated the presence of dopamine and NE; 5-HT was not detected in these samples. The anteromedial portion of the *v*BNST had a roughly 1:2 ratio of dopamine:NE while the medioposterior *v*BSNT had a 1:10 dopamine:NE ratio (Figure 6.3). These ratios are quite similar to those previously reported (Kilts and Anderson, 1986). The ratiometric change between the two regions is due to a decrease in dopamine content concomitant with a three-fold increase in NE content.

**Table 6.1** Total content of dopamine and 5-HT in transgenic mouse models. The amount of dopamine and 5-HT per gram of tissue is shown for eGFP mice, synapsin transgenic mice, leptin transgenic mice, and UCP2 transgenic mice. Dopamine was identified as the sole biogenic amine in the caudate putamen of all mouse types. In the substantia nigra, 5-HT was the only detectable biogenic amine. The ventral tegmental area (VTA) contained both dopamine and 5-HT. (*, $p < 0.05$, Student's t-test, WT vs. Leptin KO)

| Animal Type | Brain Region | Dopamine Content (μg/g) | 5-HT Content (μg/g) |
|---|---|---|---|
| eGFP Negative | Caudate Putamen | 9.6 ± 1.68 | - |
| eGFP Positive | Caudate Putamen | 7.3 ± 0.85 | - |
| eGFP Negative | VTA | 0.7 ± 0.15 | 1.0 ± 0.16 |
| eGFP Positive | VTA | 0.7 ± 0.23 | 0.8 ± 0.51 |
| Synapsin WT | Caudate Putamen | 5.0 ± 0.97 | - |
| Synapsin TKO | Caudate Putamen | 4.7 ± 0.60 | - |
| Synapsin WT | Substantia Nigra | - | 1.0 ± 0.20 |
| Synapsin TKO | Substantia Nigra | - | 0.7 ± 0.10 |
| UCP2 KO | Caudate Putamen | 17 ± 1.6 | - |
| UCP2\Leptin WT | Caudate Putamen | 17 ± 1.6 | - |
| Leptin KO | Caudate Putamen | 12 ± 1.0* | - |

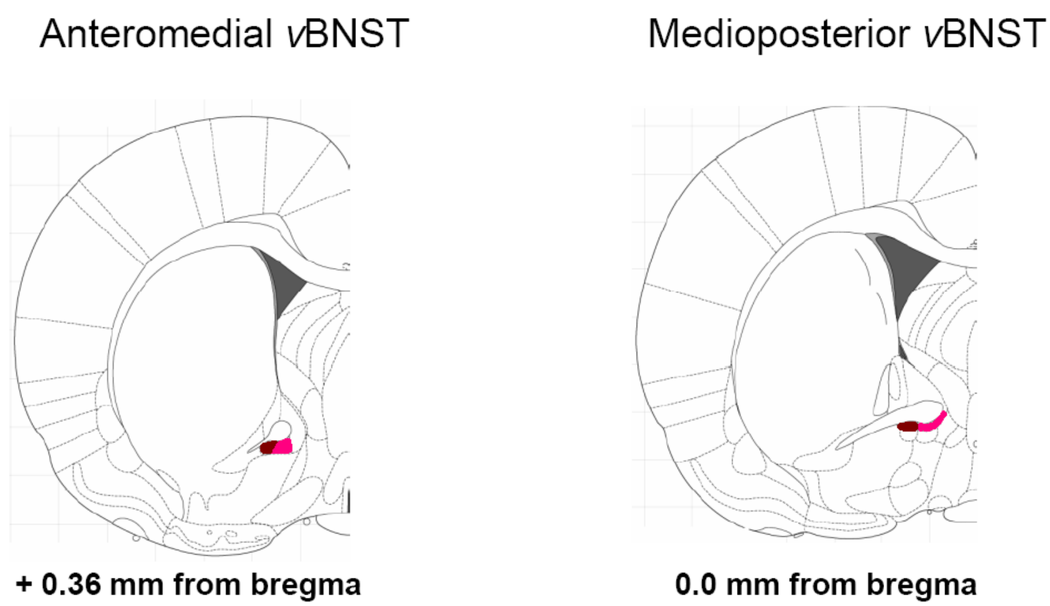


| *v*BNST | Anteromedial (μg/g, n = 12 trials) | Medioposterior (μg/g, n = 12 trials) |
|---|---|---|
| **norepinephrine** | $2.0 \pm 0.75^*$ | $3.3 \pm 1.89^*$ |
| **dopamine** | $1.2 \pm 0.25$ | $0.3 \pm 0.29^{\#}$ |
| **5-HT** | n.d. | n.d. |

**Figure 6.3** The biogenic amine profile of the ventral bed nucleus of the stria terminalis (*v*BNST) as determined by RP-HPLC. Tissue samples (shown as the colored sections) were micro-dissected by hand from brain slices and analyzed for the anteromedial and medioposterior sections of the *v*BNST. Slice schematics and sterotaxic coordinates for both regions are shown in the top panel, both colored regions were removed and homogenized. The total content distribution of dopamine, norephinephrine, and 5-HT are shown in the bottom panel. The ratio of norepinephrine to dopamine increases as you move posterior within the *v*BNST.

*Biogenic Amine Distribution in Murine Adrenal Glands*

The ability to measure biogenic amine concentrations by RP-HPLC is not limited to brain tissue homogenates. The technique used for brain homogenate can be extended to tissues taken from the peripheral nervous system. Of particular interest is the biogenic amine profile of the adrenal gland which is responsible for the release of E and NE into the blood stream upon induction of a stress response. The adrenal gland consists of chromaffin clusters (containing about 20 cells each) oriented adjacent to the vascular system (Barbara et al., 1998) (Kajiwara et al., 1997) (Figure 6.4A). The individual chromaffin cells are capable of releasing either E or NE, which diffuses to the vasculature and is carried by the blood stream to peripheral targets. Whole adrenal glands were homogenized in 500 µL of 0.1 N perchloric acid. The only biogenic amines detected in these samples were NE, E, and dopamine. There were large amounts of E and NE (180 and 350 µg/g respectively) and a relatively small of dopamine (< 10 µg/g); furthermore, the E:NE ratio was found to be 2 (Figure 6.4B). These data are consistent with that found in the literature for the content of adrenal glands analyzed by RP-HPLC (Ally et al., 1986).

*Analyzing Iontophoretic Ejections*

RP-HPLC was used to help quantify the contribution of EOF to the ejection rate of analytes by iontophoresis (Herr et al., 2008). An electron micrograph of an iontophoretic electrode with four open capillaries is shown in Figure 6.5A. A bolus of analyte is ejected through one of these capillaries by the application of a driving force, in this case, current (Figure 6.5A). To determine the relative rates of ejection for neutral and charged molecules, ten minute ejections of dopamine, HQ, and acetamidophenol (AP) were done into 500 µL of 0.1 N perchloric acid using a modified recording chamber shown in Figure 6.5B. Figure 6.6A shows the successful isocratic separation and detection of ejected dopamine and AP

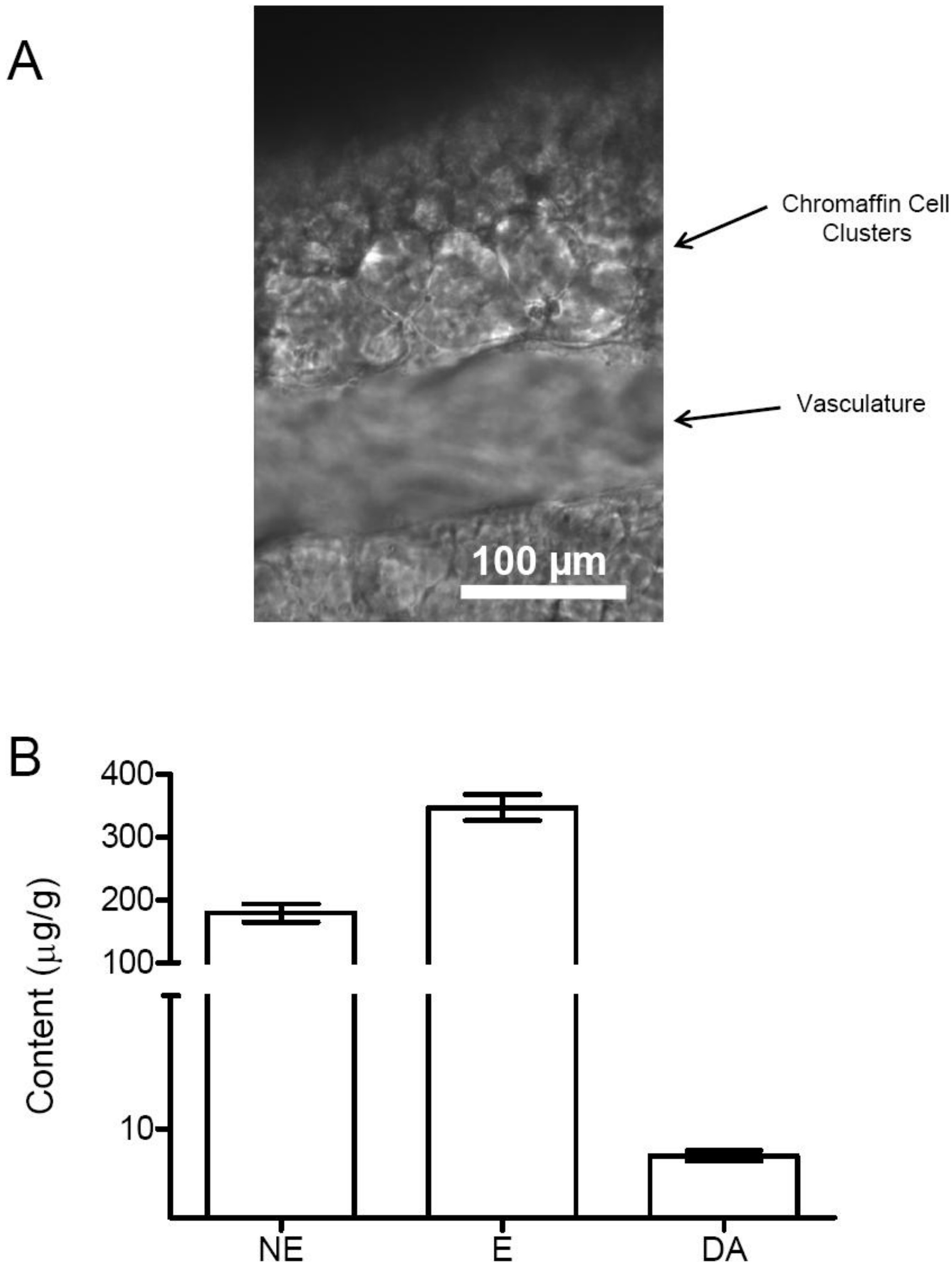


**Figure 6.4** Adrenal glands contain biogenic amines in high concentrations as reported by RP-HPLC total content analysis. A) A light micrograph of an adrenal slice shows chromaffin cell clusters arranged around the venous blood supply. Photo courtesy of Jelena Petrovic. B) Whole glands (n = 4) where homogenized in 500 µL of 0.1 N perchloric acid, and their content analyzed by RP-HPLC. There is roughly a 2-fold higher content of E in adrenal slices compared to NE; DA content is very low in comparison.

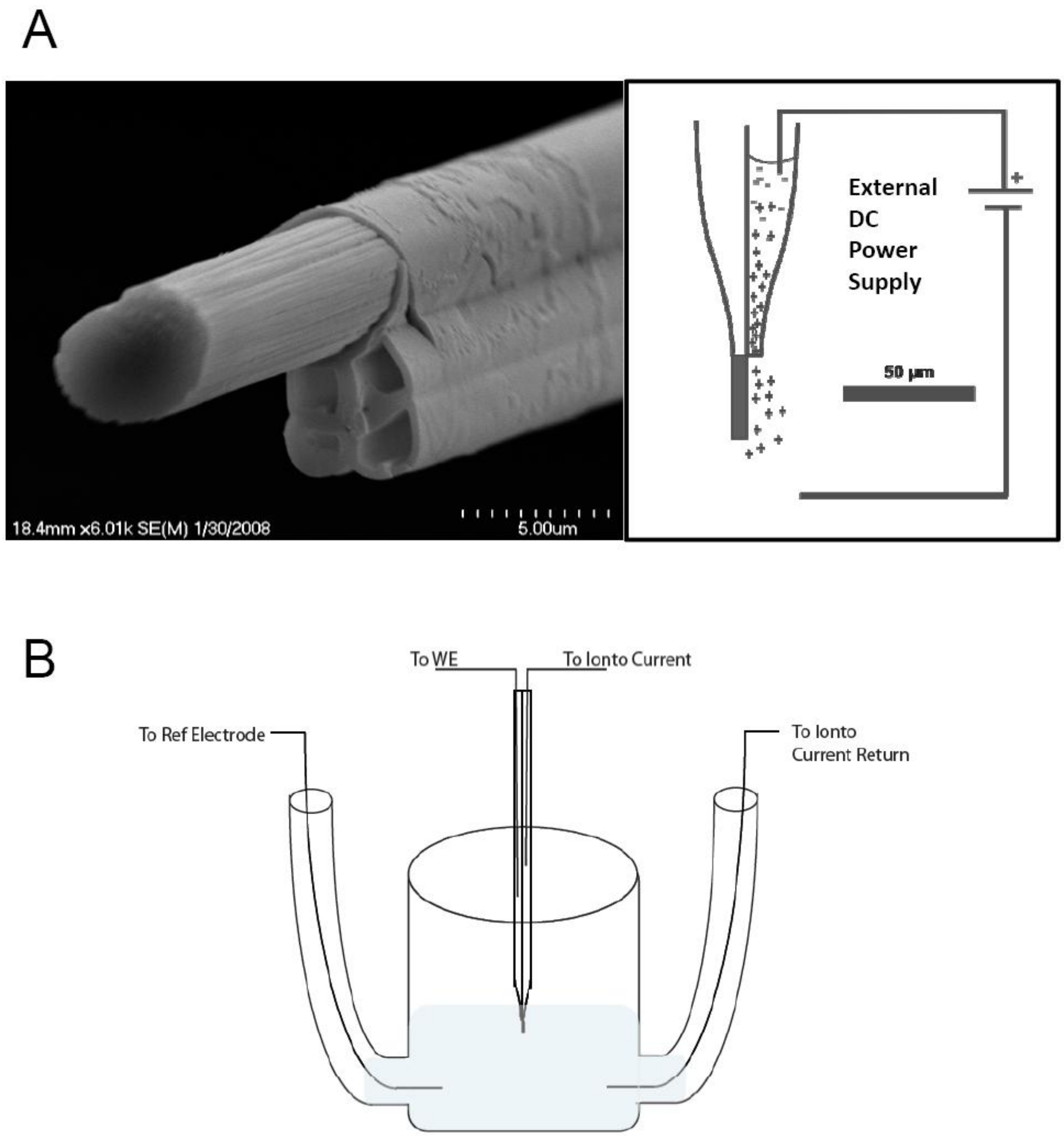


**Figure 6.5** Iontophoretic ejections of electroactive analytes for RP-HPLC analysis. A) An electron micrograph showing an iontophoretic electrode with the carbon fiber sensor oriented on the top of four open capillaries. The open capillaries can be used to eject chemicals into the area surrounding the electrode by applying a current of the same polarity as the species being ejected. B) The apparatus used to collect the total amount of ejected material. An ejection was done into 500 µL of perchloric acid with connections made for the reference electrode, working electrode, iontophoretic current applied, and the current return.

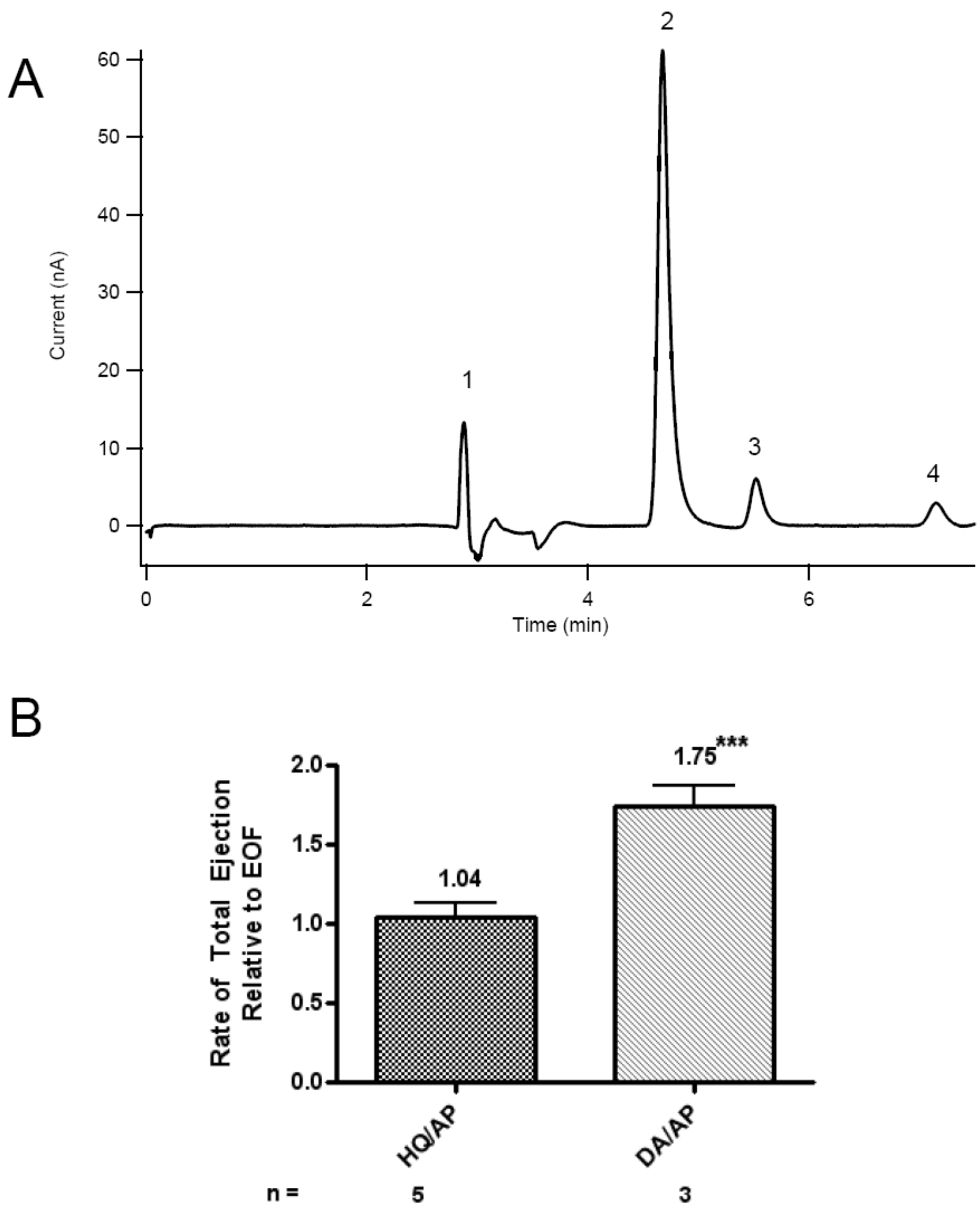


**Figure 6.6** Analytes ejected from the barrel of an electrophoretic probe quantified using RP-HPLC analysis. A) Isocratic separation of iontophoretically ejected dopamine (DA) and acetamidophenol (AP) from the internal standard HQ. Separations were performed as described in Figure 1 with the exception that 10 % methanol was used. Peak identifications: 1- solvent front (perchloric acid), 2- HQ (internal standard), 3- DA, 4- AP. B) The amount of ejected compound was used to quantify the rate of ejection for HQ, DA, and AP (n, the number of barrels tested). HQ and AP are both neutral compounds and are therefore ejected at the same rate. DA is positively charged leading to a faster ejection rate than the neutral AP (***, $p < 0.001$, t-test).

(the EOF marker for these experiments). Figure 6.6B shows the rate of total ejection relative to EOF for a charged analyte, dopamine, and an uncharged analyte, HQ. The HQ:AP ratio was 1.04 while the DA:AP ratio was 1.75 (Figure 6.6B, $n \geq 3$ electrodes) indicating that HQ is ejected at the same rate as EOF while dopamine is ejected at a faster rate than EOF. These conclusions support those obtained using FSCV that show the rate of ejection for charged molecules is higher than that of uncharged molecules (Herr et al., 2008).

**Discussion**

Independent validation of a result by multiple analytical techniques is critical in neuroscience where divergent theories cannot be supported or refuted with a single technique. For example, one of the key requirements for complete validation of new *in vivo* biosensors is validation via established analytical techniques (Phillips and Wightman, 2003). A similar set of standards should be adopted when evaluating newly formed transgenic animals or novel brain regions. RP-HPLC is a technique that can be used to help validate conclusions drawn from electrochemical evidence because it provides a different viewpoint on the state of biogenic amines.

*Isocratic Elutions of Biogenic Amines*

RP-HPLC using isocratic elution with a single pH buffer is adequate for the separation of biogenic amines. Biogenic amines are baseline resolved when run on a reversed phase C18 column using citric acid mobile phase (pH 3.5) containing 5 % methanol as an organic modifier (Figure 6.1). Although adequate for these purposes, there are limitations to a separation of biological samples by isocratic elution. Closer examination reveals two clusters of retained compounds, the first of which occurs prior to 10 minutes. Within the first cluster are peaks 2 and 3 (NE and E) which are not completely resolved from one another. These less retained analytes would benefit from a lower methanol concentration which would increase their overall $t_R$ and resolution. However, a second pair of peaks (dopamine and DOPAC) are late eluting compounds (> 20 min.) indicating that they are highly retained on the column. As is typical in an isocratic elution, these late eluting peaks have become short and broad; an undesirable quality for chromatographic peaks (Neue, 1997). Lowering the methanol concentration would only exacerbate these problems potentially eliminating these peaks altogether. This classical problem is most easily addressed using a gradient elution. A linear increase in the concentration of organic modifier could be used to maintain positive separation for peaks 2-5 while improving the shapes of peaks 6 and 7 by forcing them off of the column more quickly. Gradient elutions have previously been coupled with electrochemical detectors for the determination of brain analytes (Smolders et al., 1995; Kilts et al., 1996; Yun et al., 1998). The investigation of gradient methodologies in this work was hampered by instrumentation but should remain the top priority for future method development.

The isolation of biogenic amines from tissue homogenates can be used to quantify their concentration. Tissue samples taken from the caudate putamen of the mouse indicate the presence of two electroactive neurotransmitters, ascorbate and dopamine (Figure 6.2). An overwhelming large ascorbate peak is expected when analyzing biological samples because ascorbic acid is found in the extracellular space at a concentration of 400 µM (Brahma et al., 2000). The dopamine peak arises from dopamine residing in vesicles of dopamine neurons that synapse with medium spiny neurons in the dorsolateral striatum (Jones et al., 1995). Ascorbate is not retained on a reversed phase column so it elutes within the solvent front. The retention times of HQ and dopamine in Figure 6.2 differ from those shown in Figure 6.1 because a higher methanol concentration (10 % instead of 5 %) was used to improve peak shape. Experiments done at lower methanol concentrations were used to confirm the absence of early eluting compounds (NE) that would have become unretained at a methanol concentration of 10 %. Other areas of the striatum such as the nucleus accumbens have a small amount of NE present in addition to the dopamine (Park *et al.*, in preparation). However, no detectable NE was found in the mouse caudate by RP-HPLC.

*Neurotransmitter Contents in Genetically Altered Mice*

Transgenic mouse models with altered neurotransmitter release have been analyzed by RP-HPLC to help determine the origin source of altered neurotransmitter dynamics in these animals. It is beyond the scope of this chapter to discuss all of the electrochemical release data associated with these genotypes; however, additional information is provided in other chapters. Here we will focus on the power of RP-HPLC to confirm or refute the assumption that the dopamine stores in these animals remain unchanged.

Mice expressing eGFP are used to positively identify neurons expressing tyrosine hydroxylase, the rate limiting enzyme in dopamine synthesis (Kessler et al., 2003). Positive identification of dopamine neurons is beneficial to researchers studying isolated neurons, diffuse terminal fields, or brain regions where anatomical landmarks are not present (Miller *et al*., in preparation). Before these mice could be used regularly, they were evaluated for any possible changes in dopaminergic transmission by Dr. Charles Miller. The evaluation of neurotransmitter content by RP-HPLC was one component of this evaluation. Total content measurements were taken in caudate putamen, a dopamine terminal field and in the VTA, the location of dopamine cell bodies. Dopamine was the only biogenic amine detected in the striatal homogenate, while both dopamine and 5-HT were detected in the VTA (Table 6.1). The caudate putamen results are not surprising for reasons discussed earlier, and neither are those from the VTA. Dopamine neurons in this region are capable of somatodentric release; therefore, a certain level of dopamine stores must be maintained (John et al., 2006). In addition, 5-HT neurons from the dorsal raphe nucleus modulate cell firing at dopamine neurons in the VTA (Adell and Artigas, 2004). Regardless of the region or the neurotransmitter of interest, there was no observed change in biogenic amine concentrations in eGFP positive animals.

Synapsin TKO animals release larger amounts of dopamine than their WT counterparts (Chapter 3). These mice lack a presynaptic protein, synapsin, which regulates the availability of vesicles for release (Greengard et al., 1993; Lonart and Simsek-Duran, 2006). Our work has demonstrated that this disruption leads to enhanced stimulated release in dopamine neurons only (Kile *et al.*, submitted). The question follows: Does this enhancement of release relate back to an increase in overall dopamine availability? Dopamine total content measurements taken from the caudate putamen of the mouse brain indicate an equivalent amount of dopamine in WT and synapsin TKO animals (Table 6.1). This result implies that the changes in stimulated dopamine release in synapsin TKO animals are not related to a change in the overall amount of brain dopamine. Total content measurements indicated no 5-HT content difference in the SNr, where no difference in electrically stimulated 5-HT release was found electrochemically. These data taken with those already discussed in Chapter 3 strongly indicate that the change in stimulated dopamine release in synapsin TKO animals is related to changes in release probabilities or presynaptic architecture rather than a change in vesicle size or number.

Striatal dopamine content is reduced in leptin deficient animals, but unchanged in UCP2 deficient animals. Mice genetically altered to be leptin deficient have phenotypes such as obesity, diabetes, and decreased movement (Chapter 5). Leptin is known to modulate striatal dopamine stores at the cell bodies (Roseberry et al., 2007). Total content analysis in the caudate putamen was performed to confirm the hypothesis that mice lacking leptin have less dopamine projections from the substantia nigra to the caudate (Chapter 5). The total content was taken on three animal genotypes: wild type animals, animals lacking leptin, and animals lacking UCP2. Leptin insensitivity leads to a significant ($p < 0.05$) decrease in the striatal content of dopamine as determined by RP-HPLC (Table 6.1). This result is consistent with previous work indicating decreased dopaminergic innervation in this brain region as measured by DAT binding (South and Huang, 2008). Interestingly, knocking out UCP2 alone does not enhance the amount of dopamine in the striatum even though it enhances stimulated dopamine release (Chapter 5). The RP-HPLC data refutes the hypothesis that the changes in stimulated dopamine release seen in these animals is due solely to changes in terminal innervation.

There are three primary sources of error contributing to the content data shown in Table 6.1. The first source of error deals with any inconsistencies in the dissection area whether in the slice depth or the ability to efficiently isolate the area of interest prior to homogenization. This variability is unavoidable and can be seen in the relatively large SEM vales shown in Table 6.1. Smaller brain regions (VTA and SNr) have a larger percent SEM than the caudate because dissection error in these regions is more likely. The variability sources discussed above do not account for the wide range of reported striatal dopamine contents in Table 6.1. This range is due to differences in the sampling region (mainly the anterior-posterior depth of the caudate slice taken). The RP-HPLC slice used for total content analysis was designed to be the same as the slice used for the electrochemical measurements. The electrochemical measurements were done in different striatal locations for different experiments due to study specific parameters. There is a significant anterior to posterior gradient of dopamine innervation in the mouse brain affecting the total content measurement taken from tissue samples at different depths. Finally, there is variability between transgenic mouse lines due to the simple fact that they are transgenic animals. For example, the synapsin TKO animals were bred on a mixture of three different mouse backgrounds while the eGFP mice were on a pure C57 BL/6 background. This difference alone will impart large amounts of measurement variability. These error sources are not a limitation of the technique; they are a reminder that littermate WT animals must be used whenever possible to eliminate as much animal to animal variability as possible.

*Biogenic Amine Profiles by RP-HPLC*

Total content analysis by RP-HPLC is important for studies in brain regions where multiple biogenic amines contribute to the electrochemical signal. Electrically evoked neurotransmitter release *in vivo* produces a FSCV signal in the *v*BNST that is composed of NE and dopamine (Park *et al.*, accepted). The cyclic voltammograms of NE and dopamine are not sufficiently different to positively identify the signal's origin (Heien et al., 2003). In addition, the relative amounts of dopamine and NE are differ you move from an anteromedial position (bregma + 0.36) to a medioposterior position (bregma + 0.0). The total content profile of NE and dopamine by RP-HPLC in these two regions indicate that there is more NE and less dopamine in the medioposterior region leading to a larger NE:dopamine ratio (Figure 6.3). These data are in good agreement with previous RP-HPLC studies performed in this brain region (Kilts and Anderson, 1986). They also support the electrochemical and pharmacological evidence that NE composes a greater percentage of the current signal in the medioposterior region (Park *et al.,* submitted). A small number of studies have indicated the presence of 5-HT in this brain region; however, any 5-HT present in these samples was below our detection limits.

As stated in the results section, RP-HPLC can also be used to evaluate biogenic amine distributions in peripheral tissues of the neuroendocrine system. Adrenal glands consist of chromaffin cell (the biogenic amine releasing cell) clusters immediately adjacent to a vein wall (Figure 6.4). The presence of large amounts of NE and E are expected because the main function of the adrenal gland is direct infusion of NE and E into the blood stream. Whole adrenal glands were analyzed by RP-HPLC to determine the ratio of NE:E and the presence of any other electroactive substances (Figure 6.4). There is twice as much epinephrine in mouse adrenal slices as norepinephrine which is consistent with literature reports (Ally et al., 1986; Vollmer et al., 1992). Interestingly, a small amount (relative to the E concentration) of dopamine was also found. The role of dopamine in the adrenal gland has not been well established; however, upregulation of tyrosine hydroxylase has been demonstrated in response to prolonged stress (Tank et al., 2008).

*Evaluating Iontophoretic Ejections by RP-HPLC*

Iontophoresis is a drug delivery system that uses an applied current to drive analytes (charged or uncharged) through an open capillary tube (Figure 6.5A). Uncharged particles are expelled from the barrel by means of EOF (the movement of bulk ionic solution under an applied potential) only. Positively charged particles are expelled from the barrel because they are repelled by the positive current applied to the capillary; they also move along with the EOF. The contribution of EOF to the overall rate of drug application is variable, preventing accurate determination of the amount of material ejected. RP-HPLC was used to help quantify the contribution of EOF to the overall ejection rate facilitating more quantifiable iontophoretic ejections (Herr et al., 2008). Iontophoretic ejections were performed into a small volume for RP-HPLC analysis of total analyte flux into the surrounding solution (Figure 6.5B). For the study shown, AP was used as a marker of EOF. RP-HPLC successfully resolved the three compounds used in this experiment: AP, HQ, and dopamine (Figure 6.6A). As expected, there is no difference in the amount of HQ ejected when compared to AP (Figure 6.6B). HQ is an uncharged molecule that should only be ejected from the barrel at a rate equal to the EOF. Dopamine, however, is ejected at a faster rate than AP because it is also experiencing a repulsion event due to the application of a positive current pulse. These relationships are in good agreement with those obtained using FSCV (Herr et al., 2008). Charged molecules are ejected more quickly than uncharged molecules resulting in a locally higher analyte concentration (higher FSCV signal) and an overall higher flux of material (larger RP-HPLC peak area) into the surrounding volume.

## Literature Cited


Adell A, Artigas F (2004) The somatodendritic release of dopamine in the ventral tegmental area and its regulation by afferent transmitter systems. Neurosci Biobehav Rev 28:415-431.

Ally AI, Vieira L, Reuhl KR (1986) Trimethyltin as a selective adrenal chemosympatholytic agent in vivo: effect precedes both clinical and histopathological evidence of toxicity. Toxicology 40:215-229.

Barbara JG, Poncer JC, McKinney RA, Takeda K (1998) An adrenal slice preparation for the study of chromaffin cells and their cholinergic innervation. J Neurosci Methods 80:181-189.

Brahma B, Forman RE, Stewart EE, Nicholson C, Rice ME (2000) Ascorbate inhibits edema in brain slices. J Neurochem 74:1263-1270.

Filipov NM, Stewart MA, Carr RL, Sistrunk SC (2007) Dopaminergic toxicity of the herbicide atrazine in rat striatal slices. Toxicology 232:68-78.

Greengard P, Valtorta F, Czernik AJ, Benfenati F (1993) Synaptic vesicle phosphoproteins and regulation of synaptic function. Science 259:780-785.

Hadden N (1971) Basic liquid chromatography. [s.l.]: Varian Aerograph.

Heien ML, Phillips PE, Stuber GD, Seipel AT, Wightman RM (2003) Overoxidation of carbon-fiber microelectrodes enhances dopamine adsorption and increases sensitivity. Analyst 128:1413-1419.

Herr NR, Kile BM, Carelli RM, Wightman RM (2008) Electroosmotic flow and its contribution to iontophoretic delivery. Anal Chem 80:8635-8641.

John CE, Budygin EA, Mateo Y, Jones SR (2006) Neurochemical characterization of the release and uptake of dopamine in ventral tegmental area and serotonin in substantia nigra of the mouse. J Neurochem 96:267-282.

Jones SR, Garris PA, Kilts CD, Wightman RM (1995) Comparison of dopamine uptake in the basolateral amygdaloid nucleus, caudate-putamen, and nucleus accumbens of the rat. J Neurochem 64:2581-2589.

Kajiwara R, Sand O, Kidokoro Y, Barish ME, Iijima T (1997) Functional organization of chromaffin cells and cholinergic synaptic transmission in rat adrenal medulla. Jpn J Physiol 47:449-464.

Kessler MA, Yang M, Gollomp KL, Jin H, Iacovitti L (2003) The human tyrosine hydroxylase gene promoter. Brain Res Mol Brain Res 112:8-23.

Kilts CD, Anderson CM (1986) The Simultaneous Quantification of Dopamine, Norepinephrine and Epinephrine in Micropunched Rat Brain Nuclei by On-line Trace Enrichment RP-HPLC with Electrochemical Detection: Distribution of Catecholamines in the Limbic System. Neurochem Int 9:437-445.

Kilts CD, Knight DL, Nemeroff CB (1996) The simultaneous determination of neurotensin and its major fragments by on-line trace enrichment RP-HPLC with electrochemical detection. Life Sci 59:911-920.

Lonart G, Simsek-Duran F (2006) Deletion of synapsins I and II genes alters the size of vesicular pools and rabphilin phosphorylation. Brain Res 1107:42-51.

Neue UD (1997) RP-HPLC columns : theory, technology, and practice. New York: Wiley-VCH.

Phillips PEM, Wightman RM (2003) Critical guidelines for validation of the selectivity of in-vivo chemical microsensors. Trends in Analytical Chemistry: TRAC 22:6p.

Ramstrom M, Zuberovic A, Gronwall C, Hanrieder J, Bergquist J, Hober S (2009) Development of affinity columns for the removal of high-abundance proteins in cerebrospinal fluid. Biotechnol Appl Biochem 52:159-166.

Roseberry AG, Painter T, Mark GP, Williams JT (2007) Decreased vesicular somatodendritic dopamine stores in leptin-deficient mice. J Neurosci 27:7021-7027.

Smolders I, Sarre S, Michotte Y, Ebinger G (1995) The analysis of excitatory, inhibitory and other amino acids in rat brain microdialysates using microbore liquid chromatography. J Neurosci Methods 57:47-53.

South T, Huang XF (2008) High-fat diet exposure increases dopamine D2 receptor and decreases dopamine transporter receptor binding density in the nucleus accumbens and caudate putamen of mice. Neurochem Res 33:598-605.

Tank AW, Xu L, Chen X, Radcliffe P, Sterling CR (2008) Post-transcriptional regulation of tyrosine hydroxylase expression in adrenal medulla and brain. Ann N Y Acad Sci 1148:238-248.

Vollmer RR, Baruchin A, Kolibal-Pegher SS, Corey SP, Stricker EM, Kaplan BB (1992) Selective activation of norepinephrine- and epinephrine-secreting chromaffin cells in rat adrenal medulla. Am J Physiol 263:R716-721.

Vriend J, Dreger L (2006) Effects of haloperidol and melatonin on the in situ activity of nigrostriatal tyrosine hydroxylase in male Syrian hamsters. Life Sci 78:1707-1712.

Yun EK, Prince AJ, McMillin JE, Welch LE (1998) High-performance liquid chromatographic separation and electrochemical detection of cephalosporins. J Chromatogr B Biomed Sci Appl 712:145-152.

Zhang MY, Kagan N, Sung ML, Zaleska MM, Monaghan M (2008) Sensitive and selective liquid chromatography/tandem mass spectrometry methods for quantitative analysis of 1-methyl-4-phenyl pyridinium (MPP+) in mouse striatal tissue. J Chromatogr B Analyt Technol Biomed Life Sci 874:51-56.

Zhao XE, Suo YR (2008) Simultaneous determination of monoamine and amino acid neurotransmitters in rat endbrain tissues by pre-column derivatization with high-performance liquid chromatographic fluorescence detection and mass spectrometric identification. Talanta 76:690-697.

# Chapter 7

Disease State Mouse Models

## Introduction

Obesity alters human physiology in part by limiting the arterial blood supply to the heart, decreasing the ability for the pancreas to measure blood sugar levels, and slowing digestion. The effects of obesity are not limited to the periphery; changes have been seen in brain structures such as the hypothalamus and cortex. The relationship between increased body weight and neurotransmission is important; food is one of a handful of naturally rewarding substances (Stoeckel et al., 2008; Stice et al., 2009). The physiological drive for food intake originates in the hypothalamus where the hormones ghrelin and leptin regulate hunger and satiety (Broberger, 2005; Bomberg et al., 2007). Leptin in particular has been shown to modulate dopamine levels in the mesoaccumbens pathway altering the rewarding benefits of food intake (Figlewicz and Benoit, 2009). A complete understanding of how brain chemistry is altered during the obese state may provide insight into possible anti-obesity treatments.

Leptin has long been implicated as the ‘fat’ hormone because it is partly responsible for the cessation of food intake. Free floating leptin binds to hypothalamic receptors inducing a feeling of satiety (Figlewicz and Benoit, 2009); furthermore, the action of leptin appears to decrease dopamine release from hypothalamic nerve endings (Brunetti et al., 1999). Leptin insensitivity or leptin resistance has been implicated as a cause of obesity in

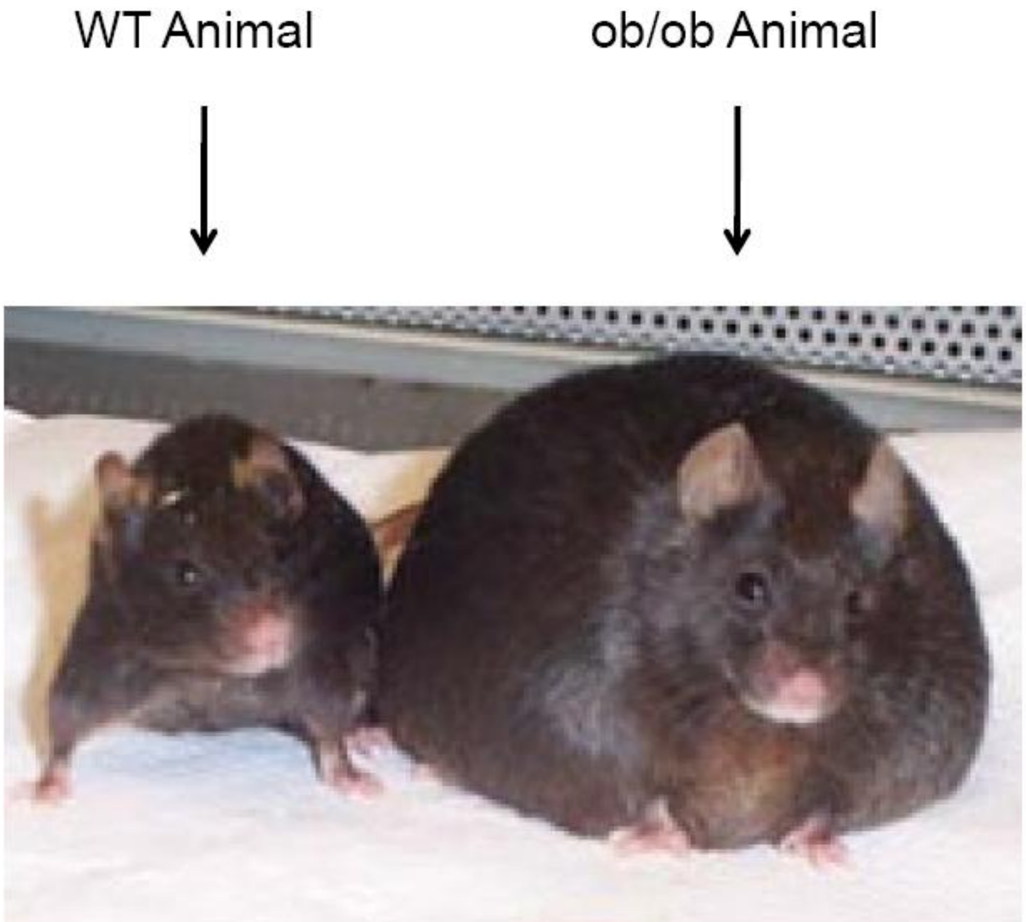


**Figure 7.1** Mice lacking the hormone leptin are prone to hyperphagia leading to morbid obesity. The mouse shown on the left is a normal C57 strain mouse. The mouse on the right is the same strain of animal lacking leptin and given an unrestricted access to food pellets. The *ob/ob* animal has a total body mass roughly seven times his WT littermate. Both mouse strains are available from Jackson Laboratories. Photo courtesy of http://www.genomenewsnetwork.org.

some cases (Myers et al., 2008). Mice genetically altered to no longer produce leptin (*ob/ob* mice) are a good obesity model because they exhibit phenotypical hyperphagia (overeating), a process that requires dopamine (Szczypka et al., 2000). The hyperphagia in *ob/ob* mice results in a profoundly obese animal susceptible to diabetes (Figure 7.1). The *ob/ob* transgenic animal has previously been used to evaluate the relationship between leptin, obesity and dopamine release. Leptin was shown to act in the midbrain as a positive modulator of dopamine release in these animals (Fulton et al., 2006; Roseberry et al., 2007), much different from its negative modulation in the hypothalamus (Brunetti et al., 1999). However, studies done in normal mice indicate that the simple act of high fat feeding is able to alter $D_2$, $D_4$, and DAT levels in the mouse striatum and TH levels in the ventral tegmental area (VTA) (South and Huang, 2008; Li et al., 2009).

Fragile X syndrome (FXS) is the most commonly inherited form of cognitive deficiency in humans. FXS is a triple repeat disorder in which the proliferation of an CGG repeat within the promoter region of *Fmr1* leads to gene inactivation (Bassell and Warren, 2008). The *Fmr1* gene codes for fragile X mental retardation protein (FMRP), believed to be necessary for the proper transcription of many other mRNAs in the cell (Brown et al., 2001; Darnell et al., 2001). In particular, FMRP appears to regulate mRNAs expressed upon activation of metabotropic glutamate receptors regulating synaptic plasticity (Bureau et al., 2008). The Dutch Consortium (1994) generated a FXS disease state model by directly knocking out the *Fmr1* gene. A large amount of research has been done on these mouse models aimed primarily at understanding how synaptic plasticity is altered in FXS (Bear et al., 2008). There has been little evidence suggesting dopamine as a component of FXS despite phenotypic hyperactivity disorders in some FXS patients. However, FMRP was recently shown to be required for dopamine modulation of synaptic plasticity in the prefrontal cortex (PFC) through action of $D_1$ receptors (Wang et al., 2008). Additionally, amphetamine was able to improve object recognition performance in *Fmr1* KO mice coincident with a preferential increase in PFC dopamine levels over WT animals (Ventura et al., 2004).

This chapter focuses on preliminary release experiments performed in obesity and mental retardation disease state models. The *ob/ob* disease state mouse model for obesity results in decreased dopamine release and uptake as measured in striatal brain slices. This is consistent with previous work demonstrating decreased dopaminergic acitivity due to leptin deficiency as well as hyperphagia. The Fragile X syndrome disease state model showed no alterations in neurotransmitter release from the caudate putamen, *v*BNST, or SNr consistent with the theory that Fragile X syndrome results from disruption of postsynaptic signaling.

## Materials and Methods

A full description of techniques used in this chapter can be found in Chapter 2.

## Disclaimer

Part of this chapter contains data taken in collaboration with the lab of Dr. Brad Lowell at Beth Israel Deaconess Hospital in Boston, Massachusetts. My direct contact person at this lab provided me with the genetic identities of the *ob/ob* mice and WT control mice used in this study. This contact person was recently removed from his/her position due to academic misconduct in regards to the study relating UCP2 upregulation to neurotransmission in obesity. The genetic identities of the animals provided to me have in one form or another been confirmed by the Lowell lab as being correct; therefore, I stand behind the results shown here and the conclusions drawn from them.

## Results

*Stimulated Dopamine and 5-HT Release in ob/ob Animals*

The effect of leptin deficiency on stimulated biogenic amine release was evaluated using brain slices. Dopamine release was evoked with a single pulse electrical stimulation and detected with FSCV in striatal brain slices containing the caudate putamen from WT mice and *ob/ob* mice. Data pooled from multiple animals (4 sites within each animal) of each genotype showed that *ob/ob* animals release significantly less ($p < 0.001$, one-way anova, $n = 9$ both genotypes) dopamine than WT animals (Figure 7.2A). This was not the case for 5-HT release evoked from the SNr of WT and *ob/ob* animals using a 20 pulse 100 Hz stimulation (Figure 7.2B). Under these conditions, there was no significant difference in the amount of 5-HT released between WT and *ob/ob* animals ($p > 0.05$, one-way anova, $n = 9$ both genotypes).

Obese animals have decreased levels of DAT expression in the striatum (South and Huang, 2008). For this reason, the average $V_{max}$ of dopamine uptake was measured in the caudate putamen of WT and *ob/ob* animals using FSCV with temporal deconvolution and simplex non-linear regression (Chapter 2). The $V_{max}$ of dopamine uptake was significantly lower ($p < 0.001$) in *ob/ob* animals when compared to WT animals (Figure 7.3, one way anova, $n = 9$ both gentoypes).

*Biogenic Amine Release in Fragile X Mutant Mice*

Possible presynaptic alterations in *Fmr1* KO mice were evaluated using brain slices containing the caudate putamen, *v*BNST, or SNr (Figure 7.4). Electrically stimulated dopamine release (single pulse) monitored by FSCV was unchanged in *Fmr1* KO mice when compared to WT mice ($p > 0.05$, $n = 6$ both genotypes). Additionally, NE release in the vBNST by a 60 pulse 60 Hz stimulation was not different ($p > 0.05$, $n = 6$ both genotypes)

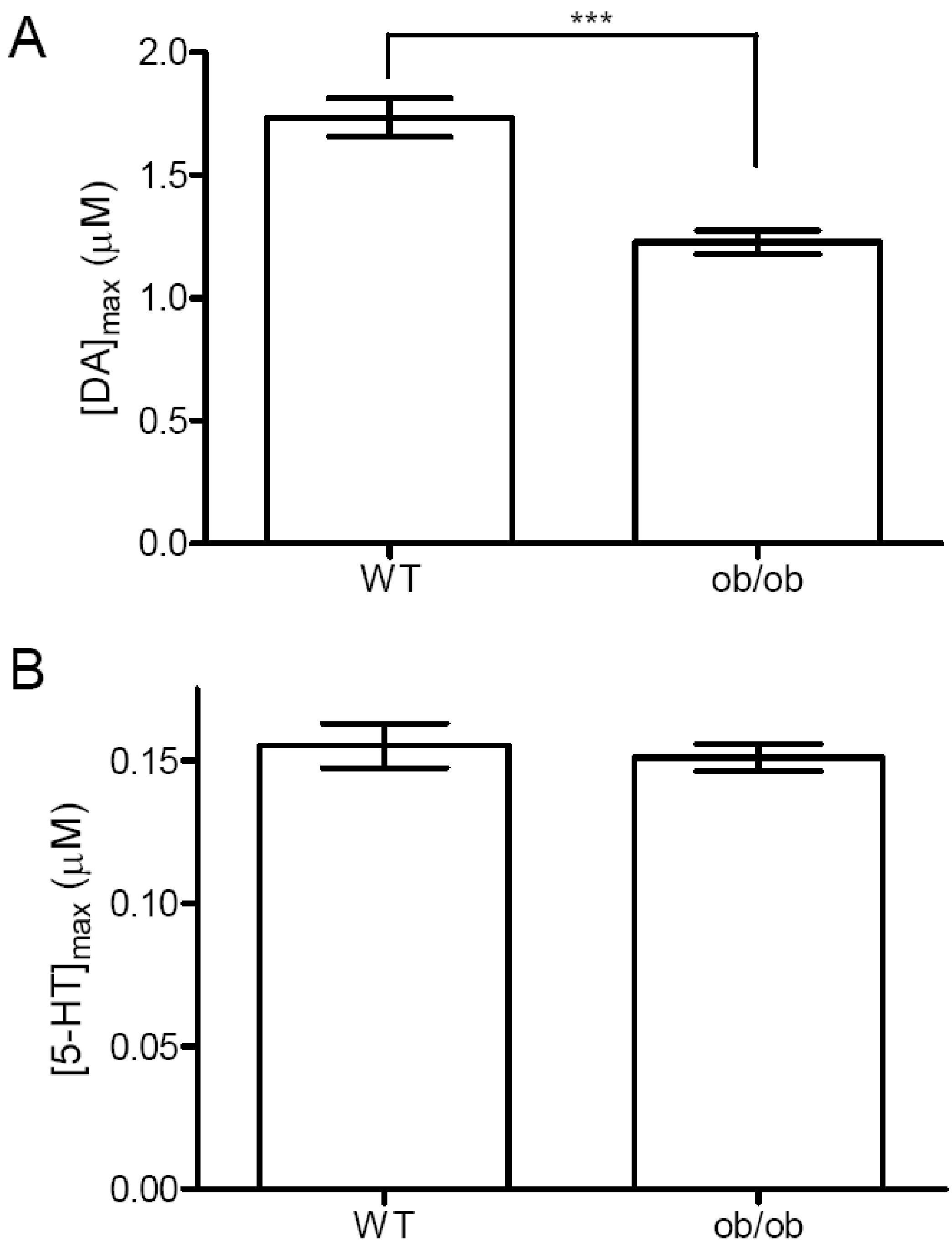


**Figure 7.2** Leptin deficiency affects striatal dopamine release but not stimulated 5-HT release in the substantia nigra. A) Stimulated dopamine release in the caudate putamen of *ob/ob* mice is significantly reduced (n = 9, *** p < 0.001, one-way anova). B) There is no significant difference in stimulated 5-HT release between WT animals or ob/ob animals ( p > 0.05, n = 9).

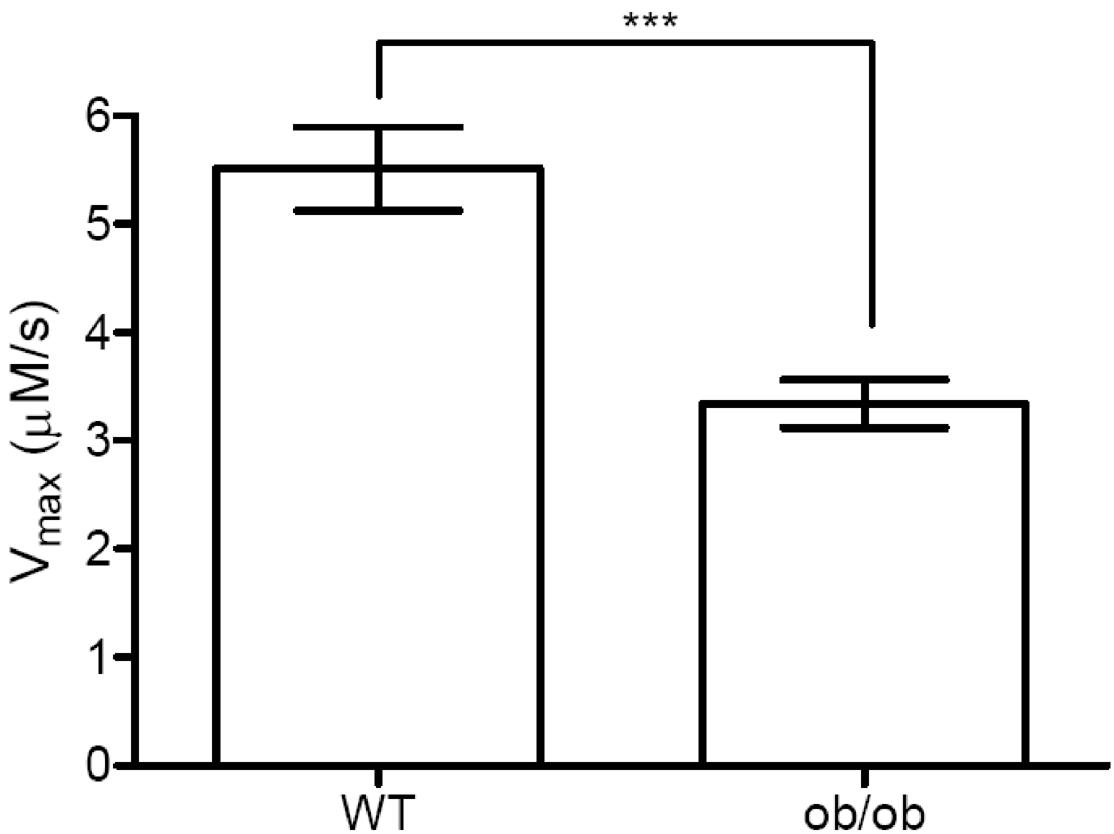


**Figure 7.3** The maximal rate of dopamine clearance is changed in *ob/ob* mice. Temporal deconvolution and simplex modeling of dopamine traces were used to assign a $V_{max}$ for dopamine uptake. As seen with dopamine release, the $V_{max}$ of dopamine uptake is significantly reduced in *ob/ob* mice compared to WT animals (***, $p < 0.001$, one-way anova, n = 5 both genotypes).

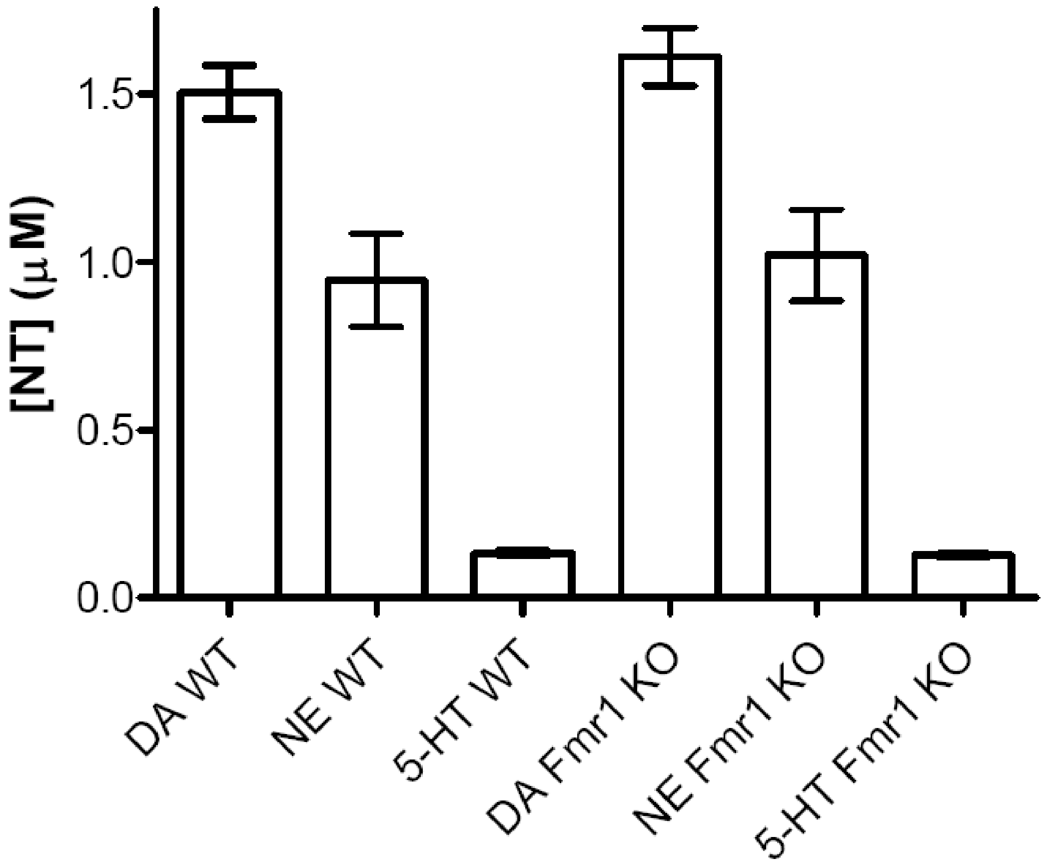


**Figure 7.4** Stimulated neurotransmitter release in three regions of the adult mouse brain. Brain slices containing the caudate putamen, *v*BNST, or SNr were taken from WT mice and *Fmr1* KO mice. Dopamine release evoked by a single pulse electrical stimulation was unchanged in *Fmr1* KO mice compared to WT mice ($p > 0.05$, $n = 6$ both genotypes). The same can be said for 5-HT release evoked by a 20 pulse 100 Hz stimulation in the SNr and NE release evoked by a 60 pulse 60 Hz stimulation in the *v*BNST ($p > 0.05$, $n = 6$ both genotypes).

between *Fmr1* KO and WT control animals. This trend was repeated in the SNr where a 20 pulse 100 Hz stimulation evoked the same amount of 5-HT release in both animals ($p > 0.05$, $n = 6$ both gentoypes).

## Discussion

### *Leptin Removal and Neurotransmitter Release*

The removal of leptin from a normal C57 inbred mouse strain results in an obese and hyperphagic animal. The obese body state in these animals leads to a host of central and peripheral nervous system abnormalities. In addition to insulin resistance, these animals have altered cardiac function, decreased supportive tissue function, and decreased physical activity (Lindstrom, 2007). Many of the peripheral effects of leptin deficiency are background strain dependent (they change depending on which mouse line the *ob/ob* mutation was generated) (Lindstrom, 2007); however, all animal types have decreased physical movement. Dopamine regulates movement by acting on medium spiny neurons in the striatum; therefore, dopamine release in these animals was evaluated using brain slices. Figure 7.2A clearly shows that dopamine release in the striatum of *ob/ob* mice is significantly reduced compared to their WT littermates, a result in direct contrast to stimulated release of 5-HT (Figure 7.2B) which is leptin independent. Taken together, these data demonstrate a dopamine specific alteration in *ob/ob* mice. Decreased dopamine release in *ob/ob* mice is not a novel finding, both somatodendritic and terminal dopamine release are disrupted in these animals (Fulton et al., 2006; Roseberry et al., 2007). In addition, leptin receptors have been found on dopamine midbrain neurons (Figlewicz and Benoit, 2009) and are protective against 6-hydroxydopamine lesion formation (Weng et al., 2007). These studies provide compelling evidence that the altered dopamine release in *ob/ob* animals is the result of decreased leptin action on midbrain neurons. However, the hyperphagia/obesity phenotypes demonstrated by *ob/ob* animals have been shown to alter DAT and $D_2$ levels in the striatum and TH levels in the VTA of WT animals (South and Huang, 2008; Li et al., 2009), alterations consistent with our $V_{max}$ (Figure 7.3) and total dopamine content measurements (Chapter 6). These studies support the data shown in Figures 7.2 and 7.3 but prevent the establishment of a direct link between leptin deficiency and dopamine release. Future work probing dopamine release in diet restricted *ob/ob* animals and high fat fed WT animals may provide clues as to the true cause of dopamine disruption in these animals.

*Fragile X Syndrome and Neurotransmitter Release*

FXS syndrome results from the silencing of the *Fmr1* gene which encodes for FMRP, a protein most closely linked to glutamate receptors. *Fmr1* KO mice are genetically altered to no longer produce FMRP serving as a reliable disease state model for the study of FXS. For the first time, FSCV has been used to directly monitor the release of neurotransmitters in brain slices from these animals. Stimulated release of dopamine in the caudate putamen, NE in the vBNST, and 5-HT in the substantia nigra are unaffected by the removal of FMRP (Figure 7.4). These findings are not terribly surprising as most FXS patients do not demonstrate phenotypes typical of disrupted biogenic amine transmission. One study in the PFC of *Fmr1* KO mice did show preferential altered dopamine transmission related to novel object recognition (Ventura et al., 2004); however, the data shown in Figure 7.4 would indicate that this dopamine effect is limited to the PFC.

## Literature Cited


(1994) Fmr1 knockout mice: a model to study fragile X mental retardation. The Dutch-Belgian Fragile X Consortium. Cell 78:23-33.

Bassell GJ, Warren ST (2008) Fragile X syndrome: loss of local mRNA regulation alters synaptic development and function. Neuron 60:201-214.

Bear MF, Dolen G, Osterweil E, Nagarajan N (2008) Fragile X: translation in action. Neuropsychopharmacology 33:84-87.

Bomberg EM, Grace MK, Wirth MM, Levine AS, Olszewski PK (2007) Central ghrelin induces feeding driven by energy needs not by reward. Neuroreport 18:591-595.

Broberger C (2005) Brain regulation of food intake and appetite: molecules and networks. J Intern Med 258:301-327.

Brown V, Jin P, Ceman S, Darnell JC, O'Donnell WT, Tenenbaum SA, Jin X, Feng Y, Wilkinson KD, Keene JD, Darnell RB, Warren ST (2001) Microarray identification of FMRP-associated brain mRNAs and altered mRNA translational profiles in fragile X syndrome. Cell 107:477-487.

Brunetti L, Michelotto B, Orlando G, Vacca M (1999) Leptin inhibits norepinephrine and dopamine release from rat hypothalamic neuronal endings. Eur J Pharmacol 372:237-240.

Bureau I, Shepherd GM, Svoboda K (2008) Circuit and plasticity defects in the developing somatosensory cortex of FMR1 knock-out mice. J Neurosci 28:5178-5188.

Darnell JC, Jensen KB, Jin P, Brown V, Warren ST, Darnell RB (2001) Fragile X mental retardation protein targets G quartet mRNAs important for neuronal function. Cell 107:489-499.

Figlewicz DP, Benoit SC (2009) Insulin, leptin, and food reward: update 2008. Am J Physiol Regul Integr Comp Physiol 296:R9-R19.

Fulton S, Pissios P, Manchon RP, Stiles L, Frank L, Pothos EN, Maratos-Flier E, Flier JS (2006) Leptin regulation of the mesoaccumbens dopamine pathway. Neuron 51:811-822.

Li Y, South T, Han M, Chen J, Wang R, Huang XF (2009) High-fat diet decreases tyrosine hydroxylase mRNA expression irrespective of obesity susceptibility in mice. Brain Res.

Lindstrom P (2007) The physiology of obese-hyperglycemic mice [*ob/ob* mice]. ScientificWorldJournal 7:666-685.

Myers MG, Cowley MA, Munzberg H (2008) Mechanisms of leptin action and leptin resistance. Annu Rev Physiol 70:537-556.

Roseberry AG, Painter T, Mark GP, Williams JT (2007) Decreased vesicular somatodendritic dopamine stores in leptin-deficient mice. J Neurosci 27:7021-7027.

South T, Huang XF (2008) High-fat diet exposure increases dopamine D2 receptor and decreases dopamine transporter receptor binding density in the nucleus accumbens and caudate putamen of mice. Neurochem Res 33:598-605.

Stice E, Spoor S, Ng J, Zald DH (2009) Relation of obesity to consummatory and anticipatory food reward. Physiol Behav.

Stoeckel LE, Weller RE, Cook EW, 3rd, Twieg DB, Knowlton RC, Cox JE (2008) Widespread reward-system activation in obese women in response to pictures of high-calorie foods. Neuroimage 41:636-647.

Szczypka MS, Rainey MA, Palmiter RD (2000) Dopamine is required for hyperphagia in Lep(*ob/ob*) mice. Nat Genet 25:102-104.

Ventura R, Pascucci T, Catania MV, Musumeci SA, Puglisi-Allegra S (2004) Object recognition impairment in Fmr1 knockout mice is reversed by amphetamine: involvement of dopamine in the medial prefrontal cortex. Behav Pharmacol 15:433-442.

Wang H, Wu LJ, Kim SS, Lee FJ, Gong B, Toyoda H, Ren M, Shang YZ, Xu H, Liu F, Zhao MG, Zhuo M (2008) FMRP acts as a key messenger for dopamine modulation in the forebrain. Neuron 59:634-647.

Weng Z, Signore AP, Gao Y, Wang S, Zhang F, Hastings T, Yin XM, Chen J (2007) Leptin protects against 6-hydroxydopamine-induced dopaminergic cell death via mitogen-activated protein kinase signaling. J Biol Chem 282:34479-34491.

# Chapter 8

Experimental Parameters and Dopamine Release

## Introduction

It is critical for an experimenter to understand how his/her parameters may affect the analytical signal. In many cases simply performing a measurement will cause a permanent and undesirable change in the experimental parameters. For example, a small dose of amphetamine (AMPH) will cause an increase in motor activation; however, too much AMPH will decrease motor activation by inducing stereotypy (White et al., 1998). The stereotypy could lead experimenters to underestimate the motor enhancement due to AMPH. This chapter focuses on the aspects of experimentation that may have residual effects on the recorded dopamine signal in brain slices. First, the waveform application frequency is discussed as it is important for accurate modeling of dopamine uptake parameters. Second, the effects on dopamine release by drugs used during an experiment such as iontophoretic ejection markers or anesthetics will be described. Finally, a more robust method for the measurement of dopamine reverse transport in brain slices will be described.

## Materials and Methods

All of experimental procedures used here are explained in complete detail in Chapter 2. The use of analog background subtraction for catecholamine measurements over long time periods has been explained in detail previously (Hermans et al., 2008). Principal component regression (PCR) has been used previously to differentiate between signals obtained for dopamine with those obtained for pH (Heien et al., 2004).

## Results

### *Dopamine Sensitivity and Application Frequency*

The response of a carbon fiber microelectrode to a 2 μM bolus of dopamine changes as a function of the waveform application frequency. The same electrode has a larger current response to dopamine when the waveform is applied at 10 Hz vs. 60 Hz (Figure 8.1A). On average, the increase in current response for electrodes cycled at 10 Hz is 70 % greater than the current response at 60 Hz (n = 5 electrodes). There is a two-fold difference in the 10-90 % rise time for the two application frequencies being 200 ms at 60 Hz and 400 ms at 10 Hz (Figure 8.1A).

### *Temporal Response of FSCV*

The signal for dopamine detected with FSCV arises primarily from dopamine that has adsorbed to the electrode (Bath et al., 2000). Because the adsorption occurs in the time between voltammetric scans, both the response time and the amplitude of the measured current depend on the repetition rate. To examine how this affects the measurement of dopamine dynamics in brain slices, release and uptake evoked by a single stimulation pulse were compared when measured with the triangular waveform applied at either 10 Hz or 60 Hz. In both cases, the concentration of dopamine increased at the first measurement point after the stimulation pulse, its concentration reached a maximum a few points later, and then the dopamine concentration returned to prestimulus values (Figure 8.1B). When the current was converted to concentration, the maximal concentrations observed with both repetition rates were quite similar. However, with the 10 Hz repetition rate the maximal response occurred 200 ms after the stimulus pulse, whereas it occurred 67 ms after the stimulus with

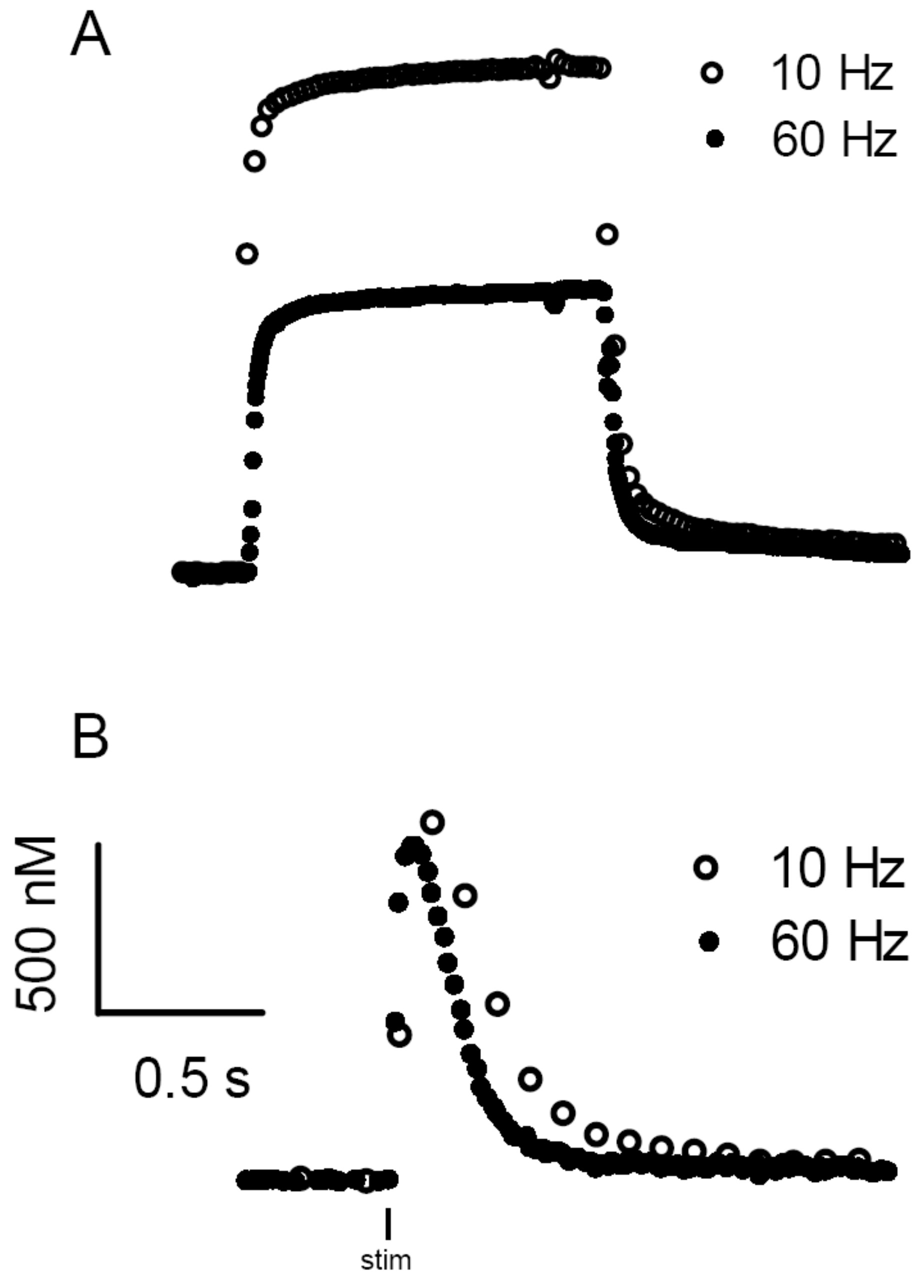


**Figure 8.1** The repetition rate of an FSCV electrode changes its sensitivity and temporal response to dopamine concentrations. A) The sensitivity of a carbon fiber microelectrode to a 2 µM bolus of dopamine is 70 % higher when the electrode is cycled at 10 Hz instead of 60 Hz. B) Stimulated dopamine release in striatal brain slices has a different time course when sampled at 10 Hz or 60 Hz. The peak dopamine concentration occurs at a later time (200 ms instead of 50 ms) when the waveform application frequency is reduced from 60 Hz to 10 Hz. The increased temporal delay at 10 Hz leads to an underestimation by 22 % in the $V_{max}$ value determined by simplex modeling.

the 60 Hz repetition frequency. Since release and uptake occur at the same rate irrespective of measurement procedure, this result clearly indicates that the response time of the electrode distorts the measurement of uptake. Further evidence of this is seen in the slower rate at which the current returns to baseline with the lower repetition frequency (Figure 8.1B). The uptake portion of both traces was fit to the Michaelis-Menten equation. The data collected at 10 Hz had a $V_{max}$ value for uptake that was 78 % of the value obtained with the data collected at 60 Hz. The lower value of the $V_{max}$ obtained with the 10 Hz sampling frequency was obtained even though the increased delay to reach the maximum was accounted for by deconvolution (Venton et al., 2002).

Similar experiments were conducted in the presence of 10 μM cocaine. The time delay is greater under these conditions but increases more with 10 Hz sampling. Furthermore, the recorded dopamine concentration is 13% greater when sampling at 10 Hz than found with 60 Hz sampling (Figure 8.2A). Additionally, the disappearance of dopamine was qualitatively slower at each concentration of cocaine tested (1 to 20 μM) with sampling at 10 Hz. However, the simplex regression procedure yielded similar values of the apparent $K_m$ value ($(K_m)_{app}$) for data acquired at both frequencies when the difference in the electrode time response was accounted for by deconvolution. The $K_i$ value at 10 Hz (0.30 μM) was the same as that found with a 60 Hz (0.32 μM) repetition rate, both values are similar to that previously reported using FSCV with 60 Hz collection (Johnson et al., 2006) (Figure 8.2B).

*Temporal Response of FSCV Compared to Amperometry*

Although 60 Hz collection frequencies were found to better model dopamine uptake in striatal brain slices, there is still concern that the adsorptive delay associated with these FSCV measurements would distort the observed time course of uptake, impeding accurate assessment of uptake rate constants. Therefore, uptake rates measured with FSCV

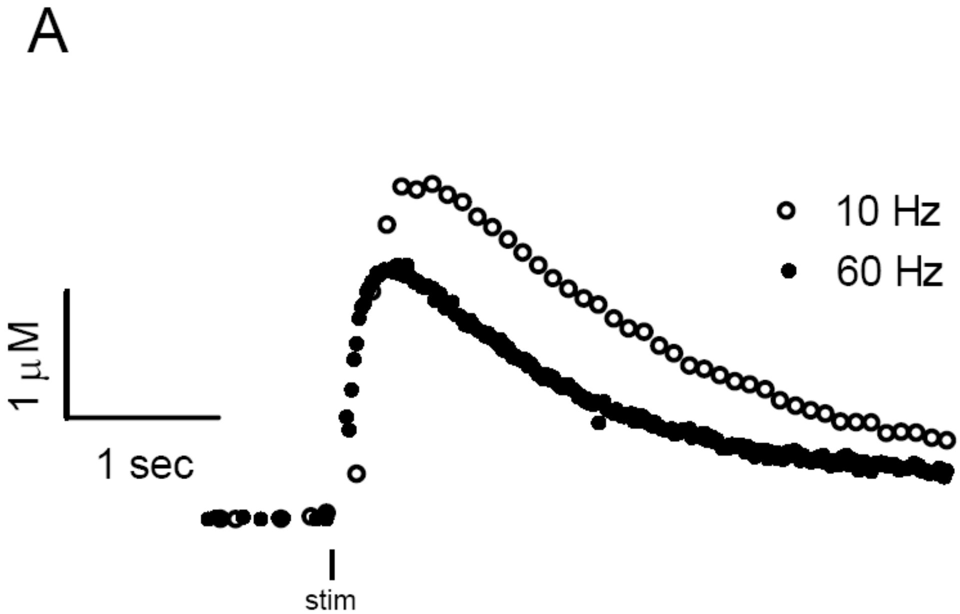


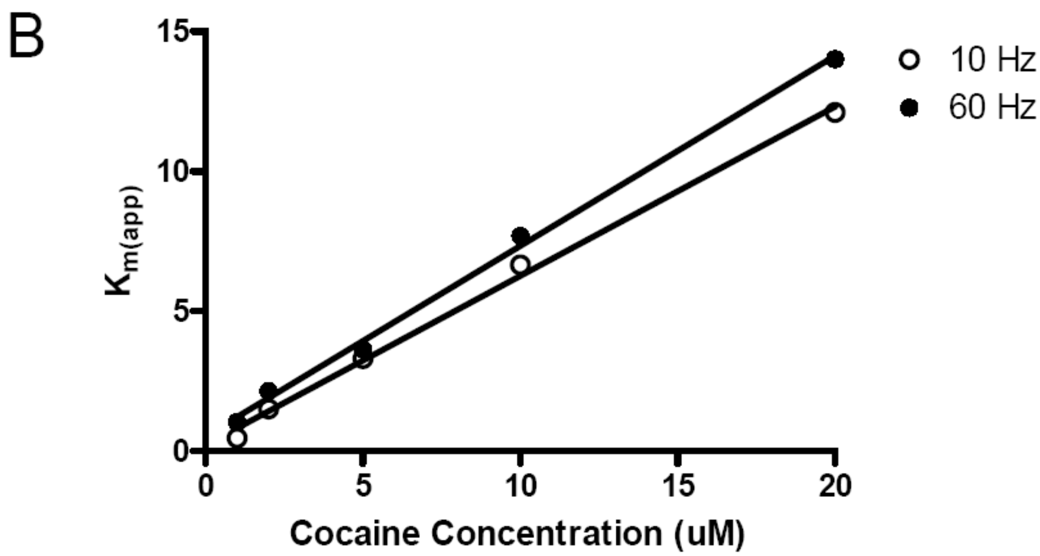


**Figure 8.2** Differences in the shape of stimulated dopamine release at 60 Hz vs. 10 Hz remain even when the uptake rate is slowed by competitive inhibition. A) Stimulated dopamine release in brain slices in the presence of 10 µM cocaine. B) The decreased rate of uptake in the presence of cocaine alleviates the insensitivity to uptake at a 10 Hz application frequency when compared to a 60 Hz application frequency. The $K_i$ values for cocaine obtained using a 10 Hz application frequency and a 60 Hz application frequency are the same being 0.30 µM and 0.32 µM respectively.

collected at 60 Hz were compared with those collected using constant potential amperometry. In the latter technique, dopamine is immediately and continuously oxidized as it reaches the electrode surface so adsorption times are not a parameter that affects the measurement (Venton et al., 2002). In this brain slice recording location, the delay time to reach a maximum value was 40 ms with FSCV repeated at 60 Hz (Figure 8.3A). The delay time was < 10 ms with amperometry (Figure 8.3A), a process that we have previously attributed to diffusion from the release site to the electrode (Venton et al., 2003). When the FSCV time delay was deconvoluted from the dopamine signal, simplex regression of the amperometric signal and FSCV data yielded similar $V_{max}$ values of 6.01 and 6.06 μM/s respectively. These similarities confirm that at 60 Hz, FSCV is able to effectively model dopamine uptake kinetics despite the presence of an adsorptive time delay at the electrode.

Ascorbic acid has been shown in improve the sensitivity of an amperometric electrode for dopamine (Venton et al., 2003). The presence of 500 μM ascorbate in the aCSF enhanced the signal due to released dopamine from electrical stimulation of brain slices by greater than two fold (Figure 8.3B). It did not significantly alter ($p > 0.05$) the time of peak oxidation or the measured uptake rate of dopamine. Ascorbic acid was also present for the release files taken in Figure 8.3A and allowed for flow cell calibration of the amperometry signal as previously described (Venton et al., 2003).

*Anesthetics and Neurotransmitter Release*

The effect of the common anesthetics, ketamine and urethane, on stimulated dopamine and 5-HT release was measured in brain slices. Bath application of 10 μM ketamine does not change stimulated dopamine release in the caudate putamen ($p > 0.05$, $n = 5$). In addition, 1 mM urethane is unable to significantly alter stimulated dopamine release in the striatum (Figure 8.4A, $p > 0.05$, $n = 5$). A similar trend is seen in stimulated 5-HT

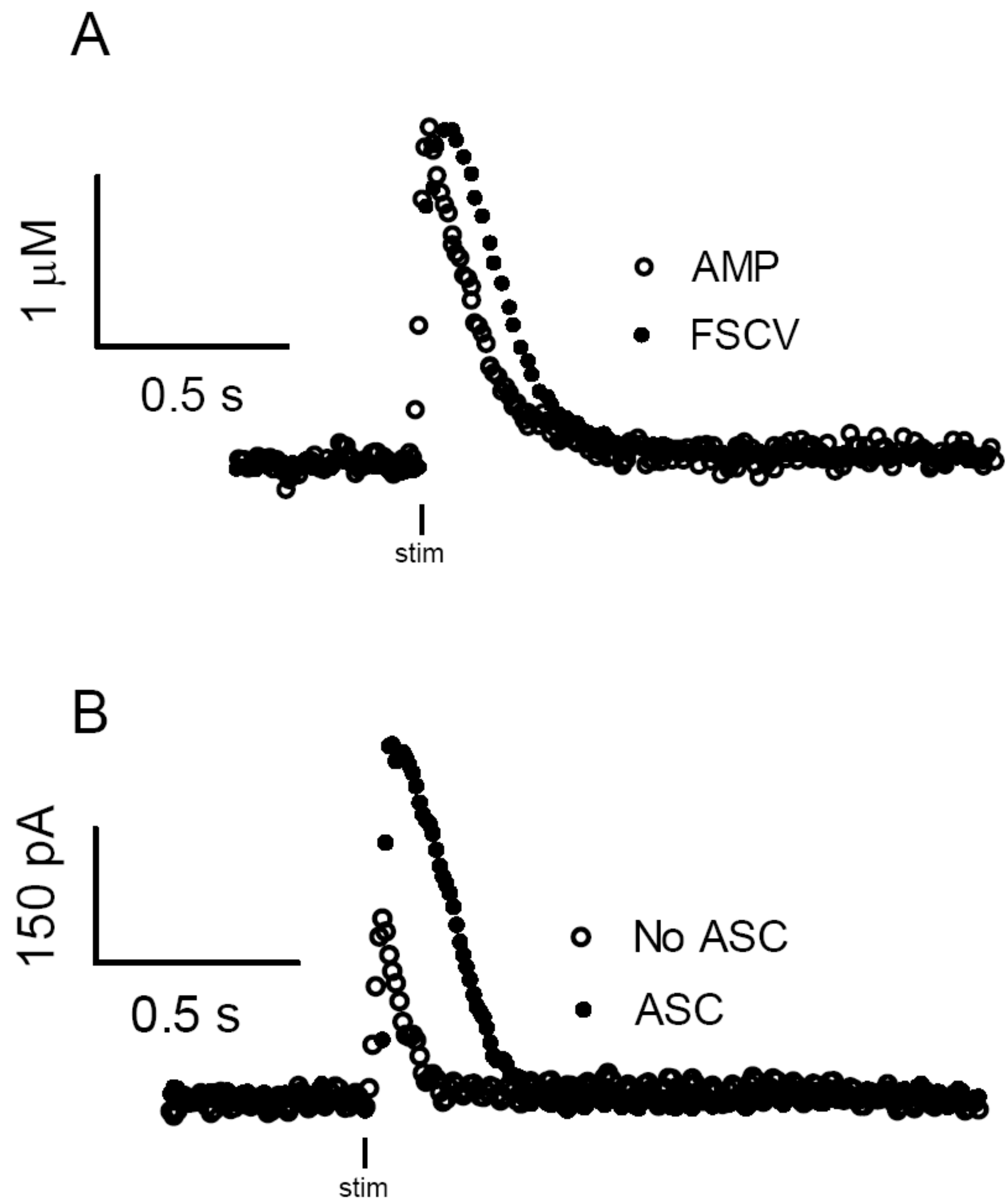


**Figure 8.3** Amperometric recordings do not exhibit the temporal delay customary of an FSCV electrode. A) Stimulated dopamine release in a striatal brain slice using FSCV at 60 Hz and amperometry. The adsorption of dopamine during FSCV causes a 40 ms delay in the rise to the peak [DA] that is not present during amperometry. A temporal deconvolution factor can be used to remove this temporal distortion; the $V_{max}$ value reported for the deconvoluted FSCV trace is the same as the amperometric trace. B) Striatal brain slices lack endogenouse ascorbic acid; supplementation of 500 μM ascorbic acid enhances the amperometric signal without altering its time course.

release in SNr containing brain slices. Ketamine does not significantly alter (Figure 8.4B, $p > 0.05$, $n \geq 3$) 5-HT release in the SNr; furthermore, there was no effect on stimulated release by urethane.

*Iontophoretic Ejection Markers and Dopamine Release*

Several compounds have shown promise as electroactive ejection markers for quantifiable iontophoretic drug application (Herr et al., 2008). Stimulated dopamine release in striatal brain slices was measured in the presence of hydroquinone (HQ), nitrophenoxyethanol (NPE), and acetamidophenol (AP) to determine any possible effects of these compounds. The ejection marker HQ has a small but insignificant effect on stimulated dopamine release (Figure 8.5, $p > 0.05$, $n = 5$). As Figure 8.5 indicates, ejection markers NPE and AP reduce stimulated dopamine release by 30 %, a reduction that is significant ($p < 0.01$, $n = 5$).

*Changes in Basal Dopamine Concentrations*

AMPH and methamphetamine (METH) are capable of inducing dopamine reverse transport, an effect that requires the dopamine transporter (Jones et al., 1998). Analog background subtracted cyclic voltammetry was combined with principal component regression analysis to accurately monitor dopamine concentration changes over long time periods (~ 40 min.) (Hermans et al., 2008). Figure 8.6A shows an example CV created based on a training set of dopamine CVs taken at the recording site. PCR was used to measure dopamine concentrations in the presence of changes in background current and capacitance. Figure 8.6B shows an average dopamine trace ($n = 5$, each drug) over 40 min. of applied AMPH or METH; for clarity, every 100$^{th}$ data point is shown. The drug was applied (10 µM) at $t = 2$ min, dopamine efflux began at 5 minutes and achieved 90 % of its maximum concentration at 10 minutes (Figure 8.6B). The maximal dopamine concentration

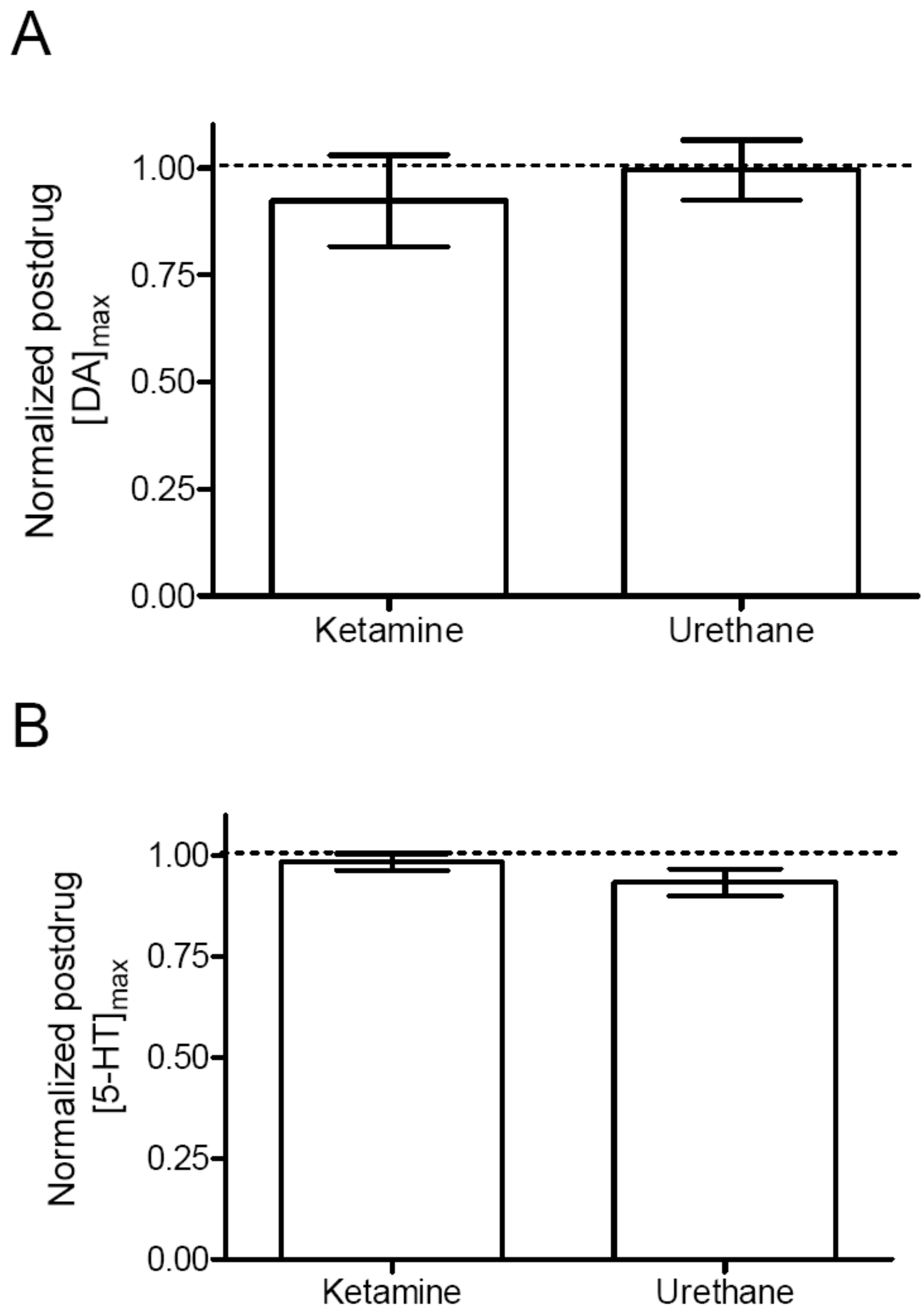


**Figure 8.4** Anesthetics used during *in vivo* experimentation do not cause changes in striatal dopamine release or 5-HT release in the SNr. A) Stimulated dopamine release in striatal brain slices is unaffected by 10 µM ketamine application nor 1 mM urethane application ($p > 0.05$, t-test, $n = 5$ both drugs). B) 5-HT release in brain slices containing the SNr is not altered by ketamine nor urethane ($p > 0.05$, t-test, $n \geq 3$ both drugs).

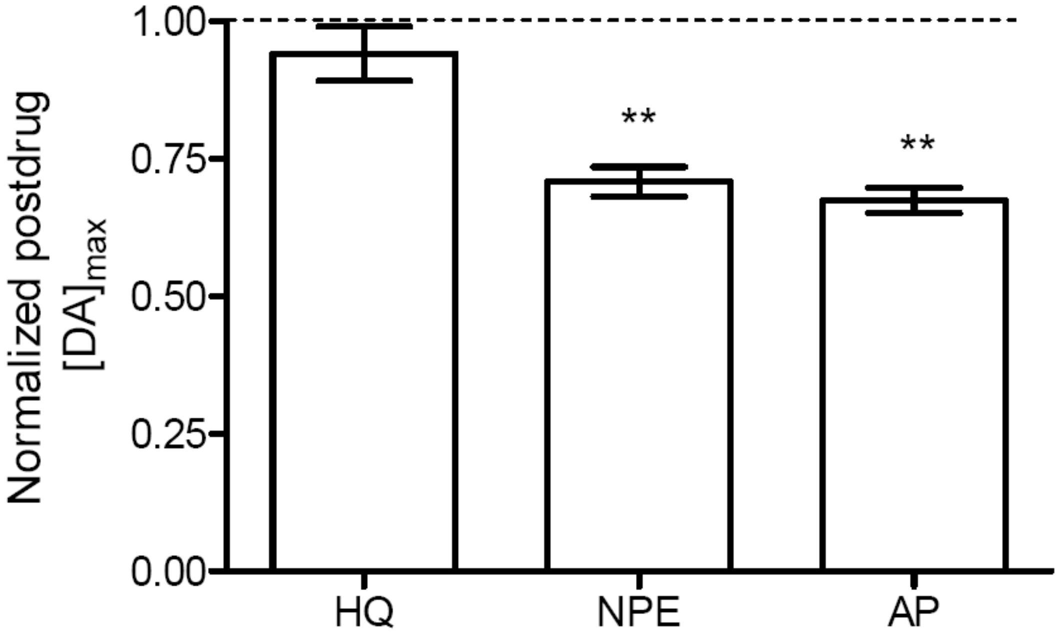


**Figure 8.5** The effect of iontophoretic marker compounds on dopamine release in striatal brain slices. Three electroactive uncharged markers used to quantify electroosmotic flow were applied to striatal brain slices so their effect on stimulated dopamine release could be evaluated. Hyrdoquinone (HQ) at 20 μM had no effect on stimulated dopamine release. Nitrophenoxyethanol (NPE) and acetamidophenol (AP) both at 20 μM significantly attenuated the dopamine signal (**, $p < 0.01$, $n = 5$ each drug).

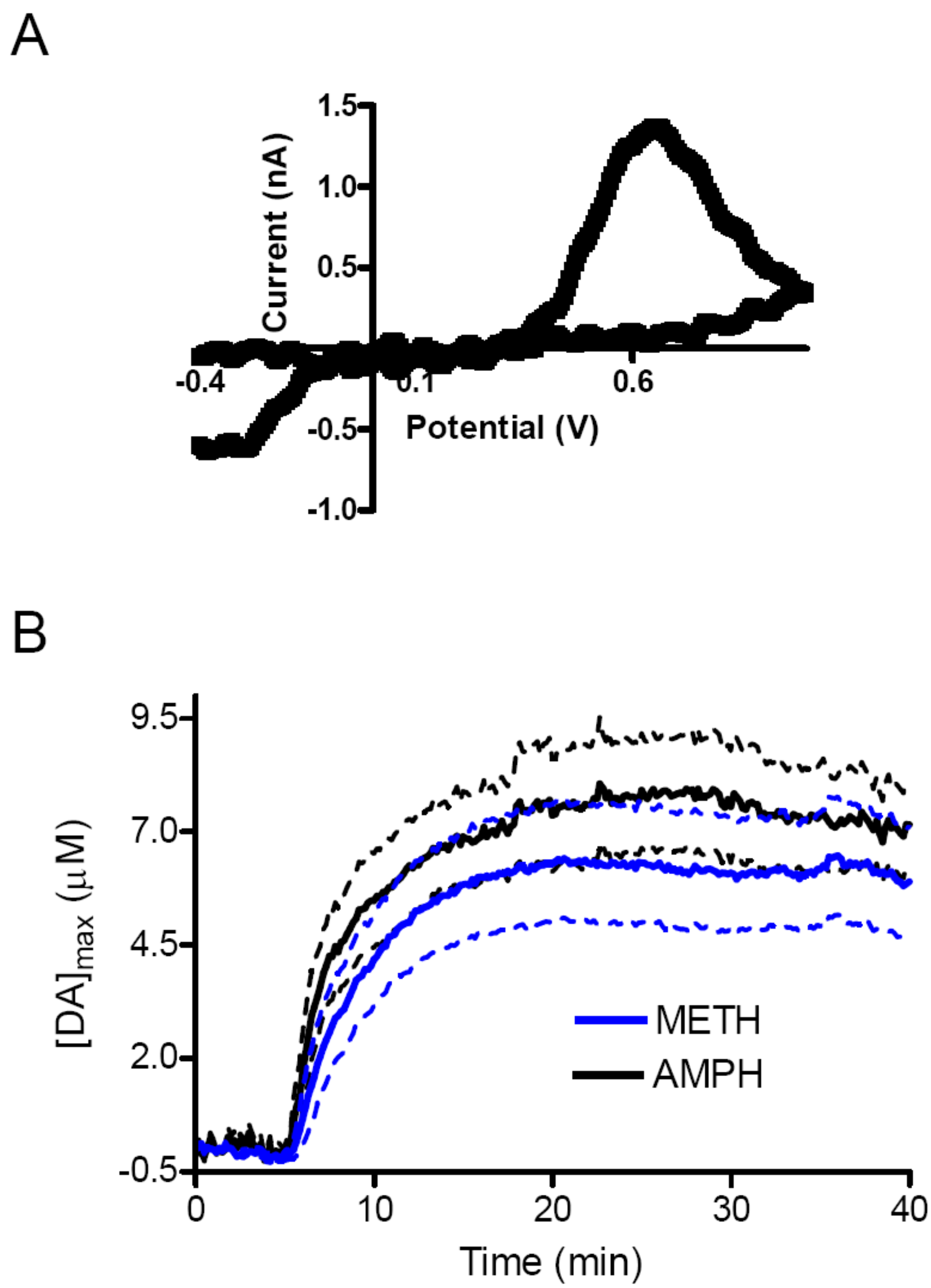


**Figure 8.6** Changes in basal dopamine concentration over long time periods can be accurately determined using principal component regression (PCR) analysis to remove contributions of electrode drift to the analytical signal. A) Dopamine training set CV used to extract a pure dopamine signal from the convoluted current trace. B) Basal dopamine concentration as determined by PCR before and after the application of 10 µM amphetamine (AMPH) or methamphetamine (METH) to striatal brain slices, every 100$^{th}$ data point shown for clarity. There are no significant ($p > 0.05$, $n = 5$ each drug) differences in the reverse transport caused by AMPH vs. METH.

achieved by either drug was on average 7.0 μM, almost 4 times higher than the average dopamine released upon electrical stimulation in this brain region and similar to that reported previously (Jones et al., 1998). There was no significant difference in either the magnitude or rate of dopamine reverse transport between the two drugs ($p < 0.05$).

## Discussion

### *Waveform Application Frequency and Temporal Response*

Carbon fibers are a desirable sensor surface for dopamine studies because they are capable of adsorbing or pre-concentrating dopamine on their surface. Pre-concentration enhances the current signal associated with the dopamine measurement and makes subtle changes in dopamine concentration more apparent. The amount of dopamine that adsorbs to the electrode surface can be controlled in part by changing the amount of time the electrode is held at a negative potential (- 0.4 V) (Figure 8.1A) (Bath et al., 2000). Additionally, modified waveforms can be used to over oxidize the carbon surface and increase the electrode's sensitivity for dopamine (Heien et al., 2003). A side effect of dopamine adsorption to the electrode is the introduction of a time delay in response to rapid changes in dopamine concentrations around the electrode (Figure 8.1A) (Bath et al., 2000). Recently, a deconvolution procedure was developed to accurately account for and remove the temporal delay associated with adsorption (Venton et al., 2002). Deconvoluted *in vivo* FSCV current traces were shown to be similar to those obtained with constant potential amperometry, which does not suffer from an adsorptive time delay (Venton et al., 2002). Until recently, this deconvolution procedure was considered sufficient for removal of the electrode time delay and accurate measurements of dopamine uptake.

Current deconvolution procedures are inadequate for the study of dopamine uptake kinetics in striatal brain slices when the adsorptive time delay is too large. This time delay is reduced by increasing the waveform application frequency from 10 Hz to 60 Hz (Bath et al., 2000). Less adsorption improves the temporal response of the electrode to rapid changes in dopamine concentration evident by a shorter delay time from stimulation to $[DA]_{max}$ (Figure 8.1B). The time to reach $[DA]_{max}$ for an electrode cycled at 60 Hz is 67 ms instead of 200 ms at the same electrode cycled at 10 Hz. The additional delay induced by the 10 Hz application frequency decreases the accuracy of the dopamine uptake measurement even when the delay of 200 ms has been accounted for by deconvolution. When both traces are fit to Michaelis-Menten kinetics using non-linear regression (Wu et al., 2001), the 10 Hz application frequency underestimates $V_{max}$ by 22 %. The underestimation in $V_{max}$ is due to a reduced electrode sensitivity to fast dopamine dynamics in the brain slice.

Slowing dopamine uptake abolishes the measurement penalty due to the increased temporal distortion at 10 Hz. The application of 10 µM cocaine slows the rate of dopamine clearance from the extracellular space without changing the electrochemical dynamics of dopamine detection (Jones et al., 1995a; Davidson et al., 2000; Uhl and Lin, 2003) (Figure 8.2A). As Figure 8.2A shows, the 10 Hz application over estimates the amount of dopamine released after the stimulation and indicates that cocaine is having a larger effect on uptake when compared to the same electrode cycled at 60 Hz. This qualitative difference is not manifested as an overestimation in $K_{m(app)}$ for a given concentration of cocaine (Figure 8.2B) and most likely reflects the reduced sensitivity of the 10 Hz electrode when the uptake rate is close to $V_{max}$. When ascending concentrations of cocaine (1-20 µM) are given and the corresponding values of $K_{m(app)}$ are plotted, a value of $K_i$ can be calculated (Jones et al., 1995a). Cocaine $K_i$ values calculated in the same location by the same electrode do not differ when the electrode is cycled at 60 Hz instead of 10 Hz giving values of 0.32 µM and 0.30 µM respectively. The $V_{max}$ and $K_{m(app)}$ data suggest that the insufficient uptake modeling at 10 Hz is dependent on the rate of uptake. In cases where uptake is slowed by an inhibitor, both frequencies can used to accurately calculate a $K_i$ for cocaine. For this reason, sampling rates of 10 Hz may still produce valid $V_{max}$ values in brain regions where dopamine uptake is slower such as the nucleus accumbens (NAc) or basolateral amygdaloid nucleus (Jones et al., 1995b).

### *Deconvoluted FSCV Mimics Amperometry*

The question remains: is a 60 Hz application frequency sufficiently fast to make the deconvolution procedure described in Venton *et al.* (2002) valid for uptake measurements in striatal brain slices? When stimulated release is measured and compared using FSCV at 60 Hz and constant potential amperometry, there is time shift of 40 ms during FSCV that is not present during amperometric detection (Figure 8.3A). The time delay is due primarily to the kinetics of adsorption at the electrode and can be completely removed by deconvolution. The maximal uptake rate for this location measured by amperometry is the same as that taken from simplex modeling of the deconvoluted FSCV signal. FSCV at 60 Hz has a sufficiently small time delay that it can be completely removed by deconvolution and accurate uptake measurements made. The robustness of uptake measurements made by FSCV at 60 Hz was also tested using mice that have faster than normal dopamine uptake (Chapter 4). Little difference was found in the $V_{max}$ values reported for these animals by FSCV and amperometry. Taken together, these data validate the deconvolution and modeling procedures; however, there is a limit to the amount of temporal distortion that can be removed using current techniques.

Amperometry has enhanced time resolution over FSCV; however, the sensitivity and calibration of amperometric electrodes remains problematic. Small currents associated with amperometric detection of dopamine in brain slices increase the challenge of using it as a primary technique for catecholamine detection. When performing amperometry in a brain slice, it is necessary to supplement the aCSF buffer with ascorbate at a concentration mimicking brain levels so that calibration of the amperometric signal can be made (Rice, 1999; Venton et al., 2003). The ascorbic acid creates a catalytic cycle close to electrode surface limiting the diffusion layer and enhancing the current response to dopamine oxidation (Venton et al., 2003). As shown in Figure 8.3B, the supplementation of a striatal brain slice with 500 µM ascorbate enhances the current signal associated with the release and uptake of dopamine without changing its temporal response. Post calibration of the electrode used in Figure 8.3A using FSCV and amperometry in a flow injection system yielded the same dopamine concentration.

*Anesthetic Effects on Stimulated Dopamine Release*

A wide range of anesthetic technologies are currently in use for survivable and non-survivable procedures in animal subjects. Accordingly, work has been done on the possible effects of these anesthetics on neurotransmitter release (Horishita et al., 2008; Rowley and Flood, 2008; Tose et al., 2009). The injectables ketamine and urethane are used in our survivable and non-survivable procedures respectively. Brain slice experiments were done to determine if either drug had an appreciable effect on dopamine or 5-HT release. The application of 1 mM urethane to brain slices did not significantly ($p > 0.05$) alter stimulated dopamine release in the caudate putamen or stimulated 5-HT release in the SNr (Figure 8.4 A and B). Urethane is widely used anesthetic in rodent preparations because it provides deep anesthesia without significant cardiovascular or respiratory depression. Urethane affects a variety of ion channels, including n-methyl-d-aspartate (NMDA) and γ-amino butyric acid (GABA) channels both of which are known to regulate dopamine release (Schmidt and Fadayel, 1996; Plaznik et al., 1997; Svensson, 2000; Hara and Harris, 2002). However, anesthetic doses of urethane do not change dopamine release or uptake *in vivo* as measured by chronoamperometry (Sabeti et al., 2003). Our results support the *in vivo* data by showing that there is no local effect of urethane on stimulated dopamine release. The effects of urethane on 5-HT release are not well documented; however, our data implies the lack of an effect.

Ketamine does not change neurotransmitter release in the caudate or the SNr (Figure 8.4 A and B). It does alter the electrode sensitivity to both neurotransmitters by 30-35 %; however, Figure 8.4 has been adjusted for the sensitivity reduction revealing no ketamine effect on release. Ketamine is an NMDA receptor (NMDAR) antagonist and has been shown to significantly increase the levels of 5-HT and dopamine *in vivo* and in brain slices (Irifune et al., 1991; Lindefors et al., 1997; Tso et al., 2004). The ketamine effect described in the literature indicates that NMDAR activation is inhibitory at dopamine and 5-HT synapses; however, our data indicates no contribution from NMDARs on stimulated release. The opening of NMDAR channels requires binding of glutamate and the cofactor glycine to the receptor followed by membrane depolarization to remove a $Mg^{2+}$ ion blocking the channel (Albensi, 2007). All three steps are required for channel opening and subsequent ion transport ($Na^{+}$, $K^{+}$, and $Ca^{2+}$) into the presynaptic terminal. The lack of glycine and glutamate tone in the brain slice coupled with the presence of $Mg^{2+}$ in the perfusion buffer would keep the NMDAR normally inactivated. Therefore, any effect by released glutamate or glycine (co-released with dopamine by the stimulation) in brain slices would occur once when the $Mg^{2+}$ block was removed by membrane depolarization. Long stimulation trains would be susceptible to the inhibition of release by presynaptic NMDAR activation because sufficient time would elapse during the stimulation for receptor occupation and channel opening (Fields et al., 2007). Exactly how NMDARs affect dopamine and 5-HT release remains unclear; however, AMPARs may negatively regulate striatal dopamine release through $H_2O_2$ formation (Avshalumov et al., 2008). The stimulation parameters used in this study (single pulse for dopamine and 20p 100 Hz for 5-

HT) are too brief to effectively probe the action of NMDARs on release. For example, dopamine release evoked by a single pulse electrical stimulation is devoid of autoreceptor effects which also regulate release by acting on presynaptic terminals (Kennedy et al., 1992). We conclude that the NMDAR is normally blocked in brain slices containing the caudate putamen or SNr, and that the release evoked by our stimulation parameters is not affected by activation of the NMDAR because the time course is too short.

*Iontophoresis Markers and Dopamine Release*

Several electroactive substances have been identified as markers to be used with iontophoretic ejections. The marker HQ did not alter stimulated dopamine release in striatal brain slices (Figure 8.5); however, both NPE and AP significantly decreased stimulated dopamine released (Figure 8.5). None of the compounds shown in Figure 8.5 appreciably altered the sensitivity of the electrode for dopamine when tested in a flow injection apparatus. The reduction of dopamine by AP is supported by Fiebich *et al.* (2006) who found striatal dopamine release to be diminished in slices incubated with a mixture of aspirin, caffeine, and acetaminophen (Fiebich et al., 2006). There is no evidence from the literature to support or refute the release effects of HQ or NPE. This work is the first documented case of NPE decreasing stimulated striatal dopamine release in brain slices.

*Dopamine Reverse Transport*

The action of AMPH on basal dopamine levels in striatal brain slices was previously evaluated using FSCV and found to require the presence of DAT (Jones et al., 1998). In that study, the current due to oxidation of dopamine was separated from the background current in a different manner than is typically used for short stimulations. For those measurements, the background current measured with AMPH present was subtracted by a single background taken without AMPH present; the difference in these backgrounds was taken as the current due to dopamine concentration changes around the electrode. This approach is valid if the only parameter changing over the files being subtracted is dopamine. Over the timeframe of reverse transport (10-40 min.), the inherent instability of the electrode causes changes in the background that are not due to changes in dopamine concentration (Hermans et al., 2008). As a result, the cyclic voltammograms used to identify dopamine are less reliable with subsequent files that are further removed in time from the original background file. PCR is able to account for components of the background not related to dopamine and remove them from the signal (Heien et al., 2004; Hermans et al., 2008). The data shown in Figure 8.6B is an example of a pure dopamine trace in which background components other than dopamine have been removed by PCR. Therefore, Figure 8.6B only shows current that arises from changes in the dopamine concentrations. PCR increases the level of certainty that the measured changes are due only to dopamine.

Analog background subtraction and PCR were used to elucidate if the structural differences between AMPH and METH affected their ability to induce reverse transport. AMPH and METH differ in structure only by the presence of a methyl group and have similar mechanisms of action: they both block the DAT, inhibit VMAT2, and cause reverse transport of cytosolic dopamine (Sulzer et al., 2005). However, their addictive properties are thought to be much different with METH being more addictive than AMPH. Figure 8.6B clearly shows that there is no significant ($p > 0.05$) difference in the rise time or $[DA]_{max}$ achieved by either drug when VMAT2 is first inhibited with tetrabenazine; therefore, the reverse transport of dopamine caused by these drugs is not different. It is possible that the increased hydrophobicity of METH allows it to more easily cross the plasma membrane. Greater METH accumulation presynaptically would enhance VMAT2 inhibition and cause greater reverse transport, a mechanism not probed in the slice experiment. However, *in vitro* work in isolated cells showed no difference in the amount of dopamine released by AMPH vs.

METH (Goodwin et al., 2009) and *in vivo* microdialysis data showed dopamine increases due to METH and AMPH in the NAc are the same (Shoblock et al., 2003). In conclusion, the addictive nature of the AMPH stimulants is not due solely to their action at the monoamine transporter and are more likely the result of global changes in brain circuitry (Kalivas, 2007).

## Literature Cited


Albensi BC (2007) The NMDA receptor/ion channel complex: a drug target for modulating synaptic plasticity and excitotoxicity. Curr Pharm Des 13:3185-3194.

Avshalumov MV, Patel JC, Rice ME (2008) AMPA receptor-dependent H2O2 generation in striatal medium spiny neurons but not dopamine axons: one source of a retrograde signal that can inhibit dopamine release. J Neurophysiol 100:1590-1601.

Bath BD, Michael DJ, Trafton BJ, Joseph JD, Runnels PL, Wightman RM (2000) Subsecond adsorption and desorption of dopamine at carbon-fiber microelectrodes. Anal Chem 72:5994-6002.

Davidson C, Ellinwood EH, Douglas SB, Lee TH (2000) Effect of cocaine, nomifensine, GBR 12909 and WIN 35428 on carbon fiber microelectrode sensitivity for voltammetric recording of dopamine. J Neurosci Methods 101:75-83.

Fiebich BL, Candelario-Jalil E, Mantovani M, Heinzmann M, Akundi RS, Hull M, Knorle R, Schnierle P, Finkenzeller G, Aicher B (2006) Modulation of catecholamine release from rat striatal slices by the fixed combination of aspirin, paracetamol and caffeine. Pharmacol Res 53:391-396.

Fields HL, Hjelmstad GO, Margolis EB, Nicola SM (2007) Ventral tegmental area neurons in learned appetitive behavior and positive reinforcement. Annu Rev Neurosci 30:289-316.

Goodwin JS, Larson GA, Swant J, Sen N, Javitch JA, Zahniser NR, De Felice LJ, Khoshbouei H (2009) Amphetamine and methamphetamine differentially affect dopamine transporters in vitro and in vivo. J Biol Chem 284:2978-2989.

Hara K, Harris RA (2002) The anesthetic mechanism of urethane: the effects on neurotransmitter-gated ion channels. Anesth Analg 94:313-318, table of contents.

Heien ML, Johnson MA, Wightman RM (2004) Resolving neurotransmitters detected by fast-scan cyclic voltammetry. Anal Chem 76:5697-5704.

Heien ML, Phillips PE, Stuber GD, Seipel AT, Wightman RM (2003) Overoxidation of carbon-fiber microelectrodes enhances dopamine adsorption and increases sensitivity. Analyst 128:1413-1419.

Hermans A, Keithley RB, Kita JM, Sombers LA, Wightman RM (2008) Dopamine detection with fast-scan cyclic voltammetry used with analog background subtraction. Anal Chem 80:4040-4048.

Herr NR, Kile BM, Carelli RM, Wightman RM (2008) Electroosmotic flow and its contribution to iontophoretic delivery. Anal Chem 80:8635-8641.

Horishita T, Eger EI, 2nd, Harris RA (2008) The effects of volatile aromatic anesthetics on voltage-gated Na+ channels expressed in Xenopus oocytes. Anesth Analg 107:1579-1586.

Irifune M, Shimizu T, Nomoto M (1991) Ketamine-induced hyperlocomotion associated with alteration of presynaptic components of dopamine neurons in the nucleus accumbens of mice. Pharmacol Biochem Behav 40:399-407.

Johnson MA, Rajan V, Miller CE, Wightman RM (2006) Dopamine release is severely compromised in the R6/2 mouse model of Huntington's disease. J Neurochem 97:737-746.

Jones SR, Garris PA, Wightman RM (1995a) Different effects of cocaine and nomifensine on dopamine uptake in the caudate-putamen and nucleus accumbens. J Pharmacol Exp Ther 274:396-403.

Jones SR, Garris PA, Kilts CD, Wightman RM (1995b) Comparison of dopamine uptake in the basolateral amygdaloid nucleus, caudate-putamen, and nucleus accumbens of the rat. J Neurochem 64:2581-2589.

Jones SR, Gainetdinov RR, Wightman RM, Caron MG (1998) Mechanisms of amphetamine action revealed in mice lacking the dopamine transporter. J Neurosci 18:1979-1986.

Kalivas PW (2007) Cocaine and amphetamine-like psychostimulants: neurocircuitry and glutamate neuroplasticity. Dialogues Clin Neurosci 9:389-397.

Kennedy RT, Jones SR, Wightman RM (1992) Dynamic observation of dopamine autoreceptor effects in rat striatal slices. J Neurochem 59:449-455.

Lindefors N, Barati S, O'Connor WT (1997) Differential effects of single and repeated ketamine administration on dopamine, serotonin and GABA transmission in rat medial prefrontal cortex. Brain Res 759:205-212.

Plaznik A, Jessa M, Nazar M (1997) The behavioral effects of NMDA antagonists in serotonin depleted rats. Pharmacol Biochem Behav 58:159-166.

Rice ME (1999) Use of ascorbate in the preparation and maintenance of brain slices. Methods 18:144-149.

Rowley TJ, Flood P (2008) Isoflurane prevents nicotine-evoked norepinephrine release from the mouse spinal cord at low clinical concentrations. Anesth Analg 107:885-889.

Sabeti J, Gerhardt GA, Zahniser NR (2003) Chloral hydrate and ethanol, but not urethane, alter the clearance of exogenous dopamine recorded by chronoamperometry in striatum of unrestrained rats. Neurosci Lett 343:9-12.

Schmidt CJ, Fadayel GM (1996) Regional effects of MK-801 on dopamine release: effects of competitive NMDA or 5-HT2A receptor blockade. J Pharmacol Exp Ther 277:1541-1549.

Shoblock JR, Sullivan EB, Maisonneuve IM, Glick SD (2003) Neurochemical and behavioral differences between d-methamphetamine and d-amphetamine in rats. Psychopharmacology (Berl) 165:359-369.

Sulzer D, Sonders MS, Poulsen NW, Galli A (2005) Mechanisms of neurotransmitter release by amphetamines: a review. Prog Neurobiol 75:406-433.

Svensson TH (2000) Dysfunctional brain dopamine systems induced by psychotomimetic NMDA-receptor antagonists and the effects of antipsychotic drugs. Brain Res Brain Res Rev 31:320-329.

Tose R, Kushikata T, Yoshida H, Kudo M, Furukawa K, Ueno S, Hirota K (2009) Orexin A decreases ketamine-induced anesthesia time in the rat: the relevance to brain noradrenergic neuronal activity. Anesth Analg 108:491-495.

Tso MM, Blatchford KL, Callado LF, McLaughlin DP, Stamford JA (2004) Stereoselective effects of ketamine on dopamine, serotonin and noradrenaline release and uptake in rat brain slices. Neurochem Int 44:1-7.

Uhl GR, Lin Z (2003) The top 20 dopamine transporter mutants: structure-function relationships and cocaine actions. Eur J Pharmacol 479:71-82.

Venton BJ, Troyer KP, Wightman RM (2002) Response times of carbon fiber microelectrodes to dynamic changes in catecholamine concentration. Anal Chem 74:539-546.

Venton BJ, Zhang H, Garris PA, Phillips PE, Sulzer D, Wightman RM (2003) Real-time decoding of dopamine concentration changes in the caudate-putamen during tonic and phasic firing. J Neurochem 87:1284-1295.

White IM, Doubles L, Rebec GV (1998) Cocaine-induced activation of striatal neurons during focused stereotypy in rats. Brain Res 810:146-152.

Wu Q, Reith ME, Wightman RM, Kawagoe KT, Garris PA (2001) Determination of release and uptake parameters from electrically evoked dopamine dynamics measured by real-time voltammetry. J Neurosci Methods 112:119-133.